

**Charles University in Prague,
Faculty of Medicine in Hradec Králové**



**11th INTERNATIONAL MEDICAL
POSTGRADUATE CONFERENCE**

New Frontiers in the Research of PhD Students

Conference of Medical Schools

November 27 - 28, 2014

Organized by
Charles University in Prague, Faculty of Medicine in Hradec Králové

Supported by
Specific Research Projekt 260061/2014

Under the auspices of his Magnificence,
Rector of the Charles University in Prague
Prof. MUDr. Tomáš Zima, DrSc.

Hradec Králové
Educational Centre of the Faculty of Medicine,
location: University Hospital

Table of content

General Information	5
Dean's Welcome	6
Programme Overview	7
Scientific Programme	8
Evaluation Committee	11
Presentations	12
Author's Index	115

Organizing committee

Prof. MUDr. RNDr. Miroslav Červinka, CSc.
Prof. MUDr. Vladimír Palička, CSc., dr. h. c.

Editor:
prof. MUDr. RNDr. Miroslav Červinka, CSc.

Technical assistance:
Ing. Miloslava Paterová
Mgr. Gabriela Štěrbová

The publication has undergone neither linguistic editing nor proof reading.
It is printed from the author's e-mail correspondence.

GENERAL INFORMATION

Venue:

Educational Centre
Charles University, Faculty of Medicine
University Hospital

Conference office:

The conference office is to be set up for information
and registration at the Educational Centre
in the University Hospital at the following opening hours:

Thursday, November 27, 10:00 - 17:30
Friday, November 28, 8:30 - 16:00

Official language:

English

Presentation time:

Lecture 15 min
Discussion 5 min

Accommodation of participants:

Hotel Nové Adalbertinum
Velké náměstí 32
500 03 Hradec Králové 2

WELCOME



Dear friends and colleagues,

I would like to welcome you to the 11th International Medical Postgraduate Conference in Hradec Králové. The conference has been progressing well since its inception, and over the years it has turned into a real international meeting. We are proud to welcome participants not only from the Czech and Slovak Republics, but also from Austria, Georgia, Germany, Hungary, Poland, Portugal the Netherlands and the United Kingdom. I personally believe that the position of this conference is well established, and it is a standard part of international activities of our faculty.

There are several reasons for organizing this conference. The first obvious reason is the opportunity to compare achieved results, to present one's data and learn from others. Nevertheless, we consider this particular meeting of postgraduate students in biomedicine also very important as a tool for international harmonization of Ph.D. studies in the European area. We are very happy that ORPHEUS (Organisation for Ph.D. Education in Biomedicine Health Sciences in the European System) is an active partner in the organization of this conference.

Another important reason for organizing this meeting is an opportunity for direct personal contacts. Nowadays, the electronic world is overloaded with information. You can find all the latest news, the latest publications, hypotheses and scientific results at various websites. However, using these electronic media an essential human quality of scientific communication is disappearing. Dear participants, take advantage of this occasion.

Those of you evaluated as the best by an expert panel of judges will receive a financial award, yet this should be considered secondary. I am sure that the idea of our meeting is similar to the idea behind the Olympic Games – winning is not the most important thing. Taking part, learning scientific news, and above all meeting new colleagues and friends is of the utmost importance. If we succeed in this, the conference has fulfilled its purpose.

I wish you very successful scientific meeting and enjoyable time in our beautiful city!

Prof. MUDr. RNDr. Miroslav Červinka, PhD.
Dean, Faculty of Medicine in Hradec Králové
Charles University in Prague

PROGRAMME OVERVIEW

Thursday – November 27, 2014

10:00 – 10:40	Meeting of the Evaluation Committee	Seminar room 4
10:40 – 11:00	Opening of the Conference	Main lecture hall
11:00 – 12:40	Presentations Part I (1 - 5)	Main lecture hall
12:40 – 13:40	Lunch	Seminar room 1
13:40 – 15:20	Presentations Part II (6 - 10)	Main lecture hall
15:20 – 15:50	Coffee break	Seminar room 1
15:50 – 17:30	Presentations Part III (11 - 15)	Main lecture hall
20:00 – 22:00	Social dinner	Hotel Nové Adalbertinum

Friday – November 28, 2014

8:30 – 10:10	Presentations Part IV (16 - 20)	Main lecture hall
10:10 – 10:40	Coffee break	Seminar room 1
10:40 – 12:20	Presentations Part V (21 - 25)	Main lecture hall
12:20 – 13:20	Lunch	Seminar room 1
13:20 – 15:00	Presentations Part VI (26 - 30)	Main lecture hall
15:00 – 16:00	Meeting of Evaluation Committee	Seminar room 4
19:00 – 23:00	Social evening, Awards, Closing ceremony	Medical Library – Portico hall

THURSDAY, NOVEMBER 27

Part I

Chair: prof. MUDr. Jan Čáp, CSc.

- 11:00 T. Avaliani (Tbilisi): ASSESMENT OF MYELOPEROXIDASE LEVELS IN VARIOUS SEVERITY CONGESTIVE HEART FAILURE PATIENT GROUPS
- 11:20 Z. Babinská (Brno): BEHAVIOURAL AND NEUROCHEMICAL CORRELATES IN ANIMAL MODEL OF DEPRESSION-ADDICTION COMORBIDITY
- 11:40 B. Bibby (Hull): IDENTIFICATION AND FUNCTIONAL VALIDATION OF MIR-330 AND MIR-187 IN REGULATING OESOPHAGEAL ADENOCARCINOMA SENSITIVITY TO CHEMORADIATION THERAPY
- 12:00 J. Biedermann (Dresden): FUNCTIONAL CHARACTERISATION OF THE ISOCITRATE 1 (IDH1) MUTATION IN GLIOMAS
- 12:20 B. Botz (Pécs): PEPTIDERGIC SENSORY NERVES EXERT IMPORTANT REGULATORY ROLE IN EXPERIMENTAL ARTHRITIS

Part II

Chair: prof. MUDr. Radek Pudil, Ph.D.

- 13:40 K. Brocklesby (Hull): DEVELOPMENT OF A PET RADIOTRACER FOR ANGIOGENESIS IMAGING IN CANCER
- 14:00 J. P. Castro (Porto): HSP90 CLEAVAGE ASSOCIATES WITH OXIDIZED PROTEINS ACCUMULATION AFTER OXIDATIVE STRESS
- 14:20 L. Pálková (Bratislava): IDENTIFICATION AND CHARACTERIZATION OF BACTERIA OBTAINED FROM HUMAN SKIN AND SKIN OF MUS MUSCULUS - A PILOT STUDY FOR PREPARING NON-STANDARD MODEL BACTERIA FOR THEIR POTENTIAL USE IN ALTERNATIVE GENE THERAPY
- 14:40 I. Fabrik (Hradec Králové - University of Defence): EARLY RESPONSES OF DENDRITIC CELLS INFECTED BY FRANCISELLA TULARENSIS
- 15:00 A. Filipová (Hradec Králové): PRIMARY CILIA INCIDENCE IN A MYOBLAST CELL LINE (C2C12)

SCIENTIFIC PROGRAMME

Part III

Chair: prof. MUDr. Martina Řezáčová, Ph.D.

- 15:50 A. Howard (Liverpool): WHAT FUNCTIONAL MAGNETIC RESONANCE IMAGING TELLS US ABOUT COMPLEX SHOULDER INSTABILITY
- 16:10 R. Chrenko (Bratislava): PREDICTORS AND CLINICAL OUTCOME IN DECOMPRESSIVE HEMICRANIECTOMY FOR MALIGNANT MIDDLE CEREBRAL ARTERY INFARCTION
- 16:30 P. Ivák (Praha): CIRCULATING MICROPARTICLES AS A MARKER OF ENDOTHELIAL DYSFUNCTION IN PATIENTS WITH CONTINUOUS-FLOW VENTRICULAR ASSIST DEVICES
- 16:50 Z. Janovská (Hradec Králové): BISPHTHOSPHONATE-RELATED OSTEONECROSIS OF THE JAW: A REVIEW OF 20 CASES
- 17:10 I. Kazimierová (Martin): ANTI-ASTHMATIC EFFECTS OF POLYPHENOLIC COMPOUNDS IN ASTHMATIC ANIMAL MODEL

FRIDAY, NOVEMBER 28

Part IV

Chair: prof. RNDr. Jan Krejsek, CSc.

- 8:30 K. Koelfat (Maastricht): FGF19 EXCHANGE ACROSS THE GUT AND LIVER IN HUMANS
- 8:50 A. Krajčová (Praha): NORMALIZING GLUTAMINE CONCENTRATION CAUSES MITOCHONDRIAL UNCOUPLING IN AN IN VITRO MODEL OF HUMAN SKELETAL MUSCLE
- 9:10 L. Kramná (Praha): HUMAN GUT VIROME IN THE SEARCH FOR TYPE 1 DIABETES TRIGGERS USING NEXT-GENERATION SEQUENCING
- 9:30 K. Krychtiuk (Vienna): LEVOSIMENDAN EXHIBITS ANTI-INFLAMMATORY EFFECTS ON HUMAN CARDIAC MYOCYTES AND ENDOTHELIAL CELLS IN VITRO
- 9:50 T. Kupsa (Hradec Králové - University of Defence): BASELINE SERUM LEVELS OF MULTIPLE CYTOKINES AND ADHESION MOLECULES IN PATIENTS WITH PRIMARY AND SECONDARY ACUTE MYELOID LEUKEMIA

Part V

Chair: prof. MUDr. Stanislav Mičuda, Ph.D.

- 10:40 T. Kvárik (Pécs): PACAP CAN AMELIORATE VASCULAR CHANGES IN THE ANIMAL MODEL OF RETINOPATHY OF PREMATURITY
- 11:00 L. Matos (Porto): INVOLVEMENT OF UNFOLDED PROTEIN RESPONSE IN CELLULAR SENESCENCE ESTABLISHMENT
- 11:20 E. J. Miles (Liverpool): USE OF PH-CYCLING CONDITIONS TO MODEL POST-ERUPTIVE MATURATION OF DENTAL ENAMEL IN VITRO
- 11:40 V. Mirtskhulava (Tbilisi): PERFORMANCE OF QUANTIFERON-TB GOLD IN-TUBE TEST IN SERIAL TESTING OF LATENT TUBERCULOSIS INFECTION AMONG HEALTHCARE WORKERS IN GEORGIA
- 12:00 V. Danihel (Plzeň): HUMAN RECOMBINANT ALKALINE PHOSPHATASE (RECAP) IN THE TREATMENT OF SEPSIS AND SEPSIS-ASSOCIATED ACUTE KIDNEY INJURY

Part VI

Chair: prof. MUDr. Milan Bayer, CSc.

- 13:20 E. Sahin (Vienna): MACROPHAGE PTEN REGULATES EXPRESSION AND SECRETION OF ARGINASE I MODULATING INNATE AND ADAPTIVE IMMUNE RESPONSES
- 13:40 J. Schovánek (Olomouc): EVALUATION OF PARAMETHERS AFFECTING SURVIVAL AND METASTATIC POTENTIAL IN PATIENTS WITH SDHB MUTATED PHEOCHROMOCYTOMA/PARAGANGLIOMA
- 14:00 M. Sułkowski (Krakow): NOVEL PROTOCOL FOR DIFFERENTIATION OF INDUCED PLURIPOTENT STEM CELLS (IPS) INTO DOPAMINE AND MELANIN PRODUCING CELLS
- 14:20 J. Svačinová (Brno): THE VIBRATION PLETHYSMOGRAPHIC METHOD OF ARTERIAL COMPLIANCE ANALYSIS IN DEPENDENCE ON TRANSMURAL PRESSURE
- 14:40 D. van Dijk (Maastricht): UNIMPAIRED ANABOLIC RESPONSE TO ORAL MEAL FEEDING IN PATIENTS WITH PANCREATIC CANCER CACHEXIA

EVALUATION COMMITTEE

Chairperson: **Professor Vladimír Palička**
Vice-Dean for International Relations
Charles University, Faculty of Medicine
Hradec Králové, Czech Republic

Members: **Professor Peter Dieter**
President of Association of Medical Schools in Europe
Association of Medical Schools in Europe (AMSE)
Berlin, Germany

Professor Margarethe Geiger
Head of Institute of Physiology
Research Centre of Physiology and Pharmacology
Medical University of Vienna
Vienna, Austria

Professor Gabor Kovacs
President of the Szentagothai Research Centre
University of Pécs
Pécs, Hungary

Dr. Thorsten Liebers
Head of Dean's Office for Laboratory and Construction Affairs
Faculty of Medicine C. G. Carus, University of Technology
Dresden, Germany

Professor Alan Shenkin
Emeritus Professor of Clinical Chemistry
Faculty of Health and Life Sciences, University of Liverpool
Liverpool, Great Britain

Professor Peter Soeters
Emeritus Professor of Surgery
Faculty of Health, Medicine and Life Sciences,
University of Maastricht
Maastricht, the Netherlands

ASSESSMENT OF MYELOPEROXIDASE LEVELS IN VARIOUS SEVERITY CONGESTIVE HEART FAILURE PATIENT GROUPS

Tamar Avaliani

E-mail: tamar_avaliani@yahoo.com

David Tvildiani Medical University, Department of Internal medicine

Co-authors: Prof. Dr. N.Bregvadze

Tutor: Prof. Sergio Tabagari, Assoc. Prof. Dr. Tamar Talakvadze

Introduction

Despite attempts to create a unified hypothesis explaining all aspects of Chronic Heart Failure (CHF) syndrome, a unified conceptual paradigm, which can respond to all questions, currently does not exist. Aggravation of CHF is not fully understood and extensive research is continued. More and more data are available about the role of inflammation and oxidative stress in pathophysiology and aggravation of CHF. Myeloperoxidase (MPO) is linked to both inflammation and oxidative stress, furthermore MPO level increases in CHF patients. This increase may be of high importance and may be used for screening and diagnosis of heart dysfunction. (1) According to existing data about MPO its primary function is to kill microorganisms in neutrophils and monocytes via the special MPO-mediated antimicrobial system. There is considerable evidence to suggest that MPO can contribute to coronary artery disease (CAD), carcinogenesis, and lung injury, etc (2, 3, 4). In our study we want to assess whether MPO system can damage healthy myocardium and thus contribute to CHF aggravation.

The aim of our study was to evaluate serum levels of MPO along with other markers of inflammation, protein-energetical malnutrition (PEM) and other characteristics of patients with CHF in the context of disease etiology and severity .

Methods

Eighty-six patients with CHF and ten healthy persons were included in our study. Patients who experienced myocardial infarction or other concomitant acute diseases, renal failure (creatinine >250 $\mu\text{mol/L}$) in past 3 months, were excluded from our analysis.

Biochemical parameters, full blood count, anthropometric data, ECG, and transthoracic ultrasound were performed . MPO levels were measured by ELISA. Total lymphocyte count (TLC) cells/ mm^3 used as an indicator of patient immune status. Serum albumin (Albumin) (g/L) was used as an indicator of protein reserves. Total cholesterol (TC) (mg/dl) and high density lipoprotein - cholesterol (HDL-C) (mg/dl) were used as a caloric depletion parameter (5). Furthermore HDL-C is a potential target for MPO-oxidation.

Statistical analyses were performed using IBM SPSS Statistics 16.0, Pearson's correlation for linear regression was used to assess correlation between MPO concentration and other inflammation and oxidation parameters. Mean value of MPO was compared among the CHF classes based on functional limitations and severity.

Results

Table 1 describes patients' demographic, clinical and laboratory characteristics by CHF functional classes (NYHA).

We found that MPO levels in the patients with CHF are significantly different ($p < 0,018$) from healthy (control) group. MPO levels were not associated with the genesis of CHF (ischemic versus non-ischemic).

MPO significantly correlates with CHF severity ($p < 0,009$), left ventricle ejection fraction (LVEF) ($p < 0,000$) and other parameters. The markers of inflammation and protein-energetic malnutrition (PEM) by CHF functional classes is given in the table 2. MPO is higher in CHF class IV compared to class III ($p < 0,014$) and compared to class II ($p < 0,003$). MPO level analysis among nutritional groups divided according to Instant Nutritional Assessment (INA) (6) shows that in the group I (Albumin > 3.5 g/dL, TLC < 1500 cells/mm³) these values don't correlate neither with albumin nor TLC values; In the II group (Albumin < 3.5 g/dL, TLC < 1500 cells/mm³) MPO significantly ($p = 0,01$) correlates only with TLC value; In the III group (Albumin < 3.5 g/dL, TLC > 1500 cells/mm³) it correlates ($p = 0,012$) with albumin concentration. Above mentioned both correlations are inverse.

MPO levels comparing in the above mentioned three groups of low nutritional status showed that in conditions of preserved albumin group (> 3.5 g/dL) MPO level is significantly lower than in the II ($p < 0,008$) and III ($p < 0,073$) groups; in the conditions of low albumin level (II and III group) MPO correlation with these values (TLC or Albumin) is associated with TLC value ($< > 1500$ cell/mm³) and shows the relationship between inflammation and nutritional status values. Beside this its correlation with other markers of inflammation and malnutrition (Table 3), it's increasing during the disease severity and relation to the PEM values confirms its significance in the disease progression and indicates that heart failure's severity (and probably progression of disease) is determined not only by the hemodynamic disturbances.

Discussion

It is well-known, that MPO system is toxic to a variety of microorganisms, bacterial toxins, and mammalian cells (tumor cells, granulocytes, lymphocytes, etc). Number of low molecular weight reducing agents, as well as serum albumin, react rapidly with the highly reactive products of the MPO system and prevent them from reaching a sensitive target of biological importance. The MPO mediated antimicrobial system has different (more or less reactive) products: among them chloramines are long-lived, thus providing a mechanism for the prolongation of the oxidant activity of the peroxidase system and can be toxic at a distance under conditions in which more reactive products are readily scavenged. So, MPO system has the potential to damage normal tissues, cells and cross-links to proteins, that produce damage (7). We found that MPO correlates with inflammation and PEM markers. MPO, inflammation and PEM markers themselves are correlation with CHF severity.

Conclusion

Relationship between investigated biomarkers of inflammation and PEM in CHF patients is very complex. MPO concentration is increasing in line with CHF aggravation, thus it can become instrument for patient's assessment in future.

References

1. Michowitz Y, Kisil S, Guzner-Gur H et al.: Usefulness of serum myeloperoxidase in prediction of mortality in patients with severe heart failure. *IMAJ*. 2008; 10: 884-888.
2. Stephan Baldus, Christopher Heeschen, Thomas Meinertz et al.: Myeloperoxidase serum levels predict risk in patients with acute coronary syndromes. *Circulation*. 2003; 108: 1440-1445.
3. Roger K. Schindhelm, Leonard P.van der Zwan, Tom Teerlink et al.: *Clinical Chemistry* 55:8. 1462-1470 (2009)

4. Wu, X., Schabath, M.B., Spitz, M.R. Myeloperoxidase promoter region polymorphism and lung cancer risk. *Methods Mol.Med.* 2003. 75,121-133.
5. A. Gonzalez Madrono, A. Mancha, F.J. Rodriguez et al. *Nutricion Hospitalaria.* 2011;26 (3):594-601.
6. Seltzer MH, Bastidas JA, Cooper DM. et al. *JPEN* 1979; 3(3): 157-9.
7. Seymour J. Klebanoff. Myeloperoxidase: friend and foe. *Journal of Leukocyte Biology.* 2005. Vol.77.

Table 1. Basic data of patients with CHF syndrome

	II functional class	III functional class	IV functional class
Age (years)	66,5±15,3	66±12,8	63,8±8,6
Sex (female/male)	14/14	15/29	2-Dec
AH (%)	30,20%	53,50%	16,30%
Systolic pressure (mmHg)	168±32,1	159±32	146±28
Diastolic pressure (mmHg)	94±16	90,5±18	85,5±11,1
Smoking (%)	50%	37.50%	12,50%
Ischemic/non ischemic	Dec-16	24/20	7-Jul
Diabetic mellitus (%)	26,10%	56.5%	17,40%
Total protein (g/L)	69,3±7,3	70±6,8	69,9±8,0
Albumin (g/L)	41±5,0	39,7±4,0	38,7±5,7
LVEF (%)	45,1±4,3	34±7,2	23,9±6,2
QTc (sec)	0,42±0,05	0,41±0,05	0,45±0,08
Creatinine (µmol/L)	91±28	92±27,3	107,1±46,4

Table 2. Inflammation and malnutrition Biochemical markers in CHF syndrome

	II functional class	III functional class	IV functional class
MPO (ng/ml)	7,7 ± 4	8,9 ± 6,4	11,8 ± 7,8
hsCRP (mg/l)	7,8 ± 7,3	13,5 ± 12,9	16 ± 13,7
Leukocytes (1×10 ⁹ /L)	7,5±1,9	7±2	8±2
TLC (cell/mm ³)	1722 ± 572	1384± 461	1210,2 ±331
TC(mg/dL)	189,5±52,5	165±47	154±48,7
HDL (mg/dL)	43±14	41±11,2	36±13
Albumin (g/L)	41±5	39,7±4	38,7±5,7

Table 3. Correlation of MPO level with markers of inflammation and malnutrition in CHF patients

Biochemical Marker	Test Statistics	P- Value
CRP	Pearson's r = 0,279	0,031
Leukocyte	Pearson's r = 0,065	0,634
TLC	Pearson's r = - 0,001	0,988
TC	Pearson's r = - 0,232	0,065
HDL	Pearson's r = - 0,230	0,002
Albumin	Pearson's r = - 0,652	0,016

BEHAVIOURAL AND NEUROCHEMICAL CORRELATES IN ANIMAL MODEL OF DEPRESSION-ADDICTION COMORBIDITY

Zuzana Babinská

E-mail: babinska@med.muni.cz

Masaryk University, Faculty of Medicine, Department of Pharmacology,
Brno, Czech Republic

Experimental and Applied Neuropsychopharmacology Research Group,
CEITEC - Central European Institute of Technology,
Masaryk University, Brno, Czech Republic

Co-authors: Petra Amchová, Jana Kučerová, Alexandra Šulcová, Liana Fattore, Petr Kačer,
Magdalena Šustková-Fišerová

Tutor: PharmDr. Jana Kučerová, Ph.D.

Introduction, Aims

According to an animal model of depression and substance use disorder comorbidity, we combined the olfactory bulbectomy model (OBX) of depression with the intravenous drug self-administration procedure to verify whether depressive-like rats display higher voluntary intake of the cannabinoid CB1 receptor agonist WIN 55,212-2 (WIN). Bulbectomized rats have been previously reported to self-administer more methamphetamine (Kucerova et al., 2012) than control rats. Consequently we used the *in vivo* microdialysis technique to verify whether OBX and SHAM (control group) rats display similar increase in the level of dopamine within the *nucleus accumbens* (NAc) shell in response to a challenge of WIN and methamphetamine.

Methods

Adult male Lister Hooded (LH) rats were divided randomly into two groups; in one group the bilateral ablation of olfactory bulbs was performed while the other group was sham operated. The midline frontal incision was made on the skull and 2 burr holes were drilled in the frontal bone 6-7 mm anterior from the bregma. Both olfactory bulbs were aspirated paying particular attention not to damage the frontal cortex. Prevention of blood loss was achieved by filling the dead space with a haemostatic sponge. Sham rats underwent identical anaesthetic and drilling procedures but their bulbs were left intact. After period of recovery a permanent intracardiac catheter was implanted through the external jugular vein to the right atrium. The catheter exited the skin in the midscapular area. After recovery, self-administration procedure was conducted in operant boxes using active and inactive lever-pressing. Pressure on lever defined as active, resulted in activation of the infusion pump delivering one intravenous infusion of WIN. After period of 4 weeks, extinction conditions were introduced. Responses to WIN were extinguished by replacing cannabinoid with vehicle allowing response to be recorded without drug consequences. All the other experimental parameters were left unchanged, so that pressing on the active lever resulted in an infusion of vehicle.

Another group of animals was used for *in vivo* microdialysis (LH and Wistar strain). During microdialysis surgery a small hole was drilled on the skull. A self-made microdialysis probe with a 2 mm dialyzing surface length was inserted vertically into the shell of the NAc and then fixed to the skull using acrylic cement. Starting 24 h from implantation of the probe, artificial cerebrospinal fluid was pumped

through the dialysis membrane at a constant rate with a microinjection pump. Dialysate samples were collected every 20 min and directly injected into a high performance liquid chromatography system in order to quantify dopamine levels. The first 3 samples were used to establish the baseline. Then the changes in dopamine levels after administration of WIN (0.3 mg/kg, LH strain) or methamphetamine (5 mg/kg, Wistar strain) were monitored.

Results

In the IV self-administration a significantly (up to 2 times) higher active lever-pressing rate was observed in OBX as compared with SHAM rats (Fig.1). Also response latency, defined as the time elapsed from the commencement of the experimental sessions until the first lever press, was significantly different between the two groups. Specifically, latency was shorter in OBX than SHAM rats, which suggests that bulbectomized rats may become more impulsive after initial cannabinoid exposure. Moreover, analysis of temporal patterns of responding revealed quantitative but not qualitative differences between OBX and SHAM rats during self-administration training, since the responding rate was typically slow and evenly distributed throughout the 2h test session in both groups. Finally, OBX and SHAM rats displayed clear cut differences in the time course of operant even when saline was substituted for WIN (extinction). Analysis of responding on the active lever showed significant differences between OBX and SHAM animals and revealed a persisting responding in OBX rats which took longer than SHAM to reach extinction criteria (4 weeks for OBX and 2 weeks for SHAM).

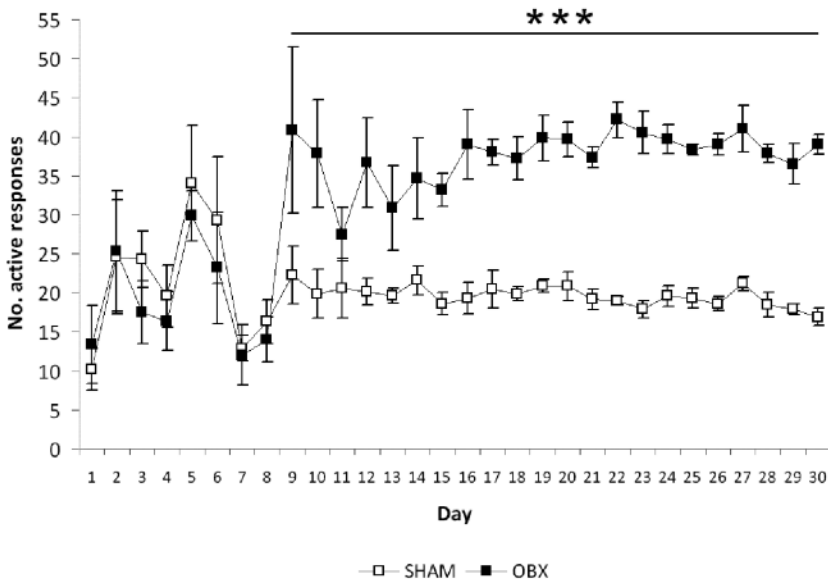


Fig.1 Mean active lever presses in SHAM and OBX LH rats during WIN self-administration.

Subsequent microdialysis experiment aimed at measuring the release of dopamine in the NAc shell of SHAM and OBX rats following an intravenous injection of WIN in LH or methamphetamine in Wistar strain. During the pre-treatment period, basal level of dopamine in the NAc shell did not differ significantly between the OBX and SHAM group of LH. Surprisingly, after an acute WIN administration, we found a significantly increased dopamine level compared to the basal level only in SHAM rats (Fig.2).

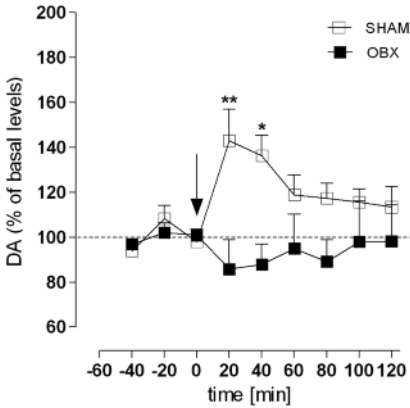


Fig.2 Effect of an intravenous administration of WIN on dopamine release in the NAc shell of SHAM and OBX LH rats.

OBX group of Wistar strain displayed lower basal level of dopamine in pg/ml (data not shown). However, relative dopamine level values after methamphetamine administration (% of individual baseline) were increased in the OBX group after methamphetamine administration as compared to SHAM (Fig.3).

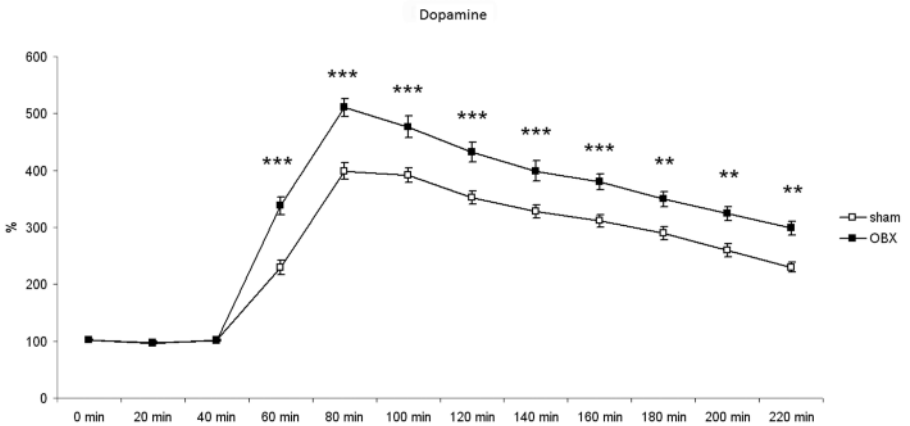


Fig.3 Effect of an intravenous administration of methamphetamine on dopamine release in the nucleus accumbens shell of SHAM and OBX Wistar rats

Discussion

Findings from the present study demonstrated that bulbectomized LH rats do self-administer higher amount of the cannabinoid CB1 receptor agonist WIN, take longer to extinguish cannabinoid-seeking behaviour than SHAM control rats and do not increase dopamine level in the NAc shell in response to a challenge of WIN as SHAM rats do. A neurobiological mechanism that may contribute to the resilience of OBX rats to extinguish not-rewarded operant responding is a dysfunction of the front-cortical neuronal circuits that are critically involved in the inhibition of on-going activity upon withdrawal of the reinforcers. Basal level of dopamine in the NAc shell did not differ significantly between the OBX and SHAM group of LH, which was probably caused by low sample size (n=3 to 4). Unlike LH, bulbectomized Wistar rats (n=8) displayed decreased dopamine basal levels and consequently increased dopamine level after methamphetamine administration, which can be explained by ceiling effect of used methamphetamine dose.

Conclusions

In conclusion, our findings showed that olfactory bulbectomy markedly affects cannabinoid self-administration, likely through a reduction of the rewarding effects of cannabinoids which animals compensate by increasing cannabinoid intake. A decreased dopamine neurotransmission in limbic brain areas might contribute to this compensatory behaviour.

Summary

To summarize, this study demonstrated that olfactory bulbectomized LH rats self-administer more cannabinoid agonist and take longer to extinguish drug-taking behaviour than SHAM group. Removal of the olfactory bulbs may disrupt activity in limbic circuits involved in the dopaminergic system, which is critical for processing drug taking and seeking behaviours. Accordingly, LH bulbectomized rats did not display a significant increase in dopamine level in the *nucleus accumbens* shell after a cannabinoid challenge, as SHAM controls did, indicating that a depressive-like state is likely to alter the rewarding perception of the drug. Bulbectomized group of Wistar rats after methamphetamine administration displayed increased dopamine level, which can be interpreted by ceiling effect of the dose used.

References

Kucerova, J., Pistovcakova, J., Vrskova, D., Dusek, L., and Sulcova, A.: The effects of methamphetamine self-administration on behavioural sensitization in the olfactory bulbectomy rat model of depression. *Int J Neuropsychopharmacol* 2012; 15, 1503-1511.

This work was supported by the project “CEITEC - Central European Institute of Technology” (CZ.1.05/1.1.00/02.0068) from European Regional Development Fund, the project of specific research at the Masaryk University (MUNI/A/0886/2013), Project PRVOUK P34, “Operational Program Prague – Competitiveness“ (CZ.2.16/3.1.00/22197, CZ.2.16/3.1.00/21537) and “National Program of Sustainability“ (NPU I (LO) MSMT - 34870/2013).

IDENTIFICATION AND FUNCTIONAL VALIDATION OF MIR-330 AND MIR-187 IN REGULATING OESOPHAGEAL ADENOCARCINOMA SENSITIVITY TO CHEMORADIATION THERAPY

Becky Ann Selina Bibby

E-mail: b.bibby@2012.hull.ac.uk

School of Biological, Biomedical and Environmental Sciences, Cancer Biology and Therapeutics Laboratory, University of Hull, UK

Co-authors: Niamh Lynam-Lennon, Stephen Maher

Tutor: Dr. Stephen Maher, PhD

Introduction

The incidence of oesophageal adenocarcinoma (OAC) has increased in western societies by 600% in the last three decades (Dulak et al, 2013). The standard treatment regimen for patients diagnosed with OAC is neoadjuvant chemoradiation therapy (neo-CRT) prior to surgical resection. Unfortunately, ~70% of patients demonstrate little or no response to neo-CRT. The identification of biomarkers predictive of patient response to neo-CRT, prior to treatment, would enable effective treatment stratification for OAC patients. Furthermore, elucidating the mechanisms that confer resistance to chemoradiation in OAC tumours will also identify novel therapeutic targets. MicroRNA (miRNA) are small, non-coding RNA that regulate gene expression via degradation or translational repression of complementary target mRNA. Dysregulated miRNA expression is associated with cancer initiation and progression. More recently it has been demonstrated that miRNA contribute to treatment sensitivity, altering cellular sensitivity to chemoradiation therapy in a number of human cancers (Hummel et al, 2010).

Aims

The initial aim was to identify miRNA, that are differentially expressed between patients who respond and patients who do not respond to neo-CRT, in a pre-treatment setting, using tumour biopsy samples from an OAC patient cohort. The functional role of select miRNA, which are differentially expressed between responders and non-responders, was further investigated in the context of chemoradiation resistance. To this end, the mRNA targets and signalling pathways of select miRNA were determined using *in vitro* OAC cell models.

Methods

Pre-treatment endoscopic biopsies were taken from patients at the point of diagnosis as previously described. Patients received a standardised neo-CRT regimen prior to surgical resection. Response to therapy was assessed by an experienced pathologist and assigned a tumour regression grade (TRG) 1-5 (Lynam-Lennon et al, 2012). Pre-treatment biopsy samples were analysed via qPCR based miRNA arrays, to identify differentially expressed miRNA between responders and non-responders to neo-CRT. *In vitro*, an isogenic model of radioresistant OAC was established by chronically irradiating OE33 cells (OE33RR) (Lynam-Lennon et al, 2012). The expression of select miRNA was manipulated using over-expression and silencing vectors and liposomal-based transfection of OAC cell lines (OE33 and OE19). The clonogenic assay was used to assess alterations in cellular sensitivity to chemotherapeutics, cisplatin and 5-fluorouracil (5-FU), and radiotherapy.

Results

Of the 742 miRNA analysed in the pre-treatment biopsy samples, from neo-CRT responders and non-responders, 67 miRNA were differentially expressed. Of the 67 differentially expressed miRNA, miR-330 and miR-187 were both downregulated in non-responders (Figure.1). MiR-330 was the most downregulated miRNA in non-responders of the patient cohort. *In vitro* miR-330 overexpression and silencing significantly altered signalling pathways associated with resistance but did not alter clonogenic sensitivity to cisplatin or 5-FU at the doses tested (Figure.2). In the isogenic radioresistance model, miR-187 was also downregulated and reconstitution of expression resensitised cells to radiation (Figure.3).

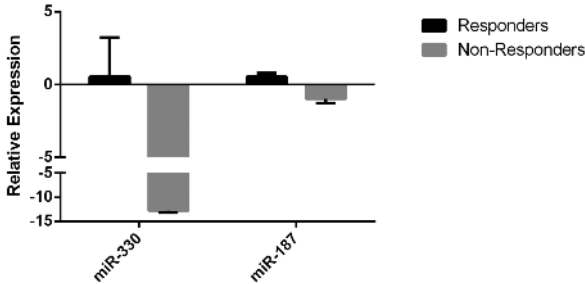


Fig.1 miR-330 and miR-187 are downregulated in OAC patients who do not respond to neo-CRT. Of the 67 differentially expressed miRNA between responders and non-responder, miR-330 was the most downregulated miRNA in non-responders in the OAC patient cohort.

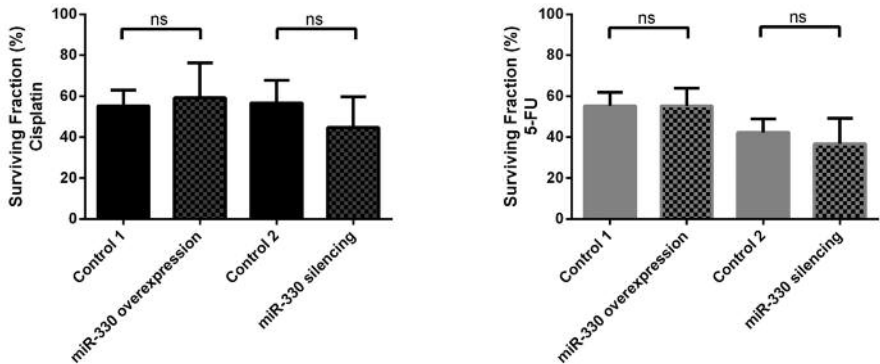


Fig.2 Overexpression and endogenous silencing of miR-330 in the OE33 cell line does not alter cellular sensitivity to chemotherapy. OE33 cells were transfected with a scrambled control plasmid (Control 1) or a plasmid encoding the miR-330 precursor sequence (overexpression). Similarly, OE33 cells were transfected with a scrambled control plasmid (Control 2) or a plasmid encoding the anti-sense miR-330 sequence (silencing). Transfected cells were subsequently seeded (following density optimisation) for clonogenic assays and treated with chemotherapeutics or the relevant vehicle control (cisplatin vs. PBS and 5-FU vs. DMSO). The surviving fraction of cells treated with cisplatin or 5-FU was calculated relative to the vehicle control treated cells (the surviving fraction of vehicle control cells was normalised).

to 100%, data not shown on the graph). Surviving fraction is calculated as [average number of colonies/(cell seeding density × plating efficiency)]. There is no significant alteration in OE33 cellular sensitivity to chemotherapy with miR-330 overexpression or silencing compared to the relevant transfected control (Control 1 and 2, respectively). Not significant= ns.

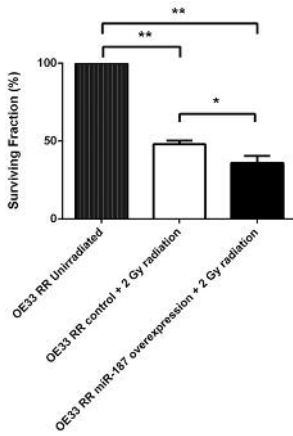


Fig.3 Restoring miR-187 in the radiation resistant OE33 cell line resensitised the cells to radiotherapy. OE33RR cells were transfected with a scrambled control plasmid (control) or a plasmid encoding the miR-187 precursor sequence (overexpression). Transfected cells and non-transfected cells were subsequently seeded (following density optimisation) for clonogenic assays and treated with 2 Gy radiation or mock irradiated. The surviving fraction of cells treated with radiation was calculated relative to the mock irradiated cells (the surviving fraction of unirradiated cells was normalised to 100%). Surviving fraction is calculated as [average number of colonies/(cell seeding density × plating efficiency)]. The overexpression of miR-187 in the OE33RR cells increased cellular sensitivity to radiotherapy ~12%. * $p < 0.05$ ** $p < 0.01$.

Discussion

In a pre-treatment setting we identified that OAC patients with downregulated miR-330 and miR-187 expression, prior to neo-CRT, did not respond to treatment. Furthermore, restoring miR-187 expression resensitised radioresistant cells to radiotherapy, suggesting miR-187 modulates cellular response and sensitivity to radiotherapy in OAC. The functional mechanism whereby miR-187 alters cellular response to radiotherapy is being further investigated, by identifying the mRNA targets and the signalling pathways modulated by miR-187. The expression of miR-330 was not downregulated in the radioresistant cells, therefore it was hypothesised that miR-330 downregulation was specifically modulating cellular response to chemotherapy. Although manipulation of miR-330 did not alter chemosensitivity *in vitro*, the downregulation of miR-330 in tumour cells may alter the tumour microenvironment and subsequently modulate sensitivity to treatment.

Conclusion

Here, we identify 67 miRNA which are differentially expressed between neo-CRT responders and non-responders. Furthermore, we identify miR-187 as a modulator of cellular sensitivity to radiotherapy. Hence, miR-187 downregulation in the tumours of patients prior to treatment may confer tumour cell resistance to the effects of radiotherapy. Although miR-330 does not alter cellular sensitivity to chemotherapy *in vitro*, in the broader context of the tumour microenvironment, miR-330 could alter tumour sensitivity to neo-CRT.

Summary

The standard treatment regimen for patients diagnosed with OAC is neo-CRT. Unfortunately, ~70% of patients demonstrate little or no response to neo-CRT. The differentially expressed miRNA between OAC responders and non-responders, identified here, are potentially biomarkers of treatment sensitivity

in patients. The most downregulated miRNA in non-responders is miR-330; future work will include further investigation of miR-330 in the context of the extracellular environment. Furthermore, we identify miR-187 as a regulator of cellular response and sensitivity to radiotherapy. Therapeutic replacement of miR-187 expression in patient tumours prior to neo-CRT may enhance tumour sensitivity to radiotherapy and improve patient outcome following neo-CRT.

References

- Dulak AM, Stojanov P, Peng S et al.: Exosome and whole genome-sequencing of esophageal adenocarcinoma identifies recurrent driver events and mutational complexity. *Nat Genet* 2013; 45(5), 478-486.
- Hummel R, Hussey DJ, Haier J. MicroRNAs: predictors and modifiers of chemo- and radiotherapy in different tumour types. *Eur J Cancer* 2010; 46(2), 298-311.
- Lynam-Lennon N, Reynolds JV, Marignol L et al.: MicroRNA-31 modulates tumour sensitivity to radiation in oesophageal adenocarcinoma. *J Mol Med* 2012; 90, 1449-1458.

FUNCTIONAL CHARACTERISATION OF THE ISOCITRATE 1 (IDH1) MUTATION IN GLIOMAS

Julia Biedermann

E-mail: julia.biedermann@mailbox.tu-dresden.de

Institut for Clinical Genetics, University of Technology Dresden, Dresden, Germany

Co-authors: K. Abou-El-Ardat, M. Conde, R. Wiedemuth, M. Peitzsch, G. Eisenhofer,
L.A. Kunz-Schughart, H.A. Temme

Tutors and Co-authors: Dr. med. Barbara Klink, Prof. Dr. med. Evelin Schröck

Introduction

Diffuse gliomas are the most prevalent brain tumors in adults and are presently incurable. According to the World Health Organization gliomas are graded I to IV depending on their histopathological and clinical characteristics [1]. While grade I gliomas are considered benign, grade IV glioblastomas (GBM) are the most aggressive tumor type and show a 2-year survival rate in less than 30 percent of the cases [2]. Better understanding of the mechanisms behind brain tumor development are therefore essential for novel therapy strategies. The most frequent mutation observed in low grade gliomas and therefrom derived GBMs is the substitution of arginine to histidine at position 132 of the enzyme isocitrate dehydrogenase 1 (IDH1 R132H) [3,4]. The heterozygous mutation is considered one of the first genetic alterations in the tumor cell and is thought to play a central role in glioma development. The wild type IDH1 is a cytoplasmic enzyme that converts isocitrate to α -ketoglutarate while reducing NADP⁺ to NADPH. In contrast, IDH1 R132H has a neomorphic enzymatic function and produces high amounts of 2-hydroxyglutarate (2-HG) while consuming NADPH [5]. The accumulation of 2-HG leads to inhibition of several α -ketoglutarate dependant enzymes resulting in genomic hypermethylation [6]. 2-HG is therefore considered to be an oncometabolite. Nevertheless, the accumulation of 2-HG alone cannot explain all observed phenomena in gliomas. For example, supraphysiological concentrations of 2-HG in corporal fluids can be observed in type I or type II D-2-hydroxyglutaric aciduria patients. Interestingly, no neoplastic disorders have been reported in these patients suffering from this disease [7]. Therefore, we aimed to investigate 2-HG independent mechanisms by which IDH1 R132H mutation contributes to gliomagenesis.

Methods

We have stably transduced three cell lines (GBM cell line U87, a primary patient-derived GBM cell line HT7606 and an immortalized astrocyte cell line SVGp12) with IDH1 c.395G>A cDNA using lentiviral vectors. Transduction success was validated on DNA, RNA and protein levels using Sanger sequencing, allele-specific PCR and Western blots respectively. Liquid chromatography-tandem mass spectrometry (LC-MS/MS) was performed to measure Krebs cycle metabolite concentrations. In order to find effects independent of 2-HG, we added the oncometabolite to empty vector controls. NADP⁺/NADPH quantification kits were used to determine the concentrations of this coenzyme. We measured cell proliferation with nonradioactive quantification assays.

Results

We confirmed the presence of IDH1 c.395G>A; p.R132H mutation in the cells transduced with the mutant variant of IDH1. As expected, levels of the oncometabolite 2-HG were strongly increased in the cells with the mutation compared to an empty vector control. Glutamate, α -ketoglutarate and subsequent Krebs cycle metabolites were down-regulated in all the cells transduced with IDH1 R132H compared to empty vector controls. No changes in Krebs cycle metabolites were observed when IDH1 wild-type cells were treated with 2-hydroxyglutarate. NADPH concentrations and NADPH/NADPt ratio significantly dropped in glioma cell lines after transduction with IDH1 R132H. There was no NADPH or NADPt depletion observed when empty vector cells were treated with 2-HG. On the other hand, the immortalized astrocytes transduced with IDH1R132H showed an increase in NADP⁺/NADPH levels. Interestingly, GBM cell line HT7606 and immortalized astrocytes transduced with IDH1 R132H showed a decreased proliferation *in vitro* 2D-cultures. GBM cell line U87 showed a significantly reduced proliferation in 3D spheroid cell cultures when expressing the mutant IDH1.

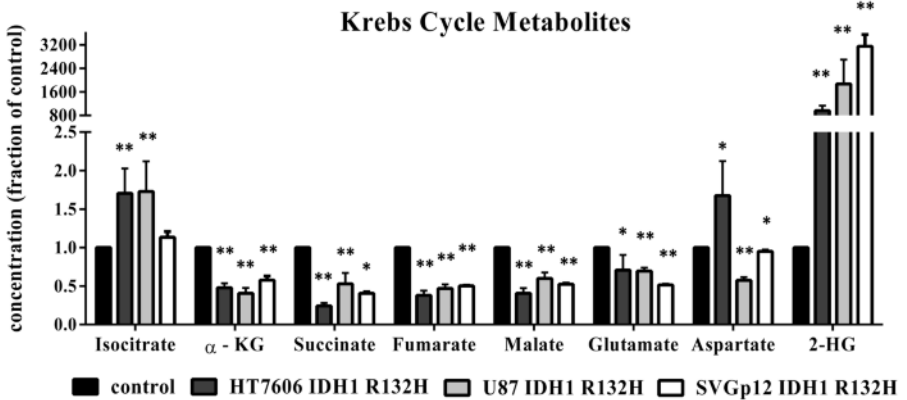


Figure 1: Concentrations of Krebs cycle metabolites were compared between empty vector controls and cells transduced with IDH1 R132H. Levels of isocitrate significantly increased, concentrations of glutamate, α -ketoglutarate and subsequent Krebs cycle metabolites decreased in cells with the IDH1 mutation. 2HG levels were up to 3400 fold increased in IDH1 mutant cells. (* $p < 0.05$, ** $p < 0.01$)

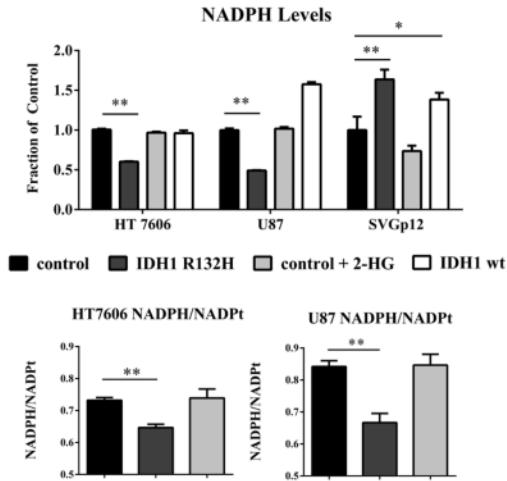


Figure 2: NADPH concentration and NADPH/NADPt ratio significantly dropped in glioma cell lines but not in immortalized astrocytes after transduction with IDH1 R132H. There was no NADPH or NADPt depletion observed when empty vector cells were treated with 2-HG. The immortalized astrocytes transduced with IDH1R132H showed an increase in NADPt. (* $p < 0.05$, ** $p < 0.01$)

Discussion and Conclusion

The mechanisms of how IDH1 R132H mutations contribute to gliomagenesis are still far from clear. The mutation is an early event and results in epigenetic changes that might lead to tumor progression. On the other hand, it is also known that patients with an IDH1 mutated tumor have a better prognosis compared to IDH1 wild-type tumors [8]. In line with this, we found that the IDH1 R132H mutation led to decreased Krebs cycle metabolites downstream of isocitrate compared to cells with wild-type IDH1. Cells with the IDH1 mutation displayed a shift in energy homeostasis and a decreased proliferation rate *in vitro*. These effects were independent of the elevation of the oncometabolite 2-hydroxyglutarate. The IDH1 mutation might have favorable and unfavorable effects on tumor progression and patient outcome [9]. In addition, some of the observed effects of the mutation appear to be dependent on the cell type. We observed an increase in NADPH levels in the immortalized astrocytes transduced with IDH1 R132H as opposed to the expected decrease seen in tumor cell lines. This, for the first time, shows that the redox homeostasis of non-cancer cells is affected differently by the mutation. Since the cell of origin of gliomas is not known and the IDH1 mutation could very likely occur in a non-transformed cell, the effects of the mutation could vary during gliomagenesis. Further studies with other possible tumor progenitor cells like neuronal stem cells could be valuable for understanding IDH1 mutations. We are currently analyzing the effect of IDH1 R132H and 2-HG on the transcriptome of our cell lines. Based on these profiles we aim to investigate possible genetic mechanisms behind the observations we have made.

Summary

The IDH1 mutation is considered to play a key role in glioma development. Due to the mutation, the oncometabolite 2-hydroxyglutarate (2-HG) accumulates in tumor cells. We were able to show 2-HG-independent effects of the mutation on three different *in vitro* models. The energy homeostasis, the redox-state as well as the proliferation were altered in IDH1 mutated cells but not in cells treated with 2HG.

References

- 1 Louis DN, Ohgaki H, Wiestler OD et al.: The 2007 WHO Classification of Tumors of the Central Nervous System. *Acta Neuropathol.* 2007; 114, 97–109.
- 2 Stupp R, Mason WP, van den Bent MJ et al.: Radiotherapy plus concomitant and adjuvant temozolomide for glioblastoma. *N Engl J Med.* 2005; 352, 987-996.
- 3 Yan H, Parsons DW, Jin G et al.: IDH1 and IDH2 mutations in gliomas. *N Engl J Med.* 2009; 360, 765–773.
- 4 Ohgaki H, Kleihues P: Genetic profile of astrocytic and oligodendroglial gliomas. *Brain Tumor Pathol.* 2011; 28, 177-183.
- 5 Dang L, White DW, Gross S et al.: Cancer-associated IDH1 mutations produce 2-hydroxyglutarate. *Nature* 2009; 462, 739–744.
- 6 Figueroa ME, Abdel-Wahab O, Lu C et al.: Leukemic IDH1 and IDH2 mutations result in a hypermethylation phenotype, disrupt TET2 function, and impair hematopoietic differentiation. *Cancer Cell* 2010; 18, 553–567.
- 7 Kranendijk M, Struys EA, Salomons GS et al.: Progress in understanding 2-hydroxyglutaric acidurias. *J Inherit Metab Dis.* 2012; 35, 571-587.
- 8 Parsons DW, Jones S, Zhang X et al.: An integrated genomic analysis of human glioblastoma multiforme. *Science* 2008; 321, 1807-1812.
- 9 Molenaar RJ, Jaroslaw TR, Maciejewski P. et al.: The driver and passenger effects of isocitrate dehydrogenase 1 and 2 mutations in oncogenesis and survival prolongation. *Biochim Biophys Acta.* 2014; 1846, 326-341.

PEPTIDERGIC SENSORY NERVES EXERT IMPORTANT REGULATORY ROLE IN EXPERIMENTAL ARTHRITIS

Balint Botz

E-mail: balint.botz@gmail.com

University of Pécs, Medical School, Department of Pharmacology and Pharmacotherapy,
Molecular Pharmacology Research Team, Pécs, Hungary

Co-authors: E. Borbely, T. Kenyer, K. Bolcskei, J. Csepregi, A. Mocsai, L. Kereskai

Advisor: Prof. Zsuzsanna Helyes M.D., Ph.D., D.Sc.

Introduction and aims

Rheumatoid arthritis (RA) is a chronic autoimmune disease characterized by progressive joint inflammation, persistent pain, and decreased life quality. It was traditionally considered as a solely immune-mediated disease, and the available treatment options focus mainly on these aspects. However, the potential impact of the nervous system via neuro-immune and neuro-vascular interactions has also been suggested [1-2]. Capsaicin-sensitive peptidergic sensory nerves express the Transient Potential Vanilloid 1 (TRPV1) ion channel that is activated by variety of irritants, such as capsaicin, as well as by several inflammatory mediators. Its permanent activation elicits massive calcium-influx into the nerve terminals resulting in a long-lasting functional impairment, therefore it offers an experimental approach to investigate their functions *in vivo*. These nerves are not only important as the primary afferents in somatic pain sensation (nociception), but they also possess potent efferent functions by releasing a range of anti/proinflammatory neuropeptide mediators [2] that regulate e.g. vascular tone and permeability, mast cells functions and leukocyte activity. Through the aforementioned pleiotropic effects these peptidergic nerves contribute to the formation of an inflammatory microenvironment, a process termed neurogenic inflammation [5]. The K/BxN serum-transfer arthritis is a disease-mimicking model of RA with translational relevance [5]. It is triggered by a systemic administration of autoantibodies resulting in a transient polyarthritis [6-8]. In the present study we investigated the role of the capsaicin-sensitive peptidergic sensory nerves in this model.

Methods

Peptidergic sensory nerves were defunctionalized by the ultrapotent capsaicin analog resiniferatoxin (RTX) [10] in 3-month-old C57Bl/6 mice, non-pretreated animals served as controls. Polyarthritis was induced by repeated ip. administration of 150-150 µl arthritogenic (K/BxN) or negative (BxN) serum with two days interval. The mechano- and thermonociceptive thresholds of the hindpaw were determined by plantar esthesiometry and hot-plate test, respectively. Joint function was assessed by grasping ability testing on a horizontal wire mesh grid. Ankle edema was evaluated by plethysmometry, disease severity by semiquantitative clinical scoring. The neutrophil-derived myeloperoxidase (MPO) activity in the inflamed joints was repeatedly measured by *in vivo* bioluminescence imaging using luminol, a compound that is selectively oxidized by MPO-derived free radicals. Matrix metalloproteinase (MMP) activity was assessed by fluorescence tomographic imaging of an enzyme-activatable selective agent (MMPsense 680) detecting the catalytic MMP-activity (MMP-2 -3 -9 and -13). Bone morphology around the tibiotarsal joints was evaluated by repeated micro-computer-tomographic (micro-CT) imaging, bone volume and density were quantified. A set of mice was sacrificed on day 10, and their

tibiotalar joints were homogenized to determine somatostatin-like immunoreactivity by radioimmunoassay [4]. At the end of the study the ankle joints were processed for histopathologic analysis. Semi-quantitative scoring was performed on the basis of 1) inflammatory cell infiltration, 2) synovial cell proliferation, 3) fibroblast count and the extent of collagen deposition [8].

Results

The ankle edema and clinical disease severity scores were considerably greater in the desensitized mice throughout the experiment (Fig. 1./a-b). In contrast, mechanical hyperalgesia was decreased in desensitized animals in the late phase of the experiment (from day 10 onwards), when compared to non-pretreated controls. Thermo-nociception was not altered in this model, although RTX-desensitized mice displayed consistently higher noxious heat thresholds (Fig. 1/c-d).

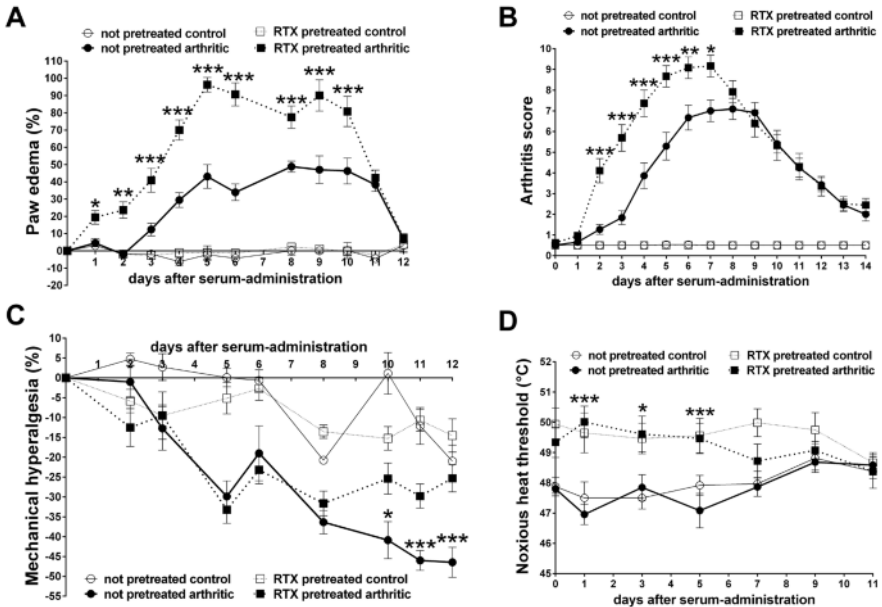


Figure 1. The change of functional parameters throughout the experiment. *A.* Hindpaw volume increase expressed as percentage of self control. *B.* Absolute values of the arthritis severity score (0-10). *C.* The decrease of mechanonociceptive threshold in percentage. *D.* The absolute values of noxious heat threshold. (mean \pm SEM, * p <0.05, ** p <0.01, *** p <0.001 vs. non-pretreated)

Consistent with these functional results, neutrophil MPO-activity was also greater in the diseased joint in the early phase (day 2), but not during the peak (day 6) of the experiment (Fig 2./a-c). Catalytic MMP activity increased dramatically in both groups following arthritis induction, being slightly greater in desensitized mice on day 5, but not in the later phase (day 8) of the study (Fig 2./b-d). The self-control assessment of bone structural imaging showed that female mice of both the control and RTX-pretreated groups displayed lower average bone mass than the age-matched males, thus these results were evaluated separately. Bone volume increased markedly around the joints of desensitized female mice, an effect which was not observed in the other groups (Fig. 2./d-e).

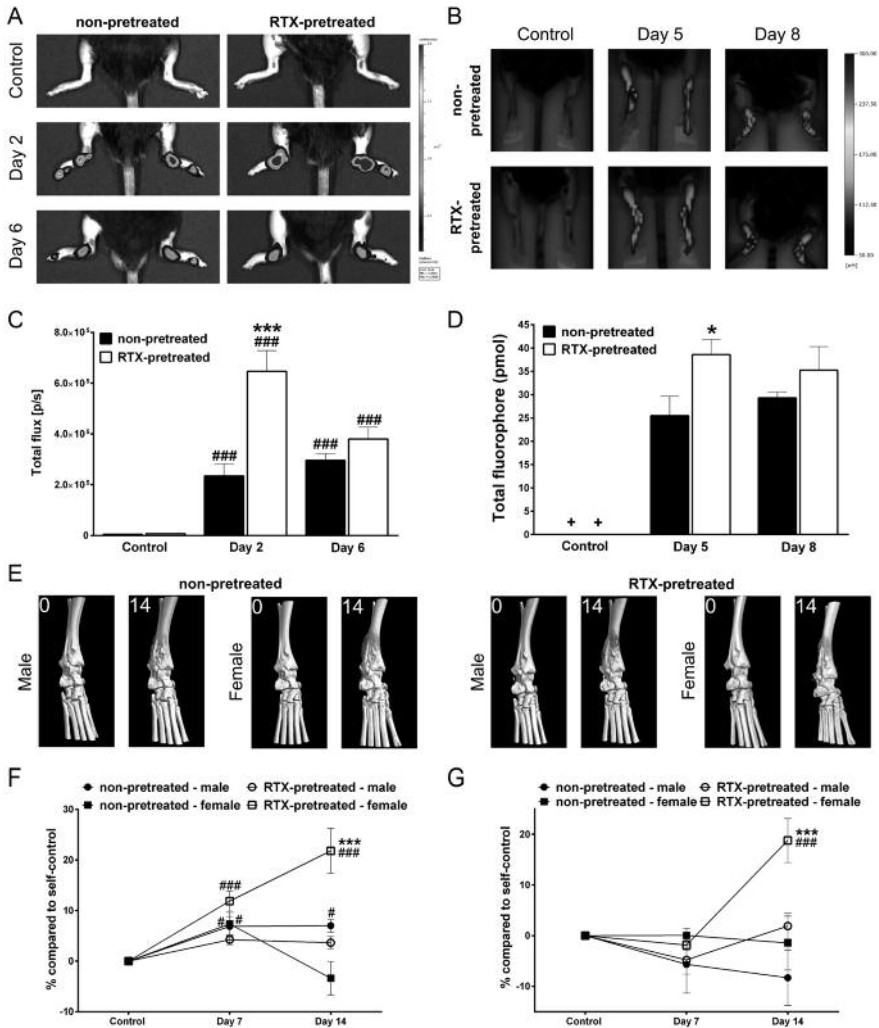
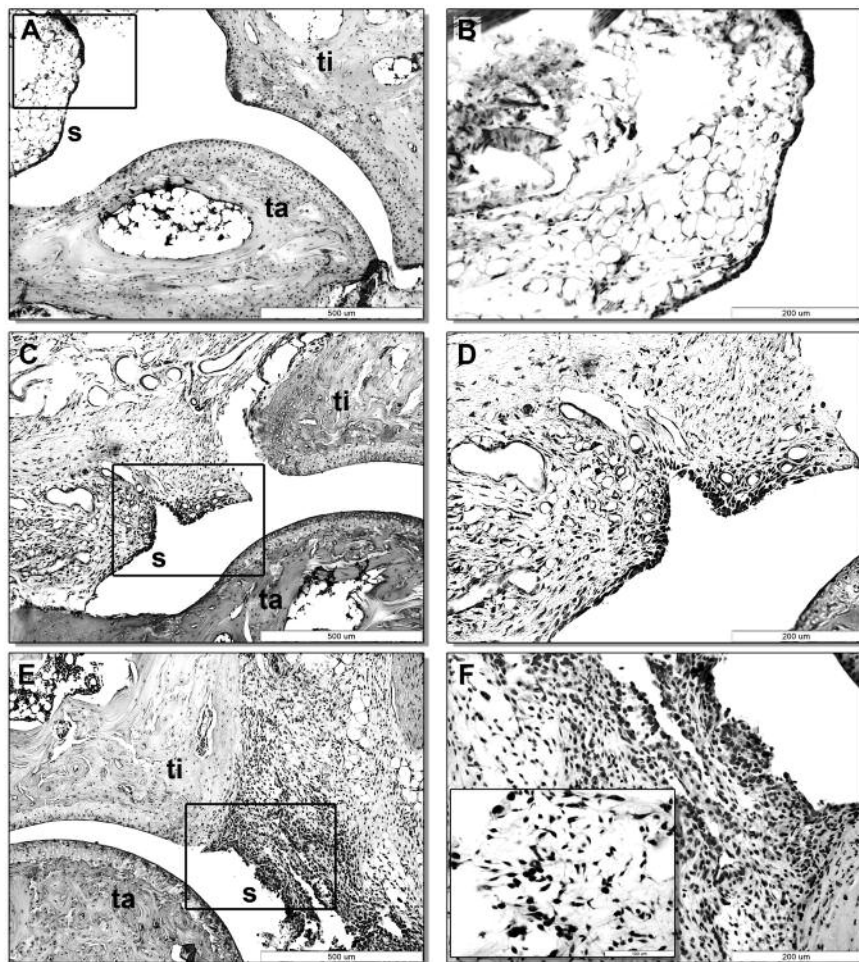


Figure 2. The change of inflammatory MPO- and MMP-activity, and periarticular bone structure. A-B. Representative images of the bioluminescence imaging of MPO-activity, and the fluorescence imaging of MMP-activity by MMPsense680 respectively. C-D. Quantification of luminal bioluminescence, and MMPsense680 fluorescence intensity in the ankle joints. E. Representative micro-CT images of the joints. F-G. Change of bone volume in the region of the tibiotarsal joint and in the periarticular region of the tibia. (mean \pm SEM, ### p <0.001 vs. controls, * p <0.05, *** p <0.001 vs. non-pretreated)

Histopathologic evaluation also revealed an increased structural damage in the joints of the RTX-pretreated mice measured by a composite arthritis score. Somatostatin-like immunoreactivity was considerably elevated in the joint homogenates of both non-pretreated and desensitized mice, being slightly greater in the former group (Fig. 3).



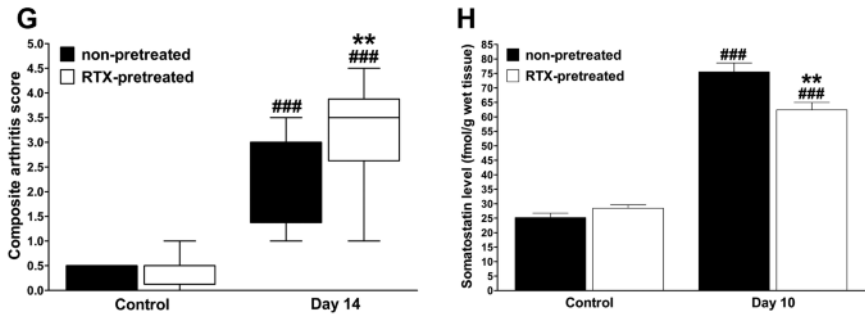


Figure 3. Histopathologic changes and somatostatin levels of the ankle joints. A-B. Representative microphotographs of an intact tibiotarsal joint (ti: tibia, ta: tarsus, s: synovium). C-D. The joint structure of a non-pretreated mouse on day 14 after arthritogenic serum administration. E-F. The significantly pronounced arthritic changes of RTX-pretreated animals. G.. Box plots representing the composite histopathologic scores. H. Somatostatin levels in ankle homogenates on day 10 (mean \pm SEM, ### p <0.001 vs. controls, ** p <0.01 vs. non-pretreated)

Discussion

The synovium and the articular capsule is densely innervated by peptidergic afferents, thus it has been hypothesized that their effect could be more substantial than simply conveying nociceptive signals to the central nervous system [1,4]. Increasing evidence suggests that selective modulation of these nerves might provide novel therapeutic approach in RA, offering a way to alleviate not only the pain, but also to ameliorate the progressive inflammation [1,3,4,6,8]. Our results prove, that these nerve terminals modulate chronic arthritis-related symptoms in a complex manner: their activation induces mechanical hyperalgesia, but inhibits edema formation and inflammatory cell functions leading to decreased inflammatory enzyme (MMP, MPO) activities. These sensory nerve endings also protect against the detrimental bone reorganization neof ormation during arthritis. Thermal hyperalgesia was absent in the model, however it is also atypical in RA. Nevertheless, we observed an increased noxious heat threshold in desensitized mice, which is a known effect of RTX. The decreased somatostatin levels in the joint homogenates after desensitization are in good correlation with the functional and in vivo imaging results, as it was previously found to alleviate arthritis in preclinical models, and also in human clinical trials [10]. It exerts not only analgesic, but also anti-inflammatory functions (e.g. by reducing MMP-expression). Thus, in our opinion, the increased disease severity of desensitized mice can be at least partially attributed to the lacking anti-inflammatory mediator-release from the peptidergic nerve terminals. As TRPV1 channels have been found to be expressed in various non-neural tissues as well (incl. immune cells), the potential effect of desensitization on these components has to be delineated by further investigations.

Conclusions

Capsaicin-sensitive peptidergic nerve endings are not only involved the development of arthritic pain, but they also attenuate the generation of inflammatory microenvironment and influence inflammatory cell activity through their locally released anti-inflammatory mediators (e.g. somatostatin), exerting an overall beneficial, protective role in inflammatory arthritis.

Summary

Our study using the K/BxN disease model of RA provided evidence that peptidergic nerve terminals represent an endogenous protective, disease-limiting mechanism, besides their known role in pain transmission. The reduced edema formation, neutrophil respiratory burst, and catalytic enzyme activity underlines the manifold influence exerted by these terminals and suggests their efferent activity as a mechanism of potential therapeutic implications.

References

1. Szabó Á, Helyes Zs, Sándor K, et al. Role of TRPV1 receptors in adjuvant-induced chronic arthritis: in vivo study using gene-deficient mice. *J Pharmacol Exp Ther* 2005; 314: 111–9.
2. Riol-Blanco L, Ordovas-Montanes J, Perro M, et al. Nociceptive sensory neurons drive interleukin-23-mediated psoriasiform skin inflammation. *Nature*. 2014;510:157-61.
3. Sousa-Valente J, Andreou AP, Urban L, et al. Transient receptor potential ion channels in primary sensory neurons as targets for novel analgesics. *Br J Pharmacol*. 2014; 171: 2508-27.
4. Helyes Zs, Szabó Á, Németh J, et al. Anti-inflammatory and analgesic effect of somatostatin released from capsaicin-sensitive sensory nerve terminals in Freund's adjuvant-induced chronic arthritis model of the rat. *Arthritis Rheum* 2004; 50: 1677–85.
5. Kouskoff V, Korganow AS, Duchatelle V, et al. Organ-specific disease provoked by systemic autoimmunity. *Cell*. 1996; 87: 811-22.
6. Kelly S, Chapman RJ, Woodhams S, et al. Increased function of pronociceptive TRPV1 at the level of the joint in a rat model of osteoarthritis pain. *Ann Rheum Dis*. 2013;doi: 10.1136/annrheumdis-2013-203413.
7. Stangenberg L, Burzyn D, Binstadt BA, et al. Denervation protects limbs from inflammatory arthritis via an impact on the microvasculature. *Proc Natl Acad Sci U S A*. 2014; 111:11419-24.
8. Botz B, Bölcskei K, Kereskai L, et al. Differential regulatory role of pituitary adenylate cyclase-activating polypeptide in the serum-transfer arthritis model. *Arthritis Rheumatol*. 2014; 66: 2739-50.
9. Szolcsanyi J, Szallasi A, Szallasi Z, et al. Resiniferatoxin: an ultrapotent selective modulator of capsaicin-sensitive primary afferent neurons. *J Pharmacol Exp Ther*. 1990; 255: 923-8.
10. Imhof AK, Glück L, Gajda M, et al. Differential antiinflammatory and antinociceptive effects of the somatostatin analogs octreotide and pasireotide in a mouse model of immune-mediated arthritis. *Arthritis Rheum*. 2011; 63 :2352-62.

DEVELOPMENT OF A PET RADIOTRACER FOR ANGIOGENESIS IMAGING IN CANCER

Kayleigh L. Brocklesby^{1,2}

E-mail: hyklb@hyms.ac.uk or kayleigh.brocklesby@icr.ac.uk

¹School of Biological, Biomedical and Environmental Sciences, University of Hull, Hull, United Kingdom,

²Radiotherapy and Imaging, The Institute of Cancer Research, London, United Kingdom

Tutor: Jennifer S. Waby (PhD)¹ and Graham Smith (PhD)²

Background

Angiogenesis is the development of blood vasculature from a pre-existing network, in response to a critical deficiency in the nutrient supply and is key for cancer development and metastasis.¹ Models of cancer progression demonstrate the core of solid tumours is hypoxic, owing to their avasculature nature. This forces the tumour to activate the angiogenic switch, driving the upregulation of pro-angiogenic factors such as vascular endothelial growth factor (VEGF)¹. Indeed, it has been shown that poor prognosis is linked with overexpression and hyper-activation of the native VEGF pathway.² This hyper-activation can be exploited to allow positron emission tomography (PET) imaging of angiogenesis. PET imaging involves the use of positron emitting radionuclides, including fluorine-18, carbon-11, copper-64, gallium-68, zirconium-89 and iodine-124.³ Neutron poor PET radioisotopes decay by conversion of a proton to a neutron causing emission of a positron which travels a short range in matter before colliding with an electron, producing two γ -photons. These are detected and used to generate an image for quantitative interpretation of disease status, without the need for repeated biopsies (Figure 1A). Current radioligands for imaging the VEGF pathway are based on VEGFA and the VEGFA mimic Bevacizumab, radiolabelled using zirconium-89 and copper-64.⁴ Small-molecule imaging of the VEGF pathway offers potentially easier access to radiolabelling precursors, improved pharmacokinetics for the radiotracer and with potential to use widely available fluorine-18 rather than expensive and difficult to source metal radioisotopes. Small-molecule VEGF imaging has, so far, focused on agents such as Sunitinib, a pan-kinase inhibitor with a poor specificity profile.⁵

Aims/Rationale

Upon binding of VEGF to its mitogenic receptor, VEGFR₂, receptor dimerization causes the exposure of an ATP binding pocket where a small-molecule can be used to block ATP binding and further downstream signalling. PET imaging could provide quantitative analysis of response to chemotherapy and, particularly, anti-angiogenic therapies. Given the lack of small-molecule VEGFR₂ radiotracers, this study aims to develop a library of VEGFR₂ specific receptor binding agents and evaluate these in relevant biological assays. A previous study using an indole-pyrimidine ether bridged core showed promising affinity and selectivity towards VEGFR₂.⁶ Using this as a basis, we wish to develop an appropriate candidate for radiolabelling with the radioisotope fluorine-18.

Methods

Chemistry/Synthesis: A library of nine compounds was synthesised and based on the following principles: cLogP values (<4), retention of VEGFR₂ affinity, selectivity and an easily incorporated motif for PET imaging.

Docking studies: Docking studies were used to confirm interactions predicted between the compounds and VEGFR₂. Docking was performed using Schrödinger Gold (2014-2) and visualised on Chemical Computing Group MOE (2013-8802).

MTS assay: Cell lines with no VEGFR₂ expression (HEK293-human embryonic kidney); low VEGFR₂ expression (HCT116-human colorectal carcinoma) and high VEGFR₂ expression (A549-human lung adenocarcinoma) were treated with 0-50µM concentrations of each compound. Following 24h treatment, effects on viability were examined using 3-(4,5-dimethyl-2-yl)-5-(3-carboxymethoxyphenyl)-2-(4-sulfophenyl)-2H-tetrazolium inner salt (MTS assay) as well as phenotypic assessment.

Immunofluorescence microscopy: HCT116, A549 and HEK293 cell lines were cultured with the IC₅₀ values of the candidates for 24h and being fixed for fluorescence microscopy and stained with 4',6-Diamidino-2-phenylindole (DAPI) to visualise the nuclear DNA to assess changes in mitosis or cell cycle.

Statistical analysis: All statistical analysis and dose-response curves were completed in GraphPad Prism 6, using an unpaired t-test. IC₅₀ values were calculated using log inhibitors vs normalised response curve.

Results

Chemistry/Synthesis: The library of nine compounds were synthesised with a minimum purity of 95% (1H/13C NMR and LCMS-Figure 1B)

MTS assay: Indicates compound 9 has the greatest affect, with phenotypic changes, on cell viability with an IC₅₀ of 60nM (HCT116) and 42nM (A549) respectively. This effect was not limited to VEGFR₂ expressing cell lines, and also observed in HEK293 cells.

Immunofluorescence microscopy: Fluorescence microscopy investigations clearly demonstrated HCT116 and A549 cell lines exhibited nuclei with fragmented DNA, which cannot be attributed to apoptosis.

Discussion

We synthesised a library of nine compounds, based around an indole-pyrimidine ether bridged core (Figure 1C) and interrogated their ability to affect cell proliferation in MTS assays. A direct consequence of VEGFR₂ inhibition is an arrest in cell proliferation, via the RAF/MEK/ERK pathway, with maintenance of metabolic activity.⁷ We therefore anticipated that cells expressing differing levels of VEGFR₂ would show a decrease in proliferation, to different degrees, when treated with our compounds. MTS results demonstrated the expected decrease in proliferation with IC₅₀ values in the nanomolar range for the lead compound 9 (42nM and 65nM, A549 and HCT116 respectively). To determine whether this was due to specific targeting of the VEGFR₂ receptor, we conducted further *in vitro* tests using HEK293 cell line which does not express VEGFR₂, similar decreases in cell proliferation was observed. This data demonstrates the decrease in proliferation is an off-target effect. Phenotypic changes were also observed which suggested the cells were undergoing apoptosis. This led to fluorescence microscopy to investigate nuclear DNA for changes in mitosis or in the cell cycle.

Fluorescence microscopy assays were conducted using HCT116 and A549 cell lines treated with the respective IC₅₀ values of 1, 5 and 9 (Figure 2). In apoptotic cells, the chromatin is condensed inside the nucleus before being broken down into well-organised fragments. Surprisingly, we discovered the cell lines were not undergoing an apoptosis-like death mechanism. We observed the cells being multi-nucleated, evidence of an arrest in mitosis during chromosome segregation, which is not a characteristic of apoptosis. Such off-target effects confirm this class of inhibitors lacks the necessary specificity for PET imaging to sit in many similarly conserved kinases. This can be attributed to the limited predicted interactions with the ATP binding site of VEGFR₂ (Figure 3). Since tyrosine kinase ATP pockets are known to be relatively conserved, this could allow the indole portion of the compounds.

Conclusions

The library of nine compounds was interrogated for potential off-target effects, through the use of MTS, western blot and immunofluorescence assays. The results indicate that the compounds are not suitable for PET imaging, as indicated by unexpectedly low IC₅₀ values. Further immunofluorescent studies further highlight the unsuitability of the indole-pyrimidine ether bridged core, due to widespread off-target effects.

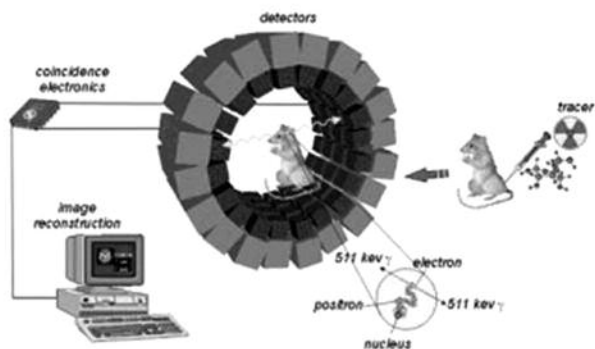
Summary

Blockade of VEGFR₂ activation can result in the arrest of cell proliferation, as well as decreased cell migration, survival and vascular permeability, thus preventing revascularisation of hypoxic tumour regions. PET imaging this process could ultimately allow for better patient stratification, with a hope to improve patient outcome. Previous studies of an indole-pyrimidine ether bridged core demonstrated promising properties of affinity and selectivity towards VEGFR₂. We focused our study around this core and designed a library of nine compounds; using cLogP values to aid library design and the incorporation of an easily radiolabelled prosthetic group. From the library of nine compounds, 9 had the greatest ability to affect cell viability in MTS assays. Further *in vitro* assays indicate this class of indole-pyrimidine ether bridged core are not selective for VEGFR₂ due to widespread toxicity, and therefore are not suitable for PET imaging agents. We are currently redesigning the compounds for greater specificity through the aid of a comprehensive literature search.

References

1. Hanahan, D.; Weinberg, R. A. Hallmarks of Cancer: The Next Generation. *Cell* 2011, 144, 646-674.
2. (a) Kaya, A.; Ciledag, A.; Gulbay, B. E.; Poyraz, B. M.; Celik, G.; Sen, E.; Savas, H.; Savas, I. The prognostic significance of vascular endothelial growth factor levels in sera of non-small cell lung cancer patients. *Respiratory Medicine* 2004, 98 (7), 632-636; (b) Salven, P.; Manpaa, H.; Orpana, A.; Alitalo, K.; Joensuu, H. Serum vascular endothelial growth factor is often elevated in disseminated cancer. *Clin. Canc. Res.* 1997, 3, 647.
3. Miller, P. W.; Long, N. J.; Vilar, R.; Gee, A. D. Synthesis of ¹¹C, ¹⁸F, ¹⁵O, and ¹³N radiolabels for positron emission tomography. *Angew. Chem. Int. Ed.* 2008, 47, 8898-9003.
4. (a) Chen, K.; Cai, W.; Li, Z.; Wang, H.; Chen, X., Quantitative PET imaging of VEGF Receptor Expression. *Mol. Imaging Biol.* 2009, 11, 15-22; (b) Cornelissen, B.; Oltenfreiter, R.; Kersemans, V.; Staelens, L.; Frankenne, F.; Foidart, J. M.; Slegers, G. *In vitro* and *in vivo* evaluation of [123I]-VEGF165 as a potential tumor marker. *Nucl. Med. Biol.* 2005, 32 (5), 431-6; (c) Gaykema, S. B.; Brouwers, A. H.; Hooge, M. N. L.-d.; Pleijhuis, R. G.; Timmer-Bosscha, H.; Pot, L.; van Dam, G. M.; van der Meulen, S. B.; Jong, J. R. d.; Bart, J.; Vries, K. d.; Jansen, L.; Vries, E. G. d.; Schroder, S. P. ⁸⁹Zr-bevacizumab PET imaging in primary breast cancer. *J. Nucl. Med.* 2013, 54 (7), 1014-1018.
5. Kuchar, M.; Oliveira, M. C.; Gano, L.; Santos, I.; Kniess, T. Radioiodinated sunitinib as a potential radiotracer for imaging angiogenesis—radiosynthesis and first radiopharmacological evaluation of 5-[¹²⁵I]iodo-sunitinib. *Biorg. Med. Chem. Lett.* 2012, 22 (8), 2850-2855.
6. Huang, S.; Li, R.; LaMontagne, K. R.; Greenberger, L. M.; Connolly, P. J. 4-amimopyrimidine-5-carbaldehyde oximes as potent VEGFR-2 inhibitors. Part II. *Bioorg. Med. Chem. Lett.* 2011, 21, 1815-1818.
7. Olsson, A.-K.; Dimberg, A.; Kreuger, J.; Claesson-Welsh, L. VEGF receptor signalling - in control of vascular function. *Nat. Rev. Mol. Cell Biol.* 2006, 7, 359-371.

A



B

Compound	Purity (%)
1	98.2
2	97.3
3	95.8
4	96.5
5	95.9
6	97.1
7	95.6
8	96.1
9	99.3

C

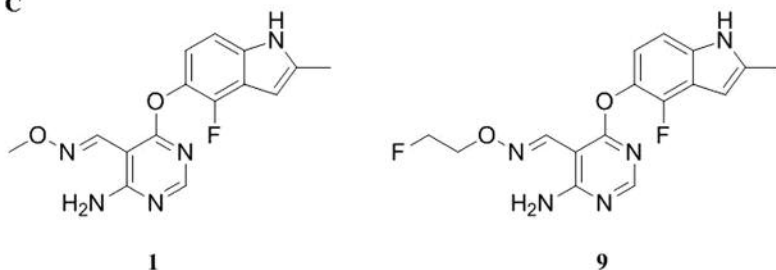


Figure 1. A) Schematic diagram representing the events in PET imaging, beginning with the annihilation of an electron emitted by the radionuclide ^{18}F , producing the two gamma rays which are detected by the ring of detectors. B) Purity of the compounds, according to LCMS (minimum required 95%) C) Schematic diagrams of the lead compounds 1 and 9.

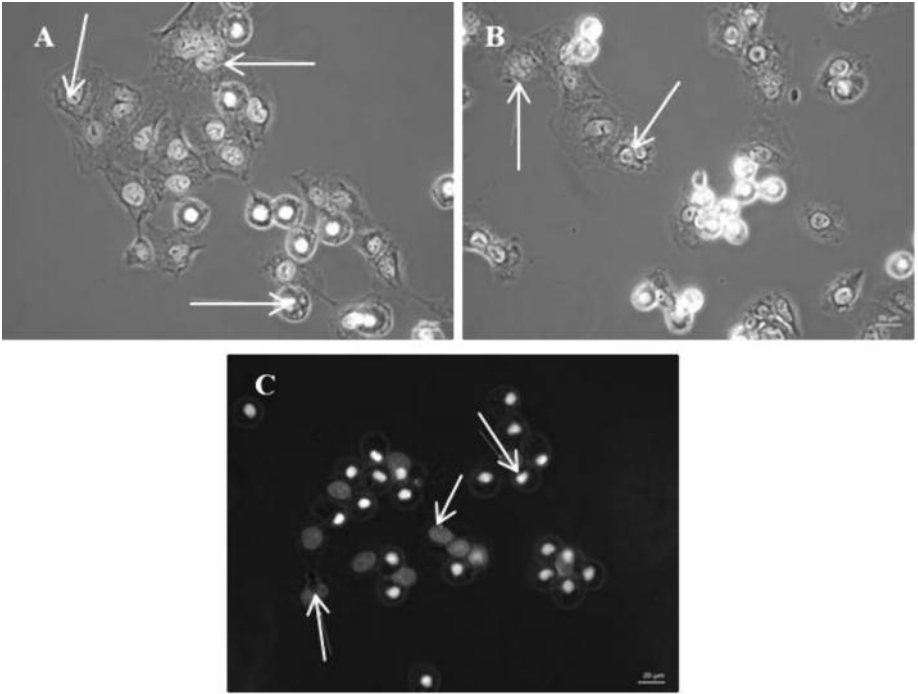


Figure 2: Fluorescence microscopy images with DAPI staining-white light merge, the arrows indicate multi-nucleated cells. A) A549 treated with 452nM of 1 B) A549 treated with 2358nM of 5 C) A549 treated with 66nM of 9.

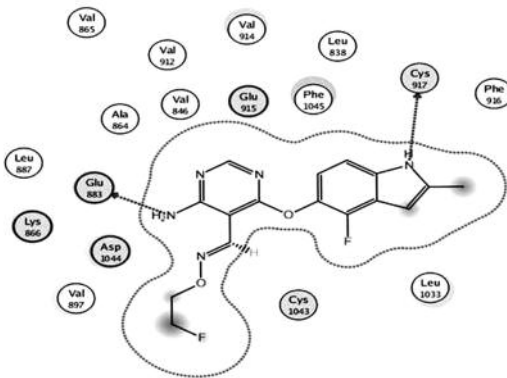


Figure 3. Predicted interactions between 9 and the VEGFR₂ ATP binding pocket. The dashed arrows indicate interactions with the specific residues, Cys919 and the amino group of 9.

HSP90 CLEAVAGE ASSOCIATES WITH OXIDIZED PROTEINS ACCUMULATION AFTER OXIDATIVE STRESS

José Pedro Castro

E-mail: josepedrocastro10@gmail.com

Department of Experimental Biology, Centre for Medical Research,
Faculty of Medicine, University of Porto, Portugal

Co-authors: Reeg S, Botelho V,

Supervisor: Henrique Almeida, MD, PhD

Co-Supervisor: Tilman Grune, MD, PhD

Introduction

To clear abnormal, mildly oxidized proteins, cells employ the 20S form of the proteasome [1]. However, if the rate of protein clearance is inferior to its formation, as occurs under oxidative stress (OS) additional oxidation results in the non-enzymatic irreversible process known as protein carbonylation and functional loss, and the promotion of protein aggregates formation and accumulation [2]. In Jurkat cells, stress promotes oxidized actin aggregates accumulation, impaired proliferation and reduced proteasome functioning, conditions frequently observed in cell senescence [3, 4]. As the heat shock protein 90, Hsp90, is a molecular chaperone that assists the degradation of oxidized proteins [5] and protects the proteasome from oxidative inactivation [6], it was hypothesized that Hsp90 functional impairment would jeopardize proteostasis under oxidative stress conditions. In fact, iron dependent Hsp90 cleavage was evidenced in the N-terminal motif, resulting in a 73kDa, less functional, fragment [7]. Therefore, we decided to verify whether Hsp90 cleavage would associate with Jurkat cells oxidized proteins accumulation during oxidative stress conditions.

Aims

To provide evidence that oxidized protein aggregates formation is associated with Hsp90 cleavage during oxidative stress.

Methods

Jurkat cells were cultured and submitted to oxidative stress by adding 100 μ M of hydrogen peroxide for 3h, 6h, 9h and 24h to the medium and comparing to 0h time-point. When employed, 500 μ M Desferoxamine (DFO) was used 18h before exposure. Cellular extracts, depending on the experiment were separated, by specific centrifuging conditions, in soluble (SF) or insoluble fractions (IF) and Western Blots with antibodies against Hsp90, Actin or LC3 proteins were employed. For protein aggregates detection, cells were fixed in PFA 4%, incubated with a specific protein aggregates fluorescent dye and visualized by fluorescence microscopy.

Results

Hsp90 cleavage occurs before actin accumulation (Fig 1A) and enhances oxidized actin degradation when compared to oxidized actin alone (Fig 1B), suggesting Hsp90 important role on oxidized proteins turnover.

Along time, proteasome inhibition and protein aggregate formation [3], which is primarily attributed Hsp90 cleavage, trigger autophagy. An important autophagic protein LC3-I is converted into LC3-II

and enhances its concentration at the insoluble fraction once protein aggregates are established (Fig 2). However, when Hsp90 cleavage was prevented by employing an iron chelator (DFO), aggregate formation and autophagy up-regulation were blunted (Fig 3), suggesting a role of Hsp90 cleavage as the chain of events precursor.

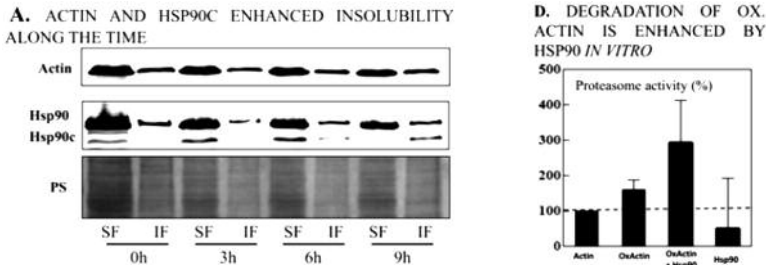


Figure 1. (A) Oxidative conditions promote Hsp90 cleavage, already evident at 3h. Hsp90c form remains in the cytoplasmic soluble fraction until 6h, when it shifts towards insolubility, which is notorious at 9h post stress. (B) In a cell free system, proteasome activity was measured after adding to the medium actin, oxidized actin, oxidized actin plus Hsp90 and Hsp90 only.

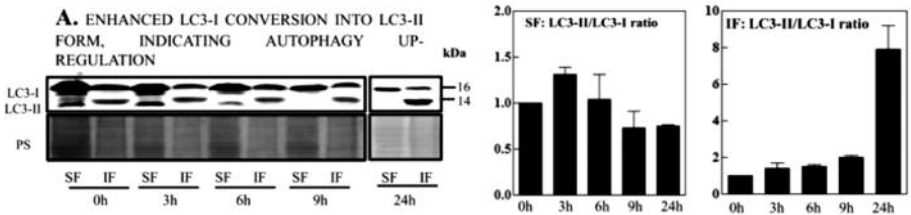


Figure 2. Data show that LC3-I conversion into LC3-II is time related, as evidenced by comparing 0h (basal) through 24h (stress time), and also shows that LC3-II shifts from the SF to the IF, suggesting its binding to the phagophore.

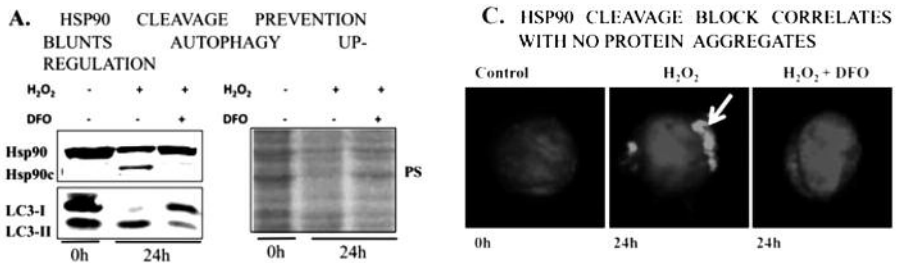


Figure 3. (A) DFO prevented Hsp90 cleavage (upper blot) and strongly inhibited the conversion of LC3-I to LC3-II (bottom blot); Ponceau S (PS) image is at the right. (B) Upon oxidative challenge, aggregates accumulate (red labeling, center image), which is prevented by previous DFO treatment.

Discussion

Hsp90 is able to degrade oxidized proteins but, when impaired due to oxidative cleavage, the process is blunted and can lead to oxidized protein accumulation into aggregates; these, in addition, can inhibit the proteasome and proliferation, important hallmarks of aged cells.

These features which range from Hsp90 cleavage to protein aggregates formation were observed in this Jurkat cell line and have a parallel with a previous report with in vivo primary T cell, whose changes were interpreted as consequent to immune cells ageing.

Conclusions

The study shows that Hsp90 is cleaved into a 73KDa form, the Hsp90c, by a non-enzymatic, time-related, iron and stress intensity dependent process. It reveals that cleavage appears early, progressively increases in the insoluble cytoplasmic fraction and later co-localizes with the actin aggregates. In addition, it demonstrates that autophagy is activated along the time, as evidenced by LC3-II protein increase in cellular extracts. Our model can represent, at least in part, what happens in vivo during senescence.

Acknowledgments

JPC was partially supported by COST Action CM1001: Chemistry of non-enzymatic protein modification-modulation of protein structure and function

Bibliography

- [1] Grune, T.; Reinheckel, T.; Davies, K. J. Degradation of oxidized proteins in mammalian cells. *The FASEB Journal* 11:526-534; 1997.
- [2] Nystrom, T. Role of oxidative carbonylation in protein quality control and senescence. *The EMBO journal* 24:1311-1317; 2005.
- [3] Castro, J. P.; Ott, C.; Jung, T.; Grune, T.; Almeida, H. Carbonylation of the cytoskeletal protein actin leads to aggregate formation. *Free Radical Biology and Medicine* 53:916-925; 2012.
- [4] Sitte, N.; Huber, M.; Grune, T.; Ladhoff, A.; Doecke, W. D.; Von Zglinicki, T.; Davies, K. J. Proteasome inhibition by lipofuscin/ceroid during postmitotic aging of fibroblasts. *FASEB journal : official publication of the Federation of American Societies for Experimental Biology* 14:1490-1498; 2000.
- [5] Whittier, J. E.; Xiong, Y.; Rechsteiner, M. C.; Squier, T. C. Hsp90 enhances degradation of oxidized calmodulin by the 20 S proteasome. *The Journal of biological chemistry* 279:46135-46142; 2004.
- [6] Conconi, M.; Petropoulos, I.; Emod, I.; Turlin, E.; Biville, F.; Friguet, B. Protection from oxidative inactivation of the 20S proteasome by heat-shock protein 90. *The Biochemical journal* 333 (Pt 2):407-415; 1998.
- [7] Beck, R.; Dejeans, N.; Glorieux, C.; Creton, M.; Delaive, E.; Dieu, M.; Raes, M.; Leveque, P.; Gallez, B.; Depuydt, M.; Collet, J. F.; Calderon, P. B.; Verrax, J. Hsp90 is cleaved by reactive oxygen species at a highly conserved N-terminal amino acid motif. *PLoS ONE* 7:e40795; 2012.

HUMAN RECOMBINANT ALKALINE PHOSPHATASE (RECAP) IN THE TREATMENT OF SEPSIS AND SEPSIS-ASSOCIATED ACUTE KIDNEY INJURY

Vojtěch Danihel^{1,3}

E-mail: danihelv@fnplzen.cz

¹Ist Dep. of Internal Med., University and Teaching Hospital Plzeň,

²Dep. of Anaesthesiology and Intensive care, University and Teaching Hospital Plzeň,

³Biomedical Centre, Faculty of Medicine in Plzeň,
Charles University in Prague, Czech republic

Co -authors: MUDr. Lenka Valešová^{1,2}, MUDr. Jiří Chvojka, PhD.^{1,3}

MUDr. Jan Beneš, PhD.^{2,3}

Tutor: prof. MUDr. Martin Matějovič, PhD.^{1,3}

Introduction

Sepsis is the most common cause of acute kidney injury (AKI). Causal treatment is not available yet. The RecAP holds a therapeutic promise for the treatment of sepsis-induced AKI. However effectiveness of the RecAP has not been tested in preclinical models that represent the complex nature of human AKI in sepsis.

Aim

To evaluate the efficacy of the RecAP and to obtain better insights into the mechanism(s) of its action in a clinically relevant porcine model of sepsis-induced acute kidney injury.

Methods

Sixteen anesthetized, mechanically ventilated, and instrumented pigs. Twelve hours after inducing progressive sepsis with stercoral peritonitis, we randomly assigned them into 2 groups: control (n=8), RecAP (n=8, dose: 1000 U/kg i.v.). The following parameters were measured at the baseline and then at 12, 18, 24 and 36 hours since sepsis induction: systemic hemodynamics (including values from Swan-Ganz catheter in pulmonary artery), kidney global blood flow (Ultrasound Doppler probe), microcirculation and tissue oxygenation of renal cortex and medulla (Laser Doppler Flowmetry, Optic fluorescence), renal vein blood pressure, renal oxygen balance, parameters of systemic inflammation and oxidative stress. The animals were followed until 36 hours after randomization or until death, if earlier.

Results

Peritonitis-induced sepsis resulted in hyperdynamic, vasoplegic circulatory state. This hemodynamic phenotype was not affected by RecAP. Both groups of animals required comparable total dose of exogenous noradrenalin to maintain adequate blood pressure. Although the RecAP didn't ameliorate sepsis-induced systemic inflammation (plasma levels of cytokines), it made it possible to wean 50% of pigs from this vasopressors support compared to 20% animals in the control group. The RecAP didn't affect neither renal macrocirculatory and microvascular perfusion, nor renal function. The incidence of AKI was 12.5% in both groups.

Summary

The RecAP molecule didn't modify hemodynamic and renal phenotype of severe sepsis. Due to relatively low incidence of AKI no firm inference can be drawn regarding the effects of RecAP on global kidney function. Therefore, the molecular and cellular effects of the RecAP are currently analysed. Finally, the signal that RecAP-treated animals required less vasopressor support deserves further evaluation in more severe model of septic shock.

The project was supported by the Research Funding of Charles University (P36) and by European Fund for Regional Development CZ.1.05/2.1.00/03.0076

EARLY RESPONSES OF DENDRITIC CELLS INFECTED BY FRANCISELLA TULARENSIS

Ivo Fabrik

E-mail: ivo.fabrik@unob.cz

Institute of Molecular Pathology, Faculty of Military Health Sciences,
University of Defence, Hradec Králové

Co-authors: M. Link, A. Härtlová, P. Řehulka, J. Stulík

Tutor: RNDr. Pavel Řehulka, Ph.D.

Introduction

Francisella tularensis is a Gram-negative coccobacillus responsible for zoonotic disease tularaemia. It is highly infectious – only ten bacteria are sufficient to cause a severe disease in humans. *Francisella* infection strategy involves invasion of phagocytic cells, rapid escape from the phagosome and proliferation in the host cytosol. Bacteria are then disseminated into lymph nodes, spleen and other organs. As for other intracellular pathogens, Th1 adaptive immunity is indispensable for the control of the infection. However, in the case of *Francisella*, the response is delayed or even absent.

Dendritic cells (DC) are the most efficient antigen presenting cells which are responsible for the priming of naïve T cells. The process is controlled by DC instructive signals governing the type of adaptive response generated (e.g. Th1/Th2/Treg), which establishes DCs as important “decision mechanism” of adaptive immunity. As professional phagocytes however, DCs are susceptible to *Francisella* invasion. It was shown, that infected cells are not properly activated and do not undergo the maturation process; all of which is required for effective Th1 priming. Hence, DC-*Francisella* interaction may affect the fate of the whole infected organism.

DC activation by bacteria in general relies on innate immunity receptors aiming conserved pathogenic structures. Activation of these sensors on the cell surface leads to complex events, including rearrangements of plasmatic membrane and the ignition of kinase-mediated cellular signaling directed into the cytosol. The primary goal of this work was therefore to map changes in membrane raft proteome and phosphoproteome of DCs infected by *Francisella* during the first ten minutes after the infection. We hope the knowledge of early events will help to understand the reasons of an atypical behavior of infected DCs which could be of interest for development of more effective treatment or vaccines.

Methods

Bacterial strains – Virulent strain *Francisella tularensis* subsp. *holarctica* FSC200 and its attenuated *Adsba* mutant lacking gene for disulfide oxidoreductase DsbA were used in infection experiments.

Bone-marrow derived DC (BMDC) – Primary BMDCs generated from murine bone marrow were used as a host infection model. Isolated bone marrow cells were kept for 9 days in RPMI-1640 with 10% FBS in the presence of recombinant GM-CSF. On 9th day, about 80-85% suspension cells were CD11c⁺. For SILAC labeling (Stable Isotope Labeling by Amino Acids in Cell Culture), we developed a modified cultivation protocol yielding cells with proteome labeling efficiency $\geq 90\%$.

Isolation of membrane rafts proteome - Following infection, BMDCs were lysed in a lysis buffer containing 0.5% TX-100. Lysates were mixed with an equal volume of ice-cold 80% sucrose. The combined lysate was overlaid with 30% and 5% sucrose and centrifuged for 24 h at 150 000g at 4 °C. Membrane raft fraction, separated as a band between 30% and 5% sucrose, was collected and proteins were digested by trypsin.

Isolation of phosphopeptides – Infected BMDCs were lysed by 1% sodium deoxycholate by placing them into boiling water bath for 5 min. Whole-cell lysate digests were subjected to HPLC fractionation based on HILIC-retention mechanisms. Phosphopeptides from collected fractions were enriched by the incubation with TiO₂ microbeads.

LC-MS – Peptides were separated on C18 column by nano-scale LC system connected through nanospray with high-resolution mass spectrometer. Data were generated by cycling of MS and MS/MS scans. Precursors were selected dynamically from previous MS scan.

Results

Primary BMDCs were infected by *F. tularensis* subs. *holarctica* WT and its *AdsbA* mutant. The latter strain was used because of its ability to provide protection against WT *in vivo*; therefore inferring the priming of effective adaptive immune response. *In vitro* experiments confirmed these results as BMDCs infected by *AdsbA* strain upregulated costimulatory molecules CD80 and CD86. In contrast, WT-infected BMDCs phenotypically resembled unstimulated cells. To find if the differences in BMDC response toward WT/*AdsbA* strains could be tracked down to bacteria-cell interactions during the first contact, changes of BMDC membrane raft proteome and phosphoproteome in first 10 minutes post infection (p.i.) were analyzed and quantified by LC-MS-based shotgun proteomics employing SILAC quantitation approach. In brief, one group of cells was grown in unmodified medium; the other was grown in medium containing isotopically labeled amino acids, which were incorporated into the proteome. In experiment, one group of cells was infected and the second was left as a control. Cell lysates were subsequently mixed and digested and changes in proteome response were devised from ratio of light/heavy peptide signals in MS. Using this approach, we were able to identify and quantify 1297 proteins in BMDC membrane rafts (from tetraplicate; 12 upregulated and 12 downregulated in WT-infected BMDCs respectively, 14 upregulated and 13 downregulated in *AdsbA*-infected BMDCs respectively; 9 proteins differentially regulated between WT/*AdsbA*-infected BMDCs). In pilot study (one replicate) focused on phosphoproteome changes in infected BMDCs during the same time p.i., we identified and quantified 9522 phosphosites with localized position in a protein sequence.

Discussion

F. tularensis WT-infected BMDC did not undergo classical phenotypic maturation and these cells would be probably only poor naïve T cells stimulators. In agreement with *in vivo* behavior, *AdsbA* mutant strain was able to elicit upregulation of BMDC co-stimulatory molecules needed for effective antigen presentation. Our results suggest these opposite outcomes of DC infection might arise from very early (10 min) *Francisella*-DC interactions. There are several events which seemed to be common for both strains, e.g. probable activation of PI3K leading to recruitment of PIP3-binding proteins into membrane rafts together with increased activation of Akt/PKB. However, we noticed that WT and *AdsbA*-infected BMDCs differed in level of tyrosine phosphorylation. Although this conclusion is currently based only on one phosphoproteomic replicate, changes in membrane raft proteome support this finding as several proteins known to be substrates of tyrosine kinases were found to be differentially regulated in rafts of WT and *AdsbA*-infected BMDCs, respectively.

Conclusions

Although these results need to be verified by independent methods and carefully interpreted, it seems that *F. tularensis* tunes the cellular signalization of DC from the earliest moments of contact. It is plausible that this subtle, yet precise, modulation is the first step leading to loss of immunity-stimulating potential in DCs.

Summary

Francisella tularensis is highly virulent intracellular bacterial pathogen known for its ability to avoid effective adaptive response of host organism. Although the exact mechanism of immunosuppression is unknown, the most efficient antigen presenting cells – dendritic cells (DCs) – challenged by *Francisella* are only poorly activated and probably incapable to provide sufficient proinflammatory stimuli to naïve T cells. To find the initial events leading to DC indifference, we focused on the cellular signalization of DCs during the first ten minutes of interaction with *Francisella*. Attenuated $\Delta dsbA$ mutant *Francisella* strain conferring the protection against WT *in vivo* was used as a positive control. Changes in membrane raft proteome and phosphoproteome of infected DCs were analyzed by LC-MS-based shotgun proteomics employing SILAC quantitation technique. Overall, we were able to identify and quantify more than 1200 proteins in membrane rafts and more than 9500 phosphosites in DCs infected by *Francisella* WT/ $\Delta dsbA$. Combination of these results sets revealed some themes common for both bacterial strains; most notably pronounced features of Akt/PKB signaling. On the other hand, WT- and $\Delta dsbA$ -infected DCs differed in the regulation of signal transduction mediated by tyrosine phosphorylation. Future work will be dedicated to a deeper interpretation of data and to a validation by a different methodology.

References

- Sjöstedt A: Intracellular survival mechanisms of *Francisella tularensis*, a stealth pathogen. *Microbes Infect* 2006; 8, 561-567.
- Fabrik I, Härtlova A, Rehulka P et al.: Serving the new masters – dendritic cells as hosts for stealth intracellular bacteria. *Cell Microbiol* 2013; 15, 1473-1483.
- Straskova A, Pavkova I, Link M et al.: Proteome analysis of an attenuated *Francisella tularensis dsbA* mutant: identification of potential *DsbA* substrate proteins. *J Proteome Res* 2009; 8, 5336-5346.
- Fabrik I, Link M, Härtlova A et al.: Application of SILAC labeling to primary bone marrow-derived dendritic cells reveals extensive GM-CSF-dependent arginine metabolism. *J Proteome Res* 2014; 13, 752-762.
- Härtlova A, Link M, Balounova J et al.: Quantitative proteomics analysis of macrophage-derived lipid rafts reveals induction of autophagy pathway at the early time of *Francisella tularensis* LVS infection. *J Proteome Res* 2014; 13, 796-804.

PRIMARY CILIA INCIDENCE IN A MYOBLAST CELL LINE (C2C12)

Alžběta Filipová

E-mail: filipoal@lfhk.cuni.cz

Department of Medical Biochemistry, Faculty of Medicine in Hradec Králové,
Charles University in Prague

Co-authors: D. Diaz-Garcia, A. Bezrouk, D. Čížková, R. Havelek, J. Vávrová, M. Řezáčová
Tutor: Prof. Martina Řezáčová, M. D., Ph.D.

Introduction

The primary cilium (PC) is a sensory, solitary, non-motile microtubule-based structure that arises from the centrosome and projects from the surface of the majority of human cells. The presence of a primary cilium on the surface of a cell is transient, limited to the quiescent G1 (G0) phase and early S phase of the cell cycle. Primary cilia, typically 200-300 nm wide and 2-10 microns long are present on most vertebrate cell types [1]. A number of different pathologies are associated with compromised cell-to-cell contact and their microenvironment. Primary cilia are one of the organelles involved in this process [2].

Aims

In this study, we used an in vitro model to evaluate the effect of ionizing radiation on cilia incidence. Ionizing radiation promotes DNA double-strand breaks in the affected cells, how this affects cell interaction with their microenvironment, at primary cilia level, remains to be seen.

Methods

The myoblast cell line C2C12 was cultured in DMEM and incubated in a 5% CO₂ atmosphere at 37°C. Cells were irradiated 48 hours after plating using a ⁶⁰Co γ -ray source at a dose rate of 0,4 - 2 Gy/min. After irradiation, cells were incubated at 37°C/5% CO₂ according to the scheduled time (1, 3 and 6 days). Non-irradiated control cells were handled in parallel. C2C12 cells were starved under low serum conditions (0,5% FBS) during the predetermined time intervals (6, 12, 24, 48, 72 and 120 hours). Control cells (10% FBS) were analyzed at 72 hours after plating. WST-1 reagent was used to determine cells viability 72 hours after irradiation (2, 6, 10 and 20 Gy) and serum starvation (0,5% FBS). Cell cycle analysis was performed after treatment. Immunostaining was performed as follows: goat serum; anti-acetylated; anti-gamma tubulin; Cy3-conjugated donkey anti-mouse secondary; Alexa 488 conjugated donkey anti-rabbit secondary antibody. Transmission electron microscopy - Images were captured with Megaview G2 digital camera and iTEM software. The statistical analysis of differences between the groups was performed by the Student's t-test and P values of ≤ 0.05 were considered significant.

Results

In our experiments, the multiplication of primary cilia occurred after irradiation with a dose capable of inducing cell cycle arrest in G2 phase (20 Gy), while irradiation dose of 6 Gy, which leads to accumulation of the irradiated cells in G1 phase, only promotes formation of solitary cilia. This observation correlates well with previous findings that centrosome multiplication occurs during a prolonged G2 phase [3]. A significant number of ciliated cells was observed 1 day after the irradiation within the

whole dose range (2-20 Gy), with the highest PC incidence three days after the treatment as compared to non-irradiated cells. However, PC incidence (%) observed in cells exposed to doses of 2, 6 and 10 Gy was significantly lower than that observed in cells irradiated by 20 Gy. Further dynamic of primary cilia formation was evaluated only after 20 Gy dose and it was found that PC incidence remained significantly higher than in non-irradiated cells even at 6 days post-irradiation. Unexpectedly, multi-ciliated cells were also detected in irradiated cells. In 2-4 % of irradiated cells two or more cilia were detected 1 day after the irradiation. A further increase in the number of cells with multiple cilia was observed 3 days after irradiation by the doses of 10 and 20 Gy (15% and 35% of cells, respectively). Cell proliferation was inhibited after serum starvation stress, decreasing the number of cells in S phase after 24 h of starvation. Cell viability was not affected and apoptotic cells were not observed. The percentage of ciliated myoblasts increased significantly as soon as after 6 hours of serum starvation as compared with the control. The PC incidence increases further during starvation, peaking at 24 hours and reaching nearly 80%. Thereafter, the percentage of ciliated cells was increased for the remaining duration of the experiment (120 hours of starvation).

Discussion

Assembly and disassembly of primary cilium is closely tied up with centrosome duplication cycle, as the basal body is formed from the mother centriole. Under normal conditions, centrosome duplication occurs precisely once per cell cycle. During S phase the mother and daughter centriole disengage and each of them nucleates a procentriole. These procentrioles elongate and mature during late S and G2 phase. Thus duplicated centrosomes are tethered together. This tether provides a loose connection between the proximal ends of the two parental centrioles and is removed during late G2 phase to allow mitotic spindle formation [4]. It seems that the formation of primary cilium requires functional appendages of mother centriole as well as a mature pericentriolar matrix [5, 6, and 7]. However, irradiated myoblasts were not only fully capable of ciliogenesis, but also formed multiple primary cilia. Our findings are in agreement with that of Conroy et al., [6], who observed occasional multiple cilia on irradiated hTERT-RPE1 retinal epithelial cell line. These cilia seem to originate from a single ciliary pocket. These observations suggest that centrosome multiplication after DNA damage could be followed by multiple primary cilia formation.

Conclusions

Taken together we suggest that centrosome multiplication and formation of multiple primary cilia is a regulatory step involved in regulation of G2/M cell cycle arrest after DNA damage induced by ionizing radiation. Although our results seem to indicate that such strong stress threatening cell survival promotes a high ciliation rate in the treated cells, further study on these results still needs to be approached as the reason behind the increased cells' multi ciliation rate under ionizing radiation is not yet completely clear, and although it coincides with a high caspase activity, care must be taken before trying to establish any direct involvement between the two processes without further evidence indicating it. Though this work raises more questions than it answers, it hints at ciliation processes not yet studied and that further research will undoubtedly clarify.

References

- [1] Fry AM, Leaper MJ, Bayliss R (2014) The primary cilium: Guardian of organ development and homeostasis. *Organogenesis* 10(1):62-68.
- [2] Nigg EA, Stearns T (2011) The centrosome cycle: Centriole biogenesis, duplication and inherent asymmetries. *Nat Cell Biol* 13(10): 1154–1160.
- [3] Graser S, Stierhof YD, Lavoie SB, Gassner OS, Lamla S, Le Clech M, Nigg EA (2007) Cep164, a novel centriole appendage protein required for primary cilium formation. *J Cell Biol* 179(2):321-30.
- [4] Ishikawa H, Kubo A, Tsukita S, Tsukita S (2005) Odf2-deficient mother centrioles lack distal/subdistal appendages and the ability to generate primary cilia. *Nat Cell Biol* 7(5):517-24.
- [5] Moser JJ, Fritzler MJ, Ou Y, Rattner JB (2010) The PCM-basal body/primary cilium coalition. *Semin Cell Dev Biol* 21(2):148-55.
- [6] Conroy PC, Saladino C, Dantas TJ, Lalor P, Dockery P, Morrison CG (2012) C-NAP1 and rootletin restrain DNA damage-induced centriole splitting and facilitate ciliogenesis. *Cell Cycle* 11(20):3769-78.
- [7] Dodson H, Bourke E, Jeffers LJ, Vagnarelli P, Sonoda E, Takeda S, Earnshaw WC, Merdes A, Morrison C (2004) Centrosome amplification induced by DNA damage occurs during a prolonged G2 phase and involves ATM. *EMBO J* 23(19):3864-73.

WHAT FUNCTIONAL MAGNETIC RESONANCE IMAGING TELLS US ABOUT COMPLEX SHOULDER INSTABILITY

Anthony Howard

E-mail: Anthony.Howard@liverpool.ac.uk

Department of Translational Medicine, Liverpool University
Liverpool, United Kingdom

Co-authors: Hawkes, D; Gibson, J; Alizadehkhayat, O; Kemp, G

Tutor: Prof. Simon Frostick

Introduction

This study investigated the spectrum disorder of complex instability, which is a cluster of similar pathologies rather than a well demarcated condition. The focus was on the patient group with shoulder instability unrelated to either trauma or structural abnormalities, Polar Type III under the Stanmore Classification. [Lewis]

This group of patients has proved difficult to treat successfully, rehabilitation being the principal solution to atraumatic instability. [Anakwenze] Within our unit these patients have achieved reduced dislocations, improved range of pain free motion and strength through a rehabilitation program. The pathogenesis and etiology of complex shoulder instability remains unclear Recent work has explored the role of motor control in joint instability using functional MRI (fMRI) studies of the brain activation in the context of ankle disorders [Francis]; the present study applied this technique for the first time to shoulder conditions.

The physical manifestation of movement in terms of muscle activation and limb movement was also explored using electromyography and motion capture video (Figure 1), although this paper reports only the fMRI findings.

Method

The patients were defined as individuals with involuntary instability of the shoulder which had not been precipitated by trauma or associated with structural abnormalities. They were assessed by two senior clinicians independent of the study to confirm they were Polar Type III (Figure 2). Patients with Ehler-Danlos Syndrome or collagen abnormalities, and those who had undergone significant shoulder surgery or other surgery that would influence shoulder function were excluded from the study. Standard MR exclusions also applied. Age-matched controls with normal shoulder function were recruited. All subjects' structural brain scans underwent a radiological assessment.

The subjects completed the Weston Ontario Shoulder Instability Index [Kirkley], the Oxford Instability Shoulder Score [Dawson] and a Beck's depression Inventory.

Structural MRI was performed using a Siemens 3 tesla Trio MR system, while fMRI images were acquired on a Siemens 1.5 tesla Symphony MR system which allowed greater shoulder movement, without any loss of neuroanatomical specificity [Han] but with an acceptable loss of sensitivity [Beli]. The study paradigm was of a block design, which encompassed both forward flexion (40 degrees) and abduction (20 degrees). The movement cycle consisted of rest then a (randomized) movement of either forward flexion or abduction, being repeated 20 times (Figure 3). The subject received standardised instructions before the scan, and during scanning the instructions as to the required movement were communicated

by changing the colour of a light projected onto the scanner, seen by the subject through a mirror on the head coil. The subjects were observed during the scan to ensure the movement commands were accurately undertaken.

The fMRI data were analysed using Brain Voyager software (BrainVoyager, Maastricht) transforming the data into Talairach space. Comparisons between the patients and controls were undertaken using a General Linear Multiple Study Model, using Bonferroni correction with a False Detection Rate of < 0.05 . The cortical maps were converted to volumes of interest, with a cluster threshold of 300, with their coordinates and Brodmann areas calculated.

Results

Standard radiological assessment of structural brain scans revealed incidental findings (not communicated to the research team, but notified to the patients' family doctor in accordance with institutional research governance policy) in 3 patients, who were excluded from the study. Three further patients will be recruited and their data analysed prior to the presentation at the AAOS conference. The following are thus preliminary results and findings.

The mean age of the patient group ($n=13$) was 23 and the controls ($n=13$) was 24 years. In the patient group the mean Oxford Shoulder Instability Score (48 - normal) was 17.5 ; the mean Western Ontario Shoulder Instability Index (Worse 2,100) was 1164 and the mean Beck's Depression Inventory score was 12 (0-42). In the control group all the shoulder stability scores were normal, and the mean Beck's depression score was 3.2 (0-16).

The level of cortical activation of the patient group was significantly higher in terms both of the extent and level of activation. In the patient group there were 23 different clusters, compared to 13 in the control group, and the patient group had a 470% higher level of cortical activation overall. In both groups there were activations in Brodmann areas 4 (primary motor cortex), 10 (anterior prefrontal cortex), 13 (insular cortex), 40 (supramarginal gyrus), 44 (inferior frontal gyrus), the caudate head and putamen; there were additional activations in Brodmann areas 6 (premotor cortex), 7 (somatosensory association cortex), 24 (anterior cingulate cortex), 37 (fusiform gyrus) and 47 (inferior frontal gyrus). Further, overall there is a difference between the centers of gravity of the activation areas, with the patient group showed more disjointed multiple centers within the same Brodmann area.

Conclusion

This is the first fMRI study of patients with Polar Type III shoulder instability. This difference in cortical activation has previously not been established. The differences observed raise the possibility that cortical activation might be changed as part of the treatment of Polar Type III shoulder instability. Further analysis of the complete dataset is required before definitive conclusions can be drawn. Unique to the patient group cortical activations are the premotor cortex (Brodmann 6) and somatosensory association cortex (Brodmann 7). The pattern of activation in inferior frontal gyrus (Brodmann 47) was not seen in the control group. This area is responsible for (amongst other functions) inhibition of movement, and may have a role in shoulder instability.

This study shows the cortical activation patterns of the grey matter, in addition DTI scans have been undertaken, which will enable assessment of the white matter connections in the two groups.

Summary

The pathogenesis and etiology of complex shoulder instability remains unclear. In the absence of structural pathology, alterations in local muscle recruitment patterns may reflect a function of the behavioral context and brain activation patterns. Functional MRI (fMRI) enables the examination of specific cortical areas involved in the production and control of motor function. fMRI has not so far been applied to shoulder conditions.

Thirteen patients with atraumatic/non structural complex shoulder instability of Polar Type III2 (mean age 23 y) and 13 healthy controls (mean age 24 y) were studied in a Siemens Symphony 1.5 Tesla MRI scanner, undertaking a randomized sequence of forward shoulder flexion and abduction during fMRI. fMRI data were analyzed using Brain Voyager software with a General Linear Model (Brain Voyager, Maastricht).

The level of cortical activation of the patient group was significantly higher both in terms of the number of regions and level of activation. Further, overall there is a difference between the centres of gravity of the activation areas, the patient group showing more disjointed multiple centres within the same cortical area.

This is the first fMRI study of patients with Polar Type III Shoulder instability. The differences in cortical activation have previously not been reported. The results raise the possibility that cortical activation might be changed as part of the treatment of Polar Type III shoulder instability.

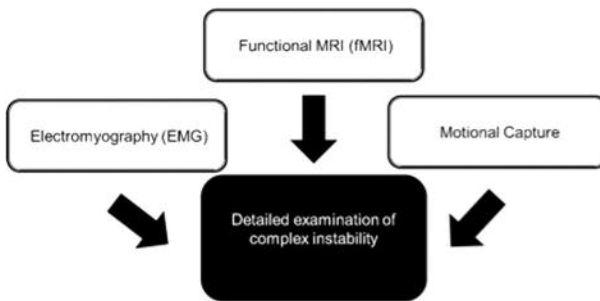


Figure 1 Diagram showing the three modalities employed to assess complex shoulder instability

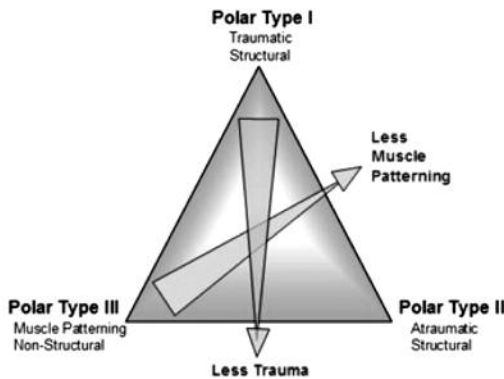


Figure 2 The Stanmore Classification of Shoulder Pathology



Figure 3 Illustration of the experimental setup in the 1.5T MR scanner

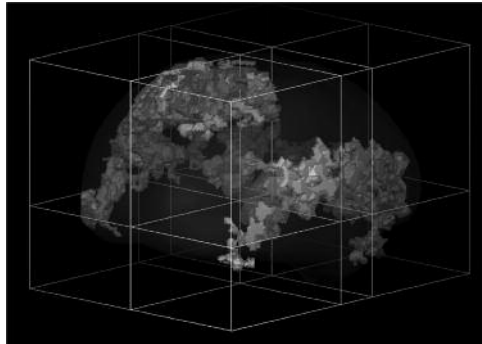


Figure 4 Multi-Subject General Linear Model of the Patient Group

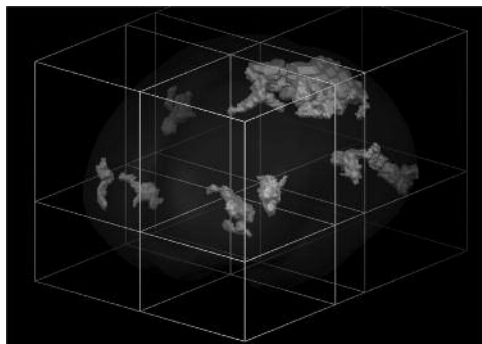


Figure 5 Multi-Subject General Linear Model of the Control Group

References

- Anakwenze, O.A. and G.R. Huffman, Evaluation and treatment of shoulder instability. *Phys Sportsmed*, 2011. 39(2): p. 149-57.
- Beli, K., et al., Comparison of fMRI activation at 3 and 1.5 T during perceptual cognitive, and affective processing. *NeuroImage*, 2003. 18: p. 813-826.
- Dawson, J., R. Fitzpatrick, and A. Carr, The assessment of shoulder instability. *Journal of Bone & Joint Surgery, British Volume*, 1999. 81-B(3): p. 420-426.
- Francis, S., et al., fMRI analysis of active, passive and electrically stimulated ankle dorsiflexion. *NeuroImage*, 2009. 44(2): p. 469-479.
- Han, K. and T. Talavage, Effects of combining field strengths on auditory fMRI group analysis: 1.5T and 3T. *J Magn Reson Imaging*, 2011. 34(6): p. 1480-1488.

PREDICTORS AND CLINICAL OUTCOME IN DECOMPRESSIVE HEMICRANIECTOMY FOR MALIGNANT MIDDLE CEREBRAL ARTERY INFARCTION

Robert Chrenko

E-mail: robertchrenko@gmail.com

Department of Neurosurgery, Landeskrankenhaus Wiener Neustadt, Wiener Neustadt, Austria
Faculty of Medicine, Comenius University in Bratislava, Slovakia

Co-authors: P. Novak, P. Slezák, P. Valkovič

Tutor: prof. MUDr. Juraj Šteňo, CSc.

Introduction

Life-threatening, space-occupying brain edema occurs in 1-10% of patients with a supratentorial infarct⁶. The prognosis for these space-occupying infarctions is poor, with case fatality rates of nearly 80%⁶. No medical treatment has been proven effective⁶. The cause of high mortality and morbidity is – apart from primary ischemic brain damage – often the development of secondary brain damage. This is caused by cytotoxic edema and subsequent intracranial hypertension (ICH)². Brain edema develops within 24-72 hours after the ischemic stroke, and can cause secondary infarcts through external vascular compression and lead to fatal brainstem compression³. The term malignant middle cerebral artery (MCA) infarction was originally defined as infarction of the entire MCA territory appearing on computed tomography (CT) scans within 48 hours, with or without infarction in other vascular territories². In fact, occlusion of either the distal internal carotid artery (ICA) or proximal MCA trunk has been characterized as a ‘malignant’ stroke in both clinical and animal studies⁸.

The surgical therapy using decompression hemicraniectomy (DHC) was previously evident to improve prognosis^{1, 4, 5, 6, 9} and is recommended as a standard therapy in selected patients with malignant MCA infarction nowadays^{7, 10}. However, decrease in mortality in operated patients is accompanied by a substantial increase in the number of functionally dependent survivors. This fact stimulates research efforts on how to further optimize the management of these patients in order to achieve improvements in the clinical outcome.

One way to achieve this goal is to exactly define the role of all the relevant predictive factors, and if appropriate to refine the criteria for surgical indication considering the role of these predictors.

Methods

This is a prospective consecutive monocentric observational study of 40 patients who underwent DHC for malignant MCA infarction at the Department of Neurosurgery at the Hospital of Wiener Neustadt in Austria during the period 2006-2012. The Department treats patients in the region of eastern Austria (Industrieviertel Niederösterreich and Burgenland) with a total of 780,000 inhabitants.

The baseline characteristics of the study population are summarized in Table 1. Selected clinical, radiological and laboratory parameters of each patient where associations with clinical outcome were anticipated were recorded according to protocol at the time of the discharge of the patient from hospital. The clinical outcome of each patient was assessed according to Barthel Index (BI) one year after the operation and recorded at that time. If the patient did not attend the follow-up examination, the clinical outcome according to BI was assessed by phone via the patient’s closest relative or caregiver. There were no patients lost of follow-up in this study.

Patients and interventions

Patients were indicated for surgery if they met the inclusion criteria as previously published⁴. If they met any of the exclusion criteria, surgery was not indicated⁴.

DHC with duraplasty was performed with the use of a dural patch, consisting of a commercially available dura substitute on the site of infarction as described⁴, and an intraparenchymal catheter to measure intracranial pressure (ICP) was inserted. Patients were postoperatively treated in the intensive care unit. A series of postoperative CT follow-up examinations was performed. After stabilization of the patient's clinical condition, they were treated in the neurosurgical or neurological department. Patients underwent intensive physiotherapy, which was continued in neurorehabilitation centers after their discharge from hospital. Reimplantation of autologous bone graft or acrylic bone substitute was performed after the resolution of the brain edema at an interval of several weeks after the operation. In selected cases the implantation of a ventriculoperitoneal shunt was indicated.

Statistical analysis

Bivariate associations between BI and continuous variables were assessed using Kendall's rank correlation coefficient tau-b. Robust linear regression (Theil-Sen estimator) was used to find a regression line presented in scatter plots. The Mann-Whitney U test was used to find relationships between BI and dichotomous variables. Multiple linear regression was then used to assess independent predictive values of the factors analyzed in the selected model. P-values less than 0,05 were considered statistically significant; all presented p-values are two-sided. Statistical analysis was performed using the statistical software StatsDirect 3.0,90, (<http://www.statsdirect.com>. England: StatsDirect Ltd., 2008).

Results

The results of the study are summarized in tables 1 - 2 and chart 1.

Number of patients	40
Gender (men:women)	23:17
Age [years]	56,3 (11,0)
Side (right:left)	22:18
Timing of surgery from symptoms begin [days]	1,7 (1,4)
Volume of infarction [ml]	376 (176)
Partial MCA : complete MCA : MCA + other	7:19:14
GCS preoperatively	11,2 (2,4)
Barthel Index - total; one year after surgery	41,6 (36,5)
Barthel Index - survivors; one year after surgery	59,5 (28,7)
Mortality; one year after surgery	12

Table 1 Baseline characteristics of the study population. (Values represent number at categorical variables and average (SD) at continuous variables).

PARAMETER	BIVARIATE ANALYSIS	MULTIVARIATE ANALYSIS	COMMENTS
Age	Tau-b= -0,32 P=0,006	r= -0,43 P=0,007	The most relevant and independent predictor
Volume of infarction	Tau-b= -0,24 P=0,04	r= -0,28 P=0,08	Relevant predictor, independence not evidenced
GCS preoperatively	Tau-b= 0,34 P=0,006	r= -0,21 P=0,20	Relevant predictor, independence not evidenced
Midline shift	Tau-b= -0,26 P=0,03	Not analysed (NA)	Relevant predictor, covariate of volume of infarction
S100B 1.postoperative day	Tau-b= 0,19 P=0,10	NA	
S100B peak postoperatively	Tau-b= 0,19 P=0,10	NA	
Timing of surgery	Tau-b= -0,06 P=0,63	NA	
Side	Mann Whitney P=0,61	NA	
Gender	Mann Whitney P=0,69	NA	
NSE 1.postoperative day	Tau-b= 0,04 P=0,70	NA	
NSE peak postoperatively	Tau-b= 0,04 P=0,44	NA	

Table 2 Patient-related parameters and their association with clinical outcome (BI) one year after surgery.

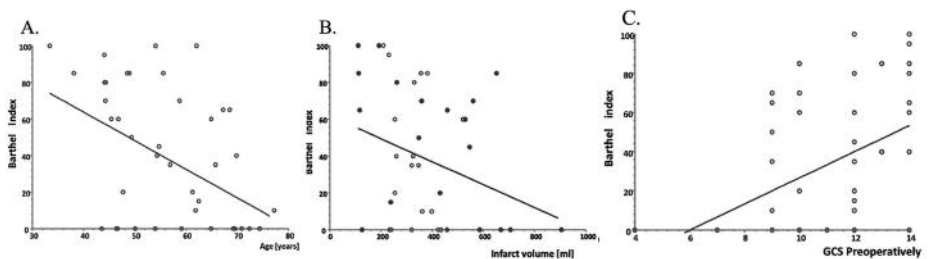


Chart 1 Non-parametric linear regression : A. between patient age and clinical outcome [BI], B. between volume of infarction [ml] and clinical outcome [BI] and C. between the preoperative level of consciousness [GCS] and clinical outcome [BI] .

Discussion

The study confirmed the highly relevant and independent predictive role of age. At the same time it also identified and exactly described the other relevant predictive factors such as volume of infarction and preoperative level of consciousness.

We assume that one of the ways to further improve the clinical outcome of patients with malignant MCA infarction can be to refine the criteria for surgical indication and – along with age – also consider the other relevant predictors. Decompressive surgery in patients up to 50 years of age is indicated given fulfillment of the standard recommended inclusion and exclusion criteria^{4,7,10}. However, in patients over 51, but especially those over 61 years of age, it seems to be advisable to restrict the criteria for surgical indication to patients with a limited volume of infarction and to patients with a favorable level of consciousness. Nevertheless, the surgical indication in patients over 71 years of age should be considered cautiously.

We assume that considering of predictor-based criteria for surgical indication can address decompressive surgery to patients with malignant MCA infarction more flexibly in order to improve clinical outcome and without an abrupt reduction in the number of candidates for surgery.

Conclusions

Age of the patient is rightly considered to be a principal indication criterion for decompressive surgery nowadays. However, we assume that in order to further improve clinical outcome it can be advisable to refine the criteria for surgical indication and – along with age – also consider the other relevant predictors, such as volume of infarction and preoperative level of consciousness.

Summary

We assume that DHC for malignant MCA has the potential to be not only a life-saving intervention but also an intervention that can further increase number of functionally independent survivors, when also considering – along with the age of the patient – the volume of infarction and preoperative level of consciousness as the criteria for surgical indication. At the same time we strongly emphasize that consideration of aforementioned criteria for surgical indication is not a definitive argument to exclude the other patients that does not meet these criteria from to be operated on. However, the exact knowing all the relevant predictors allows to inform these patients or their closest relative about the potentially less favorable prognosis and to decide pro- or contra-surgery in more appropriate manner.

References

1. Vahedi K, Vicaut E, Mateo J, et al.: (Sequential-Design, Multicenter, Randomized, Controlled Trial of Early Decompressive Craniectomy in Malignant Middle Cerebral Artery Infarction - DECIMAL Trial). *Stroke* 2007; 38, 2506-2517.
2. Hacke W, Schwab S, Horn M et al.: „Malignant,„ middle cerebral artery territory infarction: clinical course and prognostic signs. *Arch Neurol* 1996; 53, 309-315.
3. Wijdicks EF, Diringner MN: Middle cerebral artery territory infarction and early brain swelling: progression and effect of age on outcome. *Mayo Clin Proc* 1998; 73, 829-836.
4. Jüttler E, Hacke W: (Decompressive Surgery for the Treatment of Malignant Infarction of the Middle Cerebral Artery (DESTINY). A Randomized, Controlled Trial). *Stroke* 2007; 38, 2518-2525.
5. Hofmeijer J, Kappelle LJ, Algra A, et al: (Surgical decompression for space-occupying cerebral infarction (the Hemicraniectomy After Middle Cerebral Artery infarction with Life-threatening Edema Trial [HAMLET]): a multicenter, open, randomised trial). *Lancet Neurol* 2009; 8, 326–333.
6. Vahedi K, Hofmeijer J, Juettler E, et al.: (Early decompressive surgery in malignant infarction of the middle cerebral artery: a pooled analysis of three randomised controlled trials). *Lancet Neurol* 2007; 6, 215–222.
7. Veltkamp R, et al in Kommission "Leitlinien" der Deutschen Gesellschaft für Neurologie: [Akuttherapie des ischämischen Schlaganfalls.] Leitlinien für Diagnostik und Therapie in der Neurologie 09:1-17, 2012 (German)
http://www.dgn.org/images/stories/dgn/leitlinien/LL_2012/pdf/ll_22_2012_akuttherapie_des_ischmischen_schlaganfalls.pdf
8. Lanzino DJ, Lanzino G: Decompressive craniectomy for space-occupying supratentorial infarction: rationale, indications, and outcome. *Neurosurg Focus* 2000; 8(5), 1-7.
9. Gupta R, Connolly ES, Mayer S, Elkind MS: Hemicraniectomy for massive middle cerebral artery territory infarction: a systematic review. *Stroke* 2004; 35(2), 539-543.
10. Wijdicks EF, Sheth KN, Carter BS, Greer DM, Kasner SE, Kimberly WT et al.: Recommendation for the Management of Cerebral and Cerebellar Infarction With Swelling: A Statement for Healthcare Professionals From the American Heart Association/American Stroke Association. *Stroke* 2014; 45, 1222-1238

CIRCULATING MICROPARTICLES AS A MARKER OF ENDOTHELIAL DYSFUNCTION IN PATIENTS WITH CONTINUOUS-FLOW VENTRICULAR ASSIST DEVICES

Peter Ivák

E-mail: peter.ivak@ikem.cz

Department of Cardiovascular Surgery, Institute for Clinical and Experimental Medicine, Prague
Third Faculty of Medicine, Charles University in Prague, Czech Republic

Co-authors: J. Piřha, P. Wohlfahrt, I. Králová – Lesná, P. Stávek, Z. Dorazilová, J. Štěpánková,
J. Malý, M. Pokorný, and I. Netuka

Tutor: doc. MUDr. Ivan Netuka, Ph. D.

Introduction

Continuous left-ventricular assist devices (LVAD) for partial or full support of failing heart have together with heart transplantation become an important and leading therapeutic option for patients with end-stage heart failure.

Recently, LVAD are mostly used as a bridge to heart transplant, but the lack of donor organs and also design advancements and increasing reliability of LVAD are expanding possibilities of long-term use of these devices. Application of mechanical circulatory support continues to rise as permanent/destination therapy.

Generally, it is assumed that the presence of non-physiological continuous blood flow leads to higher stress of endothelial cells, and rises a concern of proatherogenic and prothrombotic changes in endothelium. Surprisingly, available data indicate that this flow pattern of significantly diminished pulsatility is well tolerated in short- and mid-term perspective. Studying long-term use of LVAD offers unique opportunity of better understanding the impact of continuous blood flow on vasculature.

Vascular endothelium plays key role in arterial wall integrity and blood flow regulation and recent studies showed that damage of endothelial cells, their activation and/or apoptosis leads to release of newly detectable biomarkers related to endothelial injury - a complex submicron membrane-shed vesicles called microparticles (MP).

Microparticles are anuclear fragments of cellular membrane shed from stressed or damaged cells, with a diameter of 0.1 to 1.0 μm . They contain surface proteins and cytoplasmic material of their parental cells. As possible end products of apoptosis of endothelial cells, circulating microparticles can act as a strong disregulators of endothelial function. The production of MP is believed to be a part of normal cell function but elevation of MP in coronary artery disease, stroke and in carotid artery disease, was well described in several studies and therefore microparticles may be associated with increased risk of major cardiovascular complications.

All these studies were performed in patients with physiological pulsatile flow, and only sparse data are available regarding the role of new potential prognostic cardiovascular risk factor - circulating MP in patients with end stage heart failure with continuous-flow LVAD. Almost no data are available describing effect of these devices on MP in short and long-term perspective. Therefore, the aim of our study was to assess the effect of the mechanical circulatory support on the concentration of circulating MP after 3, 6 and 9 months.

Methods

All the patients included in the study underwent LVAD implantation due to end stage heart failure and received axial continuous-flow device – HeartMate II (Thoratec Corp., Pleasanton, California). LVAD was implanted via sternotomy in standard fashion as a bridge to heart transplant in all patients.

Blood samples were collected from peripheral vein during 24–48 hours before and every 3 months after implantation. Circulating MP were measured in an audited lipid laboratory under continuous external quality control of CDC Atlanta, USA. The concentration of MP was determined by ELISA Zymutest MP activity test (Hyphen Biomed, France) and expressed as nanomoles per liter relative to phosphatidylserine (nM PS). The microparticles were measured in duplicate and the mean of two measurements was used for further analyses.

Institutional ethics committee approval has been obtained prior to the study initiation and all participants provided their signed informed consent.

Statistical analyses

Data are expressed as mean \pm SD, median (interquartile range-IQR), estimated marginal mean (95% confidence interval) or number (percentage). In graph estimated marginal mean and standard error of the mean (SEM) is plotted. Longitudinal changes in MP number were analyzed using generalized linear mixed-effect regression model. Because MP concentration was right-skewed, we used gamma regression. Calculations were done using SPSS 21 (IBM Corporation, NY, USA) and STATA. A two-sided p-value <0.05 was considered statistically significant.

Results

A total of 48 patients, 40 males and 8 females were included into the 9 month prospective study. Mean age of participants was 55 ± 10 years. Twenty eight patients were diagnosed with IHD and 20 with non-IHD as a cause of heart failure. Their baseline data are listed in Table 1.

In the whole group we observed a significant decrease of circulating MP before the implantation of LVAD and three months after the procedure [6.484 (95% CI 4.909-8.564) and 4.315 (95% CI 3.501-5.319), $p=0.023$]. Six months after implantation we observed again a drop in MP levels, but not statistically significant compared to levels before implantation [5.396 (95% CI 3.938-7.395) $p=0.234$]. Nine months after LVAD implantation levels of MP were significantly lower in compare to levels before implantation [3.081 (95% CI 2.386-3.980) $p=0.000$] (Figure 1). No significant differences in MP changes were detected between men and women and between patients with ischemic heart disease and patients of non-ischemic heart etiology of heart failure. In contrast, we observed smaller degree of MP decrease in smokers compared to non-smokers; these differences were of statistical significance ($p=0,039$) in third month after implantation.

Discussion

In our study we demonstrated that implantation of LVAD led to significant decrease of MP after 9 months irrespectively of the cause of heart failure. This finding may suggest improvement of endothelial function of patients treated by LVAD. Another potential explanation for significant drop of MP concentration is an overall improvement of organ perfusion and microcirculation by restoration of adequate systemic output less dependent on endothelial function. However, this favorable effect could be diminished in smokers.

Intensive research of MP and their function in several cardiovascular pathophysiological processes and also their potential role as biomarkers was conducted in recent years. Despite data indicating their importance, more information is required to confirm their clinical utility and role in improvement of management in this group of severely affected patients.

Conclusions

In conclusion, in a short term, LVAD exerted favorable effect on the vasculature, defined as decreasing number of circulating microparticles. If this effect is sustained for longer periods must be confirmed in long lasting longitudinal studies. Nevertheless, based on our recent results this laboratory method might compensate for some technical problems encountered in examination of the status of the vasculature by functional and morphological methods like ultrasound in patients with LVAD.

Summary

Left ventricular assist devices (LVAD), currently used in treatment of terminal heart failure, are working on principle of rotary pump, which generates continuous blood flow. Non-pulsatile flow is supposed to expose endothelial cells to potential damage. Therefore, we investigated longitudinal changes in concentration of circulating microparticles (MP) as a possible marker of endothelial damage before and after implantation of LVAD. Study population comprised 48 patients with end-stage heart failure indicated for implantation of the Heart Mate II LVAD. Concentrations of microparticles were measured as nanomoles per liter relative to phosphatidylserine before and every 3 months after implantation. After 9 months we observed significant decrease in concentration of MP compared to pre-implant status in the whole group; there was no difference observed between patients with ischemic etiology of heart failure (n=28) and with heart failure of non-ischemic etiology (n=20). These results indicate possibility that LVAD do not cause vascular damage 9 months after implantation. Whether these results suggest improvement of vascular wall function and of endothelium is to be definitely proved in long-term studies.

References

- Burger D, Touyz RM: Cellular biomarkers of endothelial health: microparticles, endothelial progenitor cells and circulating endothelial cells. *J Am Soc Hypertens* 2012; 6, 85-99.
- Diehl P, Aleker M, Helbing T, Sossong V, Beyersdorf F, Olchewski M, Bode C, Moser M: Enhanced microparticles in ventricular assist device patients predict platelet leukocyte and endothelial cell activation. *Interact Cardiovasc Thorac Surg* 2010; 11, 133-137.
- Ivak P, Pitha J, Wohlfahrt P, Kralova – Lesna I, Stavek P, Dorazilova Z, Stepankova J, Maly J, Pokorny M, Netuka I, Endothelial Dysfunction Expressed as Endothelial Microparticles in Patients with End Stage Heart Failure, *Physiol Res* 2014; Article in press
- Kirklin JK, Naftel DC, Pagani FD, Kormos RL, Stevenson LW, Blume ED, Miller MA, Timothy Baldwin J, Young JB: Sixth INTERMACS annual report: A 10,000-patient database. *J Heart Lung Transplant* 2014; 33, 555-564.
- Nascimbene A, Hernandez R, Geoge JK, Parker A, Bergeron AL, Pradhan S, Vijayan KV, Civitello A, Simpson L, Nawrot M, Lee VV, Mallidi HR, Delgado RM, Dong JF, Frazier OH: Association between cell-derived microparticles and adverse events in patients with nonpulsatile left ventricular assist devices. *J Heart Lung Transplant* 2014; 33, 470-477.
- Pitha J, Dorazilova Z, Melenovsky V, Kralova Lesna I, Stavek P, Stepankova J, Urban M, Maly J, Netuka I: The impact of ventricle assist device on circulating endothelial microparticles – pilot study. *Neuroendocrinol Lett* 2012; 33, 68-72.
- Schiro A, Wilkinson FL, Weston R, Smyth JV, Serracino-Inglot F, Alexander MY: Endothelial microparticles as conveyors of information in atherosclerotic disease. *Atherosclerosis* 2014; 234, 295-302.
- Singh N, Van Craeyveld E, Tjwa M, Ciarka A, Emmerechts J, Droogne W, Gordts SC, Carlier V, Jacobs F, Fieuwa S, Vanhaecke J, Van Cleemput J, De Geest B: Circulating apoptotic endothelial cells and apoptotic endothelial microparticles independently predict the presence of cardiac allograft vasculopathy. *J Am Coll Cardiol* 2012; 60, 324-331.
- Slavik L. Mikropartikule. *In vitro diagnostika* 2010; 16, 19-22. Article in Czech.

Williams JB, Jauch EC, Lindsell CJ, Campos B: Endothelial microparticle levels are similar in acute ischemic stroke and stroke mimics due to activation and not apoptosis/necrosis. *Acad Emerg Med*; 2007, 14, 685-690.

Acknowledgments

This study was funded by a grant of Ministry of Health of Czech Republic, IGA MZ NT/14019 – 3.

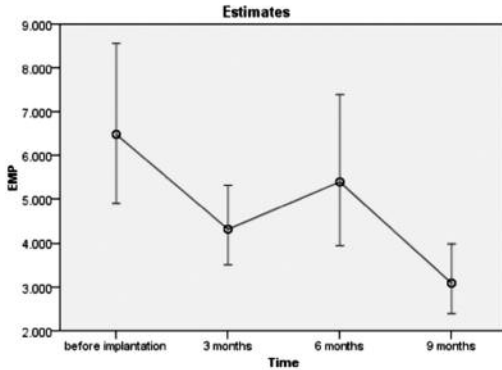


Figure 1

Longitudinal changes in circulating EMP number in patients treated by LVAD during 3, 6 and 9 months after implantation. (Estimated marginal mean and standard error of the mean). EMP – circulating microparticles

	Before implantation	month 3	month 6	month 9
n	48			
Age	55 ± 10			
Women (%)	8 (17%)			
Smokers (%)	12 (25%)			
Diabetes mellitus (%)	10 (21%)			
IHD etiology (%)*	28 (58%)			
BNP	1340 (668-2021)	337 (188-561)	304 (129-438)	336 (171 – 375)
Microparticles	6.5 [4.9 – 8.6]	4.3 [3.5 – 5.3]	5.4 [3.9 – 7.4]	3.1 [2.4 – 4.0]
Creatinine	114 ± 46	100 ± 39	102 ± 36	102 ± 27
CRP	21 (7-68)	21 (11 -29)	9 (5-20)	15 (7-20)
BMI	26.9 ± 4.6	25.8 ± 3.6	27.7 ± 4.1	29.7 ± 3.7

Table 1

Baseline data and laboratory results in 3rd, 6th, in 9th month. BNP – Brain natriuretic peptide; IHD – ischemic heart disease; CRP – C-reactive protein; BMI – Body mass index

BISPHOSPHONATE-RELATED OSTEONECROSIS OF THE JAW: A REVIEW OF 20 CASES

Zuzana Janovská

E-mail: zuzana.janovska@fnhk.cz

Department of Dentistry, Faculty of Medicine in Hradec Králové, Charles University
in Prague, and University Hospital in Hradec Králové

Co-authors: R. Mottl, R. Slezák

Tutor: doc. MUDr. Radovan Slezák, CSc.

Introduction

Bisphosphonates (BP) are inhibitors of bone resorption used mainly in the treatment of metastatic bone disease and osteoporosis. They prevent complications as pathological fracture, pain, tumor-induced hypercalcemia. Even though patient's benefit of BP therapy is huge, various side effects may develop. Bisphosphonate-related osteonecrosis of the jaws (BRONJ) is among the most serious ones. Oncologic patients receiving high doses of BP intravenously are at high risk of BRONJ development. BP impair bone turnover leading to compromised bone healing which may result in the exposure of necrotic bone in the oral cavity frequently following tooth extraction or trauma of the oral mucosa. Frank bone exposure may be complicated by secondary infection leading to osteomyelitis development [1]. No ideal treatment strategy of BRONJ has been found so far. Combination of conservative therapy aiming to reduce the symptoms and resective surgery may lead to complete recovery, provided that the procedure is correctly indicated [2].

Aims

The aim of this study was to analyse the authors' experience with BRONJ in 20 individuals.

Methods

A retrospective study of patients diagnosed and treated for BRONJ at the Department of Dentistry, University Hospital Hradec Králové during the period 2006 to 2013 was performed. Data collected and analysed were: age, gender, indication of BP therapy, type of BP and route of administration, localisation of osteonecrosis, triggering factor, type of treatment and results. Diagnosis of BRONJ was based on the results of clinical examination and radiological examination (ortopantomogram or cone-beam computed tomography). Definition and staging system published by the American Association of Oral and Maxillofacial Surgeons in 2009 has been used to determine the stage of the disease [3]. The treatment protocol consisted of antimicrobial mouth rinses (chlorhexidine, hexetidine, benzydamin) and systemic antibiotic treatment (amoxicillin, clindamycin) according to the stage of the disease. Additional surgical intervention – resection of necrotic bone with soft tissue closure in combination with systemic antimicrobial therapy was performed in two cases.

Results

During the years 2006 to 2013, BRONJ was diagnosed in 20 patients. The patients' age ranged from 43 to 84 years with a mean age 65 years. The male-female ratio was 2 : 18. Postmenopausal osteoporosis was the indication of BP administration in 11 patients, while 9 patients received BP for one of the

following oncologic diseases: renal cancer (1), breast cancer (6), multiple myeloma (2). All the oncologic patients were exposed to intravenous zoledronate as the most potent BP, whereas oral ibandronate has been most frequently used for the treatment of osteoporosis. The putative cause of BRONJ was tooth extraction in 15 cases, while in 2 cases it was a spontaneous occurrence and chronic denture trauma was the presumable triggering factor in 3 cases. Necrotic bone was most frequently found in mandible (13 patients), in 3 patients maxilla was involved, 4 patients manifested with osteonecrosis in both jaws. Complete healing defined as the absence of any mucosal breaches and exposed necrotic bone, absence of any signs of inflammation and absence of subjective complaints was achieved in 11 patients. Satisfactory healing was achieved in 3 patients. In these patients a small area of asymptomatic exposed necrotic bone up to 5 mm in diameter persisted. In 1 oncologic patient, rapid progression with the development of necrotic bone in all quadrants with severe complaints and slow sequestration process was noted. In 4 cases the therapy led to stabilisation of the disease with stationary extent of necrotic bone. In 1 case, the patient discontinued the treatment, therefore treatment results were not evaluated.

Discussion

BRONJ is a relatively rare complication which may negatively influence patients' oral health. Especially oncologic patients receiving high doses of intravenous BPs are at high risk of developing osteonecrosis. Management of the disease is a complicated task since no ideal treatment strategy has been suggested so far. Conservative treatment strategy leads to symptom reduction and decrease in the frequency of infectious complications. Surgical treatment approach with wide bone resection followed by primary soft tissue closure with pre- and postoperatively administered antibiotics may lead to complete healing. However BPs affect the whole jaw and surgical trauma to the bone could trigger progression of the osteonecrosis. Therefore, careful indication of resective surgery as well as accurate diagnostic procedure and preoperative assessment are necessary [4]. The patient's morbidity and life expectancy should be taken into account when planning surgical intervention. BRONJ seems to be a preventable complication to a certain degree since osteonecrosis is frequently a result of tooth extraction. Less often it may develop spontaneously or as a result of chronic trauma to the oral mucosa, often caused by ill-fitting dentures. Adverse effects and possible risks should be explained to the patient by the prescribing physician before the therapy onset and dental preventive measures should be taken. This requires adequate communication between the prescribing physician, the patient and the dentist [5].

Conclusion

From these data it was concluded that conservative approach in the treatment of BRONJ led to symptom regression but was not always curative. Surgical intervention, however, bears the risk of further progression of the osteonecrosis and must be carefully planned with respect to the patient's general health status and life expectancy. The treatment of BRONJ is generally difficult. Prevention plays a predominant role in the management of the this condition.

References

1. Patel V, McLeod NM, Rogers SN, et al. Bisphosphonate osteonecrosis of the jaws - a literature review of UK policies versus international policies on bisphosphonates, risk factors and prevention. *Br J Oral Maxillofac Surg* 2011;49(4):251-7.
2. Schubert M, Klatt I, Linek W, et al. The Saxon Bisphosphonate Register – Therapy and prevention of bisphosphonate-related osteonecrosis of the jaws. *Oral Oncol* 2012;48(4):349-54.
3. Ruggiero SL, Dodson TB, Assael LA, et al. American Association of Oral and Maxillofacial Surgeons position paper on bisphosphonate-related osteonecrosis of the jaws - 2009 update. *J Oral Maxillofac Surg* 2009;67(Suppl 5):2-12.
4. Ferlito S, Puzzo S, Palermo F, et al. Treatment of bisphosphonate-related osteonecrosis of the jaws: presentation of a protocol and an observational longitudinal study of an Italian series of cases. *Br J Oral Maxillofac Surg*. 2012 Jul;50(5):425-9
5. Bauer JS, Beck N, Kiefer J, et al. Awareness and education of patients receiving bisphosphonates. *J Craniomaxillofac Surg*. 2012 Apr;40(3):277-82

ANTI-ASTHMATIC EFFECTS OF POLYPHENOLIC COMPOUNDS IN ASTHMATIC ANIMAL MODEL

Ivana Kazimierová

E-mail: ivana.kazimierova@gmail.com

Department of Pharmacology, Jessenius Faculty of Medicine in Martin,
Comenius University, Slovakia

Co-authors: Lenka Pappová, Marta Jošková, Martina Šutovská, Soňa Fraňová

Tutor: doc. RNDr. Soňa Fraňová PhD

Introduction

Asthma is a chronic inflammatory disease of the airways characterized by airway hyper-reactivity, mucus hypersecretion and airway remodeling (Jung et. al., 2010). The aim of asthma treatment is to achieve symptom control and to minimize a risk of asthma exacerbation. New researches in the pharmacotherapy of asthma have demonstrated beneficial effects of polyphenols in treatment of allergic inflammation and its associated the symptoms. The aim of our study was estimated the long-term effect of polyphenolic compounds Provinol, Flavin7 and their combination with budesonide (1mM, inhalation) on experimental model of allergic asthma.

Methods

The experimental study was approved by the Ethical Committee of Jessenius Faculty of Medicine in Martin with number EK 1178/2012.

Guinea pigs were sensitized with ovalbumin (OVA) for 21 days, and simultaneously treated with Provinol (2mg/kg, p.o.), Flavin7 (2 ml/kg, p.o.), budesonide (1 mM during 5 min, nebulisation) and by half dose combinations of these substances. The airways defence mechanisms: cough reflex induced by citric acid aerosol (10^{-3} mol.l⁻¹) and specific airway resistance (sRaw) after histamine nebulisation (10^{-6} mol.l⁻¹) were assessed by in vivo method. Ciliary beat frequency was evaluated by „brushing“ method. Ciliary movement was recorded by BASLER camera. The levels of cytokines IL-4, IL-5 and IL-13 in serum and bronchoalveolar lavage fluid (BALF) were used as the inflammatory parameters and estimated by BioPlex method. Concentration of transforming growth factor - β (TGF- β) was evaluated from lung homogenates by ELISA method.

Results

The 21-day treatment of OVA sensitized guinea pigs with Provinol, Flavin7 and with their combination with budesonide caused a significant decrease the sRaw and suppression of cough reflex evaluated by in vivo method. In additional, combination Provinol+budesonide amplified the bronchodilatory and antitussive effect of substances used in monotherapy on the 21th day of measurement. After 21day of sensibilization, animals were sacrificed and was investigated the ciliary beat frequency. Tested substances modified the ciliary movement frequency on physiological values (Tab.1).

	control	OVA	PROVINOL	PROVINOL + BUDESONIDE
sRaW (ml/s)	9,55±0,47	29,52±2,43 ###	5,31 ± 1,28 ***	0,18 ± 0,05 ***
COUGH	5,33±1,04	9,17 ± 0,7 ##	4,77 ± 0,74 **	2 ± 1,03 ***
CILIARY BEAT FREQUENCY (Hz)	8,75±0,2	9,46 ± 0,35 #	8,28 ± 0,59 *	8,43 ± 0,41 *

	FLAVIN 7	FLAVIN 7 + BUDESONIDE	BUDESONIDE
sRaW (ml/s)	15,25 ± 2,7 **	18,9 ± 3,7 *	3,94 ± 0,57 ***
COUGH	4 ± 0,68 ***	4,67 ± 0,92 **	3,17 ± 1,05 ***
CILIARY BEAT FREQUENCY (Hz)	8,4 ± 0,39 *	10,14 ± 0,59	9,34 ± 0,42

Tab.1: The effect of Flavin7, Provinol and their combination on airway defense mechanisms. Data are expressed as the mean ± SEM; # $p < 0,05$, ## $p < 0,01$, ### $p < 0,001$ (control vs. OVA); * $p < 0,05$; ** $p < 0,01$, *** $p < 0,001$ (OVA vs. test substances).

Our results also confirmed the anti-inflammatory as well as anti-remodeling effect of polyphenolic compounds. Provinol, Flavin7 and their combinations with budesonide inhibited levels of IL-4, IL-5 and IL-13 formed by Th2 lymphocytes. These substances also significantly decreased a concentration of remodeling factor TGF- β in lung tissues (Tab.2).

			CONTROL	OVA	PROVINOL
Anti-inflammatory effect	SERUM	IL-4	0,65 ± 0,13	1,31 ± 0,13 ##	0,66 ± 0,14 **
		IL-5	0,72 ± 0,28	1,89 ± 0,36 ##	0,62 ± 0,2 ***
		IL-13	0,15 ± 0,13	3,75 ± 0,59 ####	2,5 ± 0,001
	BALF	IL-4	0,17 ± 0,04	2,03 ± 0,57 ##	0,22 ± 0,04 **
		IL-5	0,37 ± 0,08	1,53 ± 0,43 ##	0,55 ± 0,04 *
		IL-13	0,72 ± 0,09	3,58 ± 0,88 ##	2,01 ± 0,4
Anti-remodeling effect - TGF-β (pg/ml)			192,16 ± 77,95	459,86 ± 97,65 ##	202,29 ± 77,79 *

			PROVINOL +BUDESONIDE	FLAVIN7	FLAVIN7 +BUDESONIDE
Anti-inflammatory effect	SERUM	IL-4	0,71 ± 0,16 **	0,36 ± 0,12 ***	0,55 ± 0,1***
		IL-5	0,31 ± 0,03 ***	1,2 ± 0,4	2,18 ± 0,39
		IL-13	0,74 ± 0,17 ***	0,67 ± 0,1 ***	1,65 ± 0,34 **
	BALF	IL-4	0,36 ± 0,13 **	0,12 ± 0,02 **	0,15 ± 0,02 **
		IL-5	0,78 ± 0,25	0,34 ± 0,03**	0,45 ± 0,03 *
		IL-13	1,43 ± 0,31 *	0,8 ± 0,11	1,28 ± 0,2 **
Anti-remodeling effect - TGF-β (pg/ml)			402,87 ± 104,25	185,7 ± 95,12 *	216,95 ± 87,45

			BUDESONIDE	
Anti-inflammatory effect	SERUM	IL-4		0,58 ± 0,16 **
		IL-5		0,86 ± 0,2
		IL-13		1,5 ± 0,2 **
	BALF	IL-4		0,14 ± 0,02 **
		IL-5		0,41 ± 0,04 **
		IL-13		1 ± 0,11 **
Anti-remodeling effect - TGF-β (pg/ml)				379,82 ± 91,5

Tab.2: Results from levels of cytokines in serum and BALF and results from concentration of TGF-β analysis from lung tissue. Data are expressed as the mean ± SEM; ##p<0,01 (control vs. OVA); *p<0,05; **p<0,01, ***p<0,001 (OVA vs. test substances).

Discussion

The gold standard in asthma treatment still remains a combination of corticosteroids and long-acting β_2 agonists. However, the increasing prevalence of asthma requires to searches for new therapeutic approaches, which will lead to improvement of asthma treatment and will reduce the side-effect profile (Barnes, 2012).

The aim of the study was to elucidate the role of the polyphenolic compounds in the prevention and treatment of asthma, as potential source of new drugs. Many studies have confirmed their preventive and beneficial effect in various animal models of asthma. Polyphenols possess anti-oxidant, anti-allergic, anti-inflammatory and immune-modulating activities (Tanaka et.al., 2013). This fact is corroborated by the results of our experiment. We tested the effect of Provinol (polyphenolic compound of red wine contains: proanthocyanins, anthocyanins, catechins, hydroxycinnamic acid, flavonols, polymeric tannins) and Flavin7 (polyphenols compound of red fruit contains: quercetin, rutin, miricetin, kaempferol, luteolin, malvidin-3-glycoside, chrysin, galangin, apigenin, fisetin, catechins and others). The 3-week long application of Provinol and Flavin7 positively modulated the airway defence mechanisms, possess anti-inflammatory effect and significantly affected the concentration of TGF- β .

The inflammatory process is a consequence of allergic response to antigens, that involves the infiltration of activated eosinophils, Th2 lymphocytes and degranulation of mast cells. These lead to the release of chemical mediators that cause physiologic changes in the airways, such as smooth muscle contraction, edema, mucus hypersecretion, and, ultimately airway remodeling (Riccioni et.al., 2004). There are evidences, that anthocyanins, quercetin, kaempferol, fisetin, apigenin possess bronchodilatory effect and inhibit the synthesis of pro-inflammatory cytokines and the release of chemical mediators in allergic asthma (Park et.al., 2007; Tanaka et.al., 2013). Provinol and Flavin7 contain these substances. Therefore, we can assume, that the significant anti-asthmatic effects of polyphenolic compounds are resulting from the interaction of these monomers.

Adjuvant therapy may reduce the dose regimen as well as the presence of side-effects. Our experiment included the combination of polyphenolic compounds with clinically used antiasthmatic- budesonide, that were administered to experimental animals in half doses. Provinol and Flavin7 significantly enhanced an above mentioned effects of budesonide.

Conclusions

In conclusion, we can say that Provinol and Flavin7 could participate on prevention and treatment of allergic asthma. The combined therapy may lead to doses reduction of budesonide.

Acknowledgements

This work was supported by: the Slovak Research and Development Agency under the contract No. APVV-0305-12; CEKR II. –Project co-financed from EU sources; Grant VEGA 1/0165/14; Grant MZ 2012/35-UKMA-12; Grant Comenius University No.UK/8/2014.

References

- Barnes PJ: Severe asthma: Advances in current management and future therapy. *J Allergy Clin Immunol* 2012, 129, 48-59.
- Jung ChH, Lee JY, Park JH, Cho BJ, Sim SS, Kim ChJ.: Flavonols attenuate the immediate and late-phase asthmatic response to aerosolized-ovalbumin exposure in the conscious guinea pig. *Fitoterapia* 2010, 81, 803-812.
- Park SJ, Shin WH, Seo JW, Kim EJ. Anthocyanins inhibit airway inflammation and hyperresponsiveness in a murine asthma model. *Food and Chemical Technology* 2007, 45, 1459-1467.
- Riccioni G, Di Ilio C, D'Orazio N: Pharmacological treatment of airway remodeling: Inhaled corticosteroids or antileukotrienes? *Annals of Clin and Lab Science* 2004, 2, 34.
- Tanaka T, Takahashi R.: Flavonoids and Asthma. *Nutrients* 2013, 5, 2128-2143.

FGF19 EXCHANGE ACROSS THE GUT AND LIVER IN HUMANS

Kiran V. K. Koelfat

E-mail: k.koelfat@maastrichtuniversity.nl

Department of Surgery, Maastricht University Medical Centre and NUTRIM
School of Nutrition, Toxicology and Metabolism, Maastricht University, The Netherlands

Co-authors: F.G. Schaap, J.G. Bloemen, P.L.M. Jansen, C.H.C. Dejong, S.W.M.

Olde Damink

Tutor: Prof. Peter B. Soeters, MD, PhD

Background

FGF19 is an endocrine factor produced by the ileum in response to bile salts. The liver is considered as the primary target of this enterokine. Animal studies provided compelling evidence that FGF19 (Fgf15 in rodents) mediates negative feedback control of bile salt synthesis by bile salts. Thus, bile salts reclaimed from the intestinal lumen induce ileal FGF19 expression resulting in its release in the portal circulation. In the liver, FGF19 signaling represses the expression of the bile salt synthetic enzyme Cyp7a1. Another school of thought, however, argues that elevation of portal bile salts acts as the signal that represses de novo bile salt synthesis, as repression of Cyp7a1 in experimental animals occurs in the absence of elevated portal Fgf19/Fgf15. In this pilot study, we aimed to determine if the human gut releases FGF19 in the portal circulation. To this end, we calculated fluxes of FGF19 across the portal drained viscera (PDV), the splanchnic area and the liver.

Methods:

Blood plasma was obtained from patients (n=8) who underwent abdominal surgery (viz. liver resection). Following exposure of the liver but prior to resection, blood samples were subsequently taken from a radial artery, the portal and the central hepatic vein (within one hour). Plasma FGF19 was determined by ELISA, and total bile salts (TBS) were quantified using an enzymatic cycling assay. Net fluxes were calculated across the PDV, splanchnic area and liver, and were evaluated using a one-sample t-test.

Results:

FGF19 was markedly released by the gut ($3.7 \pm 2.3 \text{ ng} \cdot \text{kg}^{-1} \cdot \text{h}^{-1}$, $p=0.003$). There was a tendency towards net uptake of FGF19 by the liver net flux ($-2.0 \pm 2.9 \text{ ng} \cdot \text{kg}^{-1} \cdot \text{h}^{-1}$, $p=0.10$). TBS were also significantly released by the gut ($0.9 \pm 0.9 \text{ mmol} \cdot \text{kg}^{-1} \cdot \text{h}^{-1}$, $p=0.02$), indicating uptake of bile salts from the intestinal lumen. The uptake of TBS by the liver was not significant ($-0.5 \pm 2.3 \text{ mmol} \cdot \text{kg}^{-1} \cdot \text{h}^{-1}$, $p=0.55$). Splanchnic release of FGF19 and TBS were not significantly different from zero ($1.7 \pm 4.6 \text{ ng} \cdot \text{kg}^{-1} \cdot \text{h}^{-1}$ and $0.38 \pm 1.9 \text{ mmol} \cdot \text{kg}^{-1} \cdot \text{h}^{-1}$, $p=0.42$ and $p=0.59$, respectively).

Conclusions:

This is the first pilot study that demonstrates the interorgan exchange of FGF19 in humans in vivo in steady state condition. These findings indicate that FGF19 is released from the gut, implying elevation of portal FGF19 levels. Larger patient numbers are required to substantiate these findings.

NORMALIZING GLUTAMINE CONCENTRATION CAUSES MITOCHONDRIAL UNCOUPLING IN AN IN VITRO MODEL OF HUMAN SKELETAL MUSCLE

Adéla Krajčová

E-mail: adela.krajcova@seznam.cz

Laboratory for Metabolism and Bioenergetics, Department of Nutrition, Third Faculty of Medicine, Charles University in Prague, Czech Republic

Co-author: MUDr. Jakub Žiak

Tutors: Prof. MUDr. Michal Anděl, CSc., Doc. MUDr. František Duška, Ph.D.

Introduction

Hypoglutaminaemia can be seen in many critically ill patients. Until recently, supplementation of glutamine in nutrition support has been considered beneficial [1]. Nevertheless, recent studies suggest that critically ill patients with multi-organ dysfunction (MODS) do not benefit [2] or are even harmed [3] by aggressive glutamine supplementation. Mitochondrial dysfunction present in critically illness may be the key factor interfering with glutamine effects and explaining the differences in clinical outcome. Muscle mass regeneration, during recovery from wasting illnesses, is vitally dependent on the function of myoblasts [4]. These cells are generated by proliferation of satellite cells, which are attached to the muscle basement membrane. After stimulation by anabolic signals, satellite cells start to proliferate and differentiate to myoblasts, which synthesize contractile proteins and mitochondria and, finally, fuse with muscle fibers. Differentiated cells ready for fusion with muscle fibers are called myotubes. Myotubes have been used as *in vitro* model of human skeletal muscle, as their metabolic features are similar [5] to *in vivo* muscle fibers. As most rapidly dividing cell lines use glutamine as both nitrogen donor and energy substrate [6], it could be hypothesized, that hypoglutaminaemia impairs the proliferation and energy metabolism of myoblasts. This could provide a possible mechanism of enhanced lean body mass recovery with glutamine supplementation seen in some trials [7], as glutamine does not influence protein synthesis directly [8].

Aims

In this study, we ask how hypoglutaminaemia, at the degree seen in catabolic illnesses, influences the rate of proliferation and energy metabolism in human myoblasts and myotubes.

Methods

Satellite cells were isolated from muscle biopsy samples (m. vastus lateralis), obtained from patients undergoing elective hip replacement surgery (n=9), and after that exposed in duplicates to 6 different glutamine concentrations, resembling various degrees of clinical hypoglutaminaemia (0, 100, 200 and 300 μM), normal glutamine concentration in human plasma (500 μM) and concentration commonly used in cell cultures (5 000 μM). Myoblasts from the primary culture were trypsinized, manually counted and reseeded at days 5, 10, 15 and 20, which allowed to find out the proliferation rate. In addition, a subset of cells was reseeded at day 15 and allowed to differentiate into myotubes during next 7 days (in the same conditions of 6 different glutamine concentrations) to obtain an *in vitro* model of human skeletal muscle. After 3 weeks of exposure we assessed the energy metabolism of both

myoblasts and myotubes by extracellular flux analysis (Seahorse XF24 Analyzer). Seahorse XF24 Analyzer can measure oxygen consumption rate (OCR) in a microlayer, which sits above cells seeded in a 24-well microplate (4 wells were used as background control and remaining 20 wells for testing cells at 6 glutamine concentrations in tri- or tetraplicates). The measurement is performed at baseline and after the addition of up to 4 test agents (see Figure 1). The dynamics of OCR allows the assessment of mitochondrial function. In our experiment, we used the sequence of an ATPase inhibitor oligomycin, followed by an inner membrane uncoupler FCCP (Carbonyl cyanide-4-[trifluoromethoxy] phenylhydrazone). Finally, we used inhibitor antimycin A to block the respiratory chain complex III. Oxygen consumption after exposure to Antimycin A is considered non-mitochondrial. Extracellular acidification rate (ECAR), related to lactate production, was measured to reflect the rate of anaerobic glycolysis. To account for different mitochondrial density or cell count, data were normalized to citrate synthase activity.

Results

Proliferation: Fastest myoblast proliferation was observed at 300 μ M of glutamine, with a significant reduction at 0 and 100 μ M (see Figure 2).

Energy metabolism: Basal respiration. Glutamine did not influence basal OCR. After normalization to mitochondrial content, basal respiration does not differ either between myoblasts and myotubes or across glutamine concentrations. Influence of glutamine on the efficiency and capacity of the respiratory chain. After subtracting non-mitochondrial oxygen consumption, OCR at baseline reflects a sum of oxygen consumed for ATP synthesis and for energy dissipation due to leak of protons through the inner mitochondrial membrane. These two components are distinguished by measuring OCR after the addition of the F1F0 ATPase inhibitor oligomycin. ATP synthesis rate, normalized to mitochondrial content, was not different either between cell lines or across glutamine concentrations. Leak of protons through the inner mitochondrial membrane, normalized to citrate synthase activity, was significantly higher in myotubes compared to myoblasts and was influenced by glutamine concentrations. Proton leak through inner mitochondrial membrane was expressed as % of basal oxygen consumption rate, which had not been inhibited by oligomycin. Myotubes cultured at 200-300 μ M of glutamine used 80-90% of basal OCR for ATP synthesis and only 10-20% of energy was dissipated as heat. At both extremes of glutamine concentration we observed increased mitochondrial uncoupling to 30-40%, which decreased efficiency of the respiratory chain below 70% (see Figure 3). Myoblasts had significantly lower leak as compared to myotubes, which only increased with high glutamine concentrations (from 10-30%). Spare respiratory chain capacity (maximum respiration) is measured as oxygen consumption after artificial uncoupling of the inner mitochondrial membrane. If expressed as OCR normalized to mitochondrial content, maximum respiration tends to be non-significantly higher in myoblasts compared to myotubes and it is not influenced by glutamine. Similarly, when related to basal respiration, maximum respiration is 200-300% and not different between cell lines or among glutamine concentrations. Anaerobic glycolysis. Glutamine did not influence anaerobic glycolysis, glycolytic capacity or non-mitochondrial oxygen consumption.

Discussion

Glutamine concentrations, consistent with moderate clinical hypoglutaminaemia (300 μ M), bring about optimal condition of myoblast proliferation and for efficiency of aerobic phosphorylation in an in vitro model of human skeletal muscle. These data support the hypothesis of hypoglutaminaemia as an adaptive phenomenon in conditions leading to bioenergetic failure (e.g. critical illness).

Conclusion

Human myoblast proliferation is optimal at 300µM of glutamine, which is a level consistent with moderate clinical hypoglutaminaemia. Increasing glutamine concentration above this level does not improve proliferation rate and leads to significant uncoupling of the respiratory chain and a trend to impaired ATP synthesis in both myoblasts and myotubes. Glutamine does not influence respiratory chain capacity, the rate of anaerobic glycolysis or non-mitochondrial oxygen consumption in human skeletal muscle cells.

Summary

INTRODUCTION. Glutamine supplementation as a part of nutritional support seemed to be beneficial in a wide range of wasting diseases. However, recent randomized control studies suggest that critically ill patients with multi-organ failure (MODS) do not benefit or are even harmed [Heyland et al, NEJM, 2013] by aggressive glutamine supplementation. Myoblasts are crucial for muscle regeneration as they can proliferate and differentiate into myotubes, which then fuse with muscle fibres. Both myoblasts and myotubes can be cultured and used as an in vitro model of skeletal muscle.

OBJECTIVES. To assess the influence of glutamine concentration on the rate of proliferation of human myoblasts and on skeletal muscle energy metabolism in vitro.

METHODS. Myoblasts were isolated from muscle biopsy samples obtained from 6 volunteers. Cells were cultivated in six different glutamine concentrations (0, 0.1, 0.2, 0.3, 0.5 and 5 mM) for 20 days. Every 5th day cells were trypsinized and manually counted. Before the end of exposure, half of the cells were allowed to differentiate into myotubes. After 20 days of exposure to various glutamine concentration we assessed the citrate synthase activity and energy metabolism by extracellular flux analysis XF-24 (Seahorse Biosciences). This allowed us to calculate baseline oxygen consumption rate (OCR), ATP turnover rate, proton leak and spare respiratory capacity (SRC).

RESULTS. Fastest myoblast proliferation was observed at 300 µM of glutamine, with a significant reduction at 0 and 100 µM. Glutamine did not influence basal oxygen consumption, anaerobic glycolysis or respiratory chain capacity. Glutamine significantly ($p=0.015$) influenced the leak through inner mitochondrial membrane. Efficiency of respiratory chain was highest at 200-300µM glutamine (~90% of oxygen used for ATP synthesis). Increased glutamine concentration to 500 or 5000 µM caused mitochondrial uncoupling in myoblasts and myotubes, decreasing the efficiency of respiratory chain to ~70%.

CONCLUSIONS. At moderate hypoglutaminaemia (0.3mM) myoblast proliferation is fastest and ATP synthesis is most efficient. Severe hypoglutaminaemia (<0.2 mM), normal (0.5mM) or supranormal (5mM) glutamine levels lead to uncoupling of respiratory chain in an in vitro model of human skeletal muscle.

References

1. Online resource: <http://www.criticalcarenutrition.com/docs/cpgs2012/9.4a.pdf>
2. Andrews PJ, Avenell A, Noble DW, Campbell MK, Croal BL, Simpson WG, Vale LD, Battison CG, Jenkinson DJ, Cook JA; Scottish Intensive care Glutamine or Selenium Evaluative Trial TrialsGroup. BMJ. 2011;342:d1542
3. Heyland D, Muscedere J, Wischmeyer PE, Cook D, Jones G, Albert M, Elke G, Berger MM, Day AG; Canadian Critical Care Trials Group. A Randomized Trial of Glutamine and Antioxidants in Critically Ill Patients. N Engl J Med. 2013; 368: 1489-97.
4. Shi X, Garry DJ: Muscle stem cells in development, regeneration, and disease. Genes and Development: 2006 Jul 1;20(13):1692-708.
5. Ukropcova B, McNeil M, Sereda O, de Jonge L, Xie H, Bray GA, Smith SR. Dynamic changes in fat oxidation in human primary myocytes mirror metabolic characteristics of the donor. J Clin Invest. 2005 Jul;115(7):1934-41

6. Zielke HR, Sumbilla CM, Zielke CL, Tildon JT, Ozand PT. Glutamine Metabolism in Mammalian Tissues. Springer Berlin Heidelberg 1984. ISBN 978-3-642-69756-2 pp 247-254
7. Marcora S, Lemmey A, Maddison P: Dietary treatment of rheumatoid cachexia with beta-hydroxy-beta-methylbutyrate, glutamine and arginine: a randomised controlled trial. Clin Nutr. 2005 Jun;24(3):442-54.
8. Tjader I, Rooyackers O, Forsberg AM, Vesali RF, Garlick PJ, Wernerman J. Effects on skeletal muscle of intravenous glutamine supplementation to ICU patients. Intensive Care Med. 2004;30:266-75.

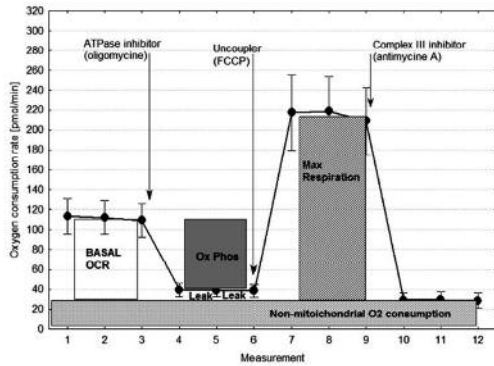


Figure 1

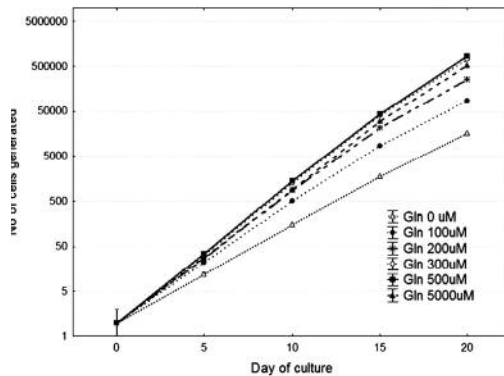


Figure 2

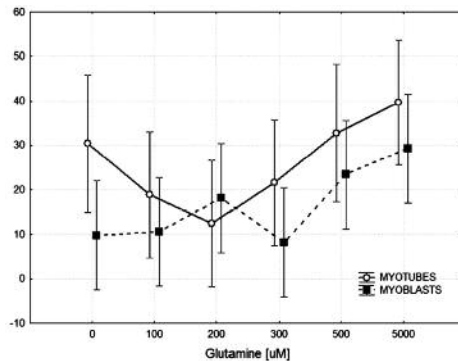


Figure 3

HUMAN GUT VIROME IN THE SEARCH FOR TYPE 1 DIABETES TRIGGERS USING NEXT-GENERATION SEQUENCING

Lenka Kramná

E-mail: lenka.kramna@lfmotol.cuni.cz

Department of Paediatrics, 2nd Faculty of Medicine, Charles University in Prague,
Prague, Czech Republic

Co-authors: K. Holková, S. Oikarinen, H. Hyöty

Tutor: doc. MUDr. Ondřej Cinek PhD.

Background and aims

The search for an association between viruses and islet autoimmunity has been limited mostly to candidate virus genera and serotypes, whereas information has been very scarce about the whole virome (i.e. the complete "virus flora"). The next-generation sequencing technologies have offered a possibility to identify all prevalent viruses in a given sample. We used this technology to contrast the stool virome between children who developed very early islet autoimmunity with subsequent type 1 diabetes, and their matched peers in the Finnish prospective Diabetes Prediction and Prevention (DIPP) birth cohort.

Materials and methods

Stool samples were collected at 3, 6 and 9 months before the first appearance of islet autoantibodies from 19 young prediabetic children who ultimately developed T1D, and 19 tightly matched controls. After mechanical enrichment of the virus fraction and nucleic acid extraction, we performed reverse transcription with tagged random primers, second strand synthesis, and partial amplification. Sequencing libraries were prepared using the Nextera XT protocol and sequenced on an Illumina MiSeq instrument. The resulting sequence reads were filtered, reduced in complexity using an unbiased de-novo assembly, and analysed for human virus motifs. The association was assessed using conditional logistic regression methods.

Results

The number of good quality sequence reads ranged from 200,000 to 1.5 million per sample, most of which belonged to multiple bacteriophages and bacteria. One or more human viruses were present in 10.4% of the samples: parechoviruses (5.2% of samples), bocaviruses (3.1%), anelloviruses (2.1%), sapoviruses (1%) and enteroviruses (1%). NGS findings were validated using virus-specific PCR. None of the human viruses or bacteriophages was associated with the appearance of islet autoimmunity.

Conclusion

The present study does not show massive changes in gut virome during this critical period, but demonstrates the ability of NGS in the evaluation of viral exposure in the pathogenesis of T1D. Further extension of this pilot dataset will allow studies of individual virus subtypes and strains, and also of sequence contigs not matching currently known organisms.

LEVOSIMENDAN EXHIBITS ANTI-INFLAMMATORY EFFECTS ON HUMAN CARDIAC MYOCYTES AND ENDOTHELIAL CELLS IN VITRO

Konstantin A. Krychtiuk

E-mail: konstantin.krychtiuk@meduniwien.ac.at

Department of Internal Medicine II – Division of Cardiology

Medical University of Vienna, Austria

Ludwig Boltzmann Cluster for Cardiovascular Research, Vienna, Austria

Co-Authors: L. Watzke, Ch. Kaun, E. Buchberger, R. Hofer-Warbinek, S. Demyanets,

J. Pisoni, S. P. Kastl, S. Rauscher, M. Gröger, A. Aliabadi, A. Zuckermann,

G. Maurer, R. de Martin, K. Huber, J. Wojta, W. S. Speidl

Tutors: Assoc.-Prof. Johann Wojta, Ph.D., Assoc.-Prof. Walter Speidl M.D.

Introduction & Aims

Levosimendan is a cardiovascular drug for the treatment of acute decompensated heart failure (HF). As an inodilator, it exhibits both positive inotropic effects by calcium sensitization and vasodilatory effects by opening ATP-sensitive potassium channels in vascular smooth muscle cells (VSMCs)¹. Clinical trials showed that levosimendan was particularly effective in HF due to myocardial infarction.^{2,3} In animal models of myocardial infarction and ischemia-reperfusion injury, levosimendan reduced the size of injured tissue.⁴ These cardioprotective effects of levosimendan might be explained in part by the observation that levosimendan opens mitochondrial ATP-sensitive K⁺-channels.⁵

The sudden obstruction of a coronary vessel leads to tissue hypoxia and cell necrosis, triggering ROS generation and initiating a cytokine cascade involving tumor necrosis factor- α (TNF- α) and interleukin-1 β (IL)-1 β , further causing activation of the endothelium and the myocardium.⁶ Expression of inflammatory cytokines, chemokines and cell adhesion molecules guides polymorphonuclear neutrophils (PMNs) into the infarcted myocardial tissue, a mechanism responsible for further tissue damage.⁷ Our aim was to examine whether levosimendan exhibits anti-inflammatory effects on human adult cardiac myocytes (HACM) and human endothelial cells.

Methods

HACM and human heart microvascular endothelial cells (HHMEC) were obtained from explanted hearts of patients undergoing heart transplantation at our institute. Human umbilical vein endothelial cells (HUVEC) were isolated from fresh umbilical cords. Cells were treated with IL-1 β (200 U/mL) for different time periods and co-treated with levosimendan at concentrations ranging from 0.1 to 10 μ M. For blocking experiments, 5-hydroxydecaonate (5-HD) was used. IL-6 and IL-8 antigen was measured by specific ELISA and mRNA was analyzed by rt-PCR. Endothelial expression of intercellular adhesion molecule-1 (ICAM-1) and E-selectin was measured by flow cytometry and rt-PCR. For adhesion experiments, PMNs were isolated from healthy volunteers and incubated on HUVEC for different time periods and surface area covered was quantified. For flow adhesion experiments, the Bioflux 200™ was used. Briefly, endothelial cell coated channels were stimulated with IL-1 β with or without levosimendan for four hours and fresh medium containing PMNs was added and a shear stress of 1 dyn/cm² was applied. Number of adherent PMNs was counted. For the analysis of nuclear shift of the NF-KB p50 and p65 subunits, Active Motif nuclear shift assays were used. For the analysis of IKB-phosphorylation we used western blotting, while NF-KB reporter gene activity was quantified by a luciferase

assay. Site specific p65-phosphorylation was examined by western blotting. All data are presented as mean \pm SD and were compared by ANOVA followed by Bonferroni correction.

Results

Incubation of HACM with IL-1 β strongly induced IL-6 and IL-8 expression evidenced by rt-PCR and ELISA. Treatment with levosimendan alone did not alter basal expression of IL-6 and IL-8 while in cells that were activated with IL-1 β , levosimendan dose- and time-dependently attenuated the expression of both cytokines by up to 75% and 65%, respectively ($p < 0.01$; Figure 1A-D). Treatment with IL-1 β strongly induced expression of ICAM-1 and E-Selectin in both HUVEC and HHMEC, while levosimendan treatment had basically no effect on steady state expression of both adhesion molecules. Co-treatment with levosimendan however, strongly reduced expression of ICAM-1 and E-Selectin in both cell types in a dose- and time dependent manner evidenced by flow cytometry and rt-PCR (Figure 1E-H). Adhesion experiments revealed that levosimendan dose-dependently reduced binding of PMNs to HUVEC under both static and flow conditions (Figure 2). To unravel the mechanism behind our findings, various experiments were performed. First, 5-HD, a blocker of mitochondrial potassium channels was added to cells treated with IL-1 β and levosimendan, showing a partly reduction in the levosimendan induced effects in endothelial cells but not in HACM. Interestingly, IKB-phosphorylation remained unaffected and no difference in nuclear p50 and p65 subunits was found in the cell nucleus. On the contrary, levosimendan treatment attenuated NF-KB reporter gene-activity in HUVEC and HACM transfected with luciferase reporter NF-KB promoters ($p < 0.001$ and $p < 0.05$ for HUVEC and HACM, respectively). Since phosphorylation at different sites of p65 have been found to influence its activity, we assayed some of them and found that levosimendan diminished the IL-1 β -induced phosphorylation of S536, but not of S276 or S529. These findings suggest a possible involvement of specific phosphorylation sites in the transactivation domain of the p65 subunit of NF-kB in the effects of levosimendan described above (Figure 3).

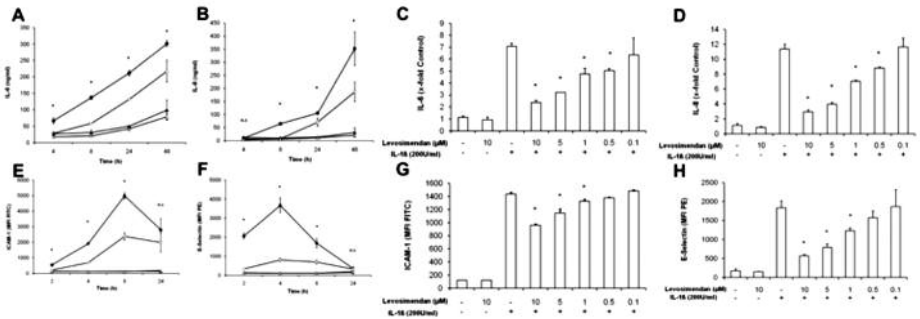


Figure 1 Effects of levosimendan on IL-6 and IL-8 expression by HACM and expression of ICAM-1 and E-Selectin by endothelial cells.

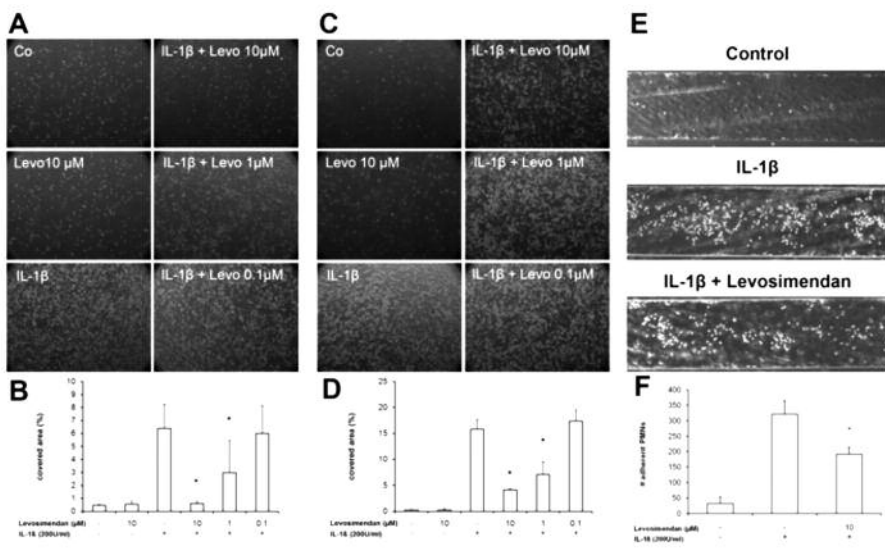
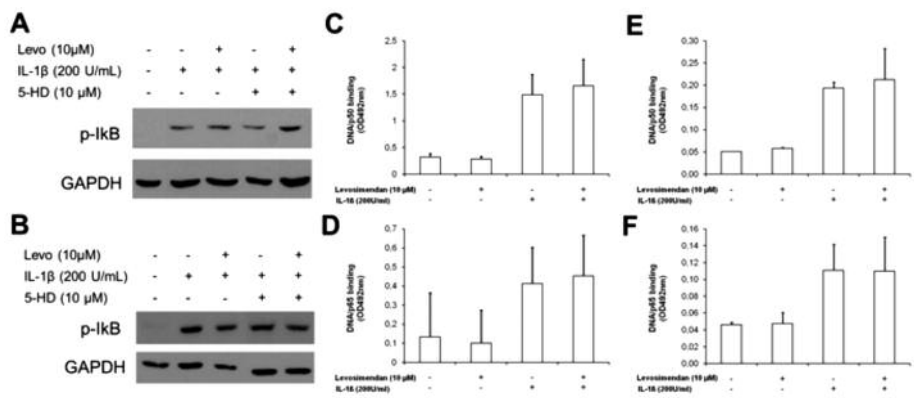


Figure 2 Levosimendan attenuates PMN adhesion to HUVEC



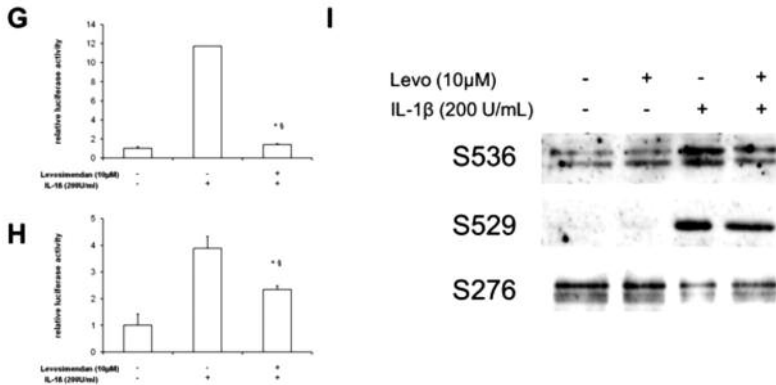


Figure 3 Involvement of the NF-κB pathway

Discussion

Here, we provide evidence for the first time that levosimendan dampens the expression of IL-6 and IL-8 in activated human cardiac myocytes. Furthermore, we illustrate that levosimendan attenuates granulocyte adhesion to endothelial cells by down-regulating the expression of ICAM-1 and E-selectin. These effects of levosimendan are partly dependent on $\text{mitoK}^+_{\text{ATP}}$ -channels and mediated by inhibition NF-κB activity. If these anti-inflammatory actions are also effective in vivo, administration of levosimendan after AMI could have beneficial effects due to a blunted reperfusion injury.

Summary

Levosimendan is an inodilator that exhibits additional cardioprotective effects via opening of $\text{mitoK}^+_{\text{ATP}}$ -channels. In clinical studies, levosimendan was particularly effective in patients suffering from acute heart failure due to myocardial infarction. Inflammatory activation plays a key role after myocardial infarction. We can show here that levosimendan attenuates IL-6 and IL-8 expression in IL-1β treated human cardiac myocytes and expression of adhesion molecules in activated human endothelial cells. Furthermore, adhesion of PMNs to endothelial cells, a critical step in reperfusion injury, is markedly attenuated under levosimendan. Anti-inflammatory effects of levosimendan are associated with decreased NF-κB activity. Anti-inflammatory effects of levosimendan could explain, at least partly, the beneficial effects of levosimendan after myocardial infarction.

References

1. Papp Z, Edes I, Fruhwald S, De Hert SG, Salmenpera M, Leppikangas H, Mebazaa A, Landoni G, Grossini E, Caimmi P, Morelli A, Guarracino F, Schwinger RH, Meyer S, Algotsson L, Wikstrom BG, Jorgensen K, Filippatos G, Parissis JT, Gonzalez MJ, Parkhomenko A, Yilmaz MB, Kivikko M, Pollesello P, Follath F. Levosimendan: Molecular mechanisms and clinical implications: Consensus of experts on the mechanisms of action of levosimendan. *Int J Cardiol.* 2012;159:82-87
2. Moiseyev VS, Poder P, Andrejevs N, Ruda MY, Golikov AP, Lazebnik LB, Kobalava ZD, Lehtonen LA, Laine T, Nieminen MS, Lie KL. Safety and efficacy of a novel calcium sensitizer, levosimendan, in patients with left ventricular failure due to an acute myocardial infarction. A randomized, placebo-controlled, double-blind study (ruslan). *Eur Heart J.* 2002;23:1422-1432
3. Husebye T, Eritsland J, Muller C, Sandvik L, Arnesen H, Seljeflot I, Mangschau A, Bjornerheim R, Andersen GO. Levosimendan in acute heart failure following primary percutaneous coronary intervention-treated acute st-elevation myocardial infarction. Results from the leaf trial: A randomized, placebo-controlled study. *Eur J Heart Fail.* 2013;15:565-572
4. Lepran I, Pollesello P, Vajda S, Varro A, Papp JG. Preconditioning effects of levosimendan in a rabbit cardiac ischemia-reperfusion model. *J Cardiovasc Pharmacol.* 2006;48:148-152
5. Kopustinskiene DM, Pollesello P, Saris NE. Levosimendan is a mitochondrial k(atp) channel opener. *Eur J Pharmacol.* 2001;428:311-314
6. Frangogiannis NG, Smith CW, Entman ML. The inflammatory response in myocardial infarction. *Cardiovasc Res.* 2002;53:31-47
7. Vinten-Johansen J. Involvement of neutrophils in the pathogenesis of lethal myocardial reperfusion injury. *Cardiovasc Res.* 2004;61:481-497

BASELINE SERUM LEVELS OF MULTIPLE CYTOKINES AND ADHESION MOLECULES IN PATIENTS WITH PRIMARY AND SECONDARY ACUTE MYELOID LEUKEMIA

Tomáš Kupsa^{1,2}

E-mail: Tomas.Kupsa@seznam.cz

¹Department of Military Internal Medicine and Military Hygiene, University of Defence, Faculty of Military Health Sciences, Hradec Kralove, Czech Republic

²4th Department of Internal Medicine – Hematology, University Hospital and Charles University, Faculty of Medicine, Hradec Kralove, Czech Republic

³Institute of Clinical Biochemistry and Diagnostics, University Hospital, Hradec Kralove, Czech Republic

Co-authors: M. Vašatová³, I. Karešová³, P. Žák²

Tutor: doc. MUDr. Jan M. Horacek, Ph.D. 

Introduction

Acute myeloid leukemia (AML) shows a high degree of heterogeneity owing to a variety of mutations and the mechanisms involved in leukemogenesis. While the treatment approach for primary and secondary AML is similar, the mechanisms of leukemogenesis differ and the outcome of secondary disease is inferior. We tested the hypothesis that secondary origin of AML influences the microenvironment measured by cytokines and soluble adhesion molecule levels more than the age itself.

Cytokines and adhesion molecules have been studied as markers of immune system activation in various diseases including hematologic malignancies and AML [1,2]. Age-related changes were suspected in several studies and older patients have often been excluded from analyses. On the other hand, age need not correlate with biological age or performance status. Based on our own experience with good results using a curative approach in patients aged 65-70 with ECOG performance status 0-2, we decided to search for age-related alterations in cytokine and adhesion molecule levels. A secondary AML usually evolves from previous myelodysplasia or myelofibrosis and is more frequent in older patients. Nevertheless, due to progress in the treatment of malignancies in younger patients (e.g. Hodgkin's lymphoma, testicular, early breast and prostate cancer) and curative treatment, some younger patients may also suffer from secondary AML.

The effect of inflammation and altered cytokine signalling on oncogenesis, leading to tumour progression, has been documented [3]. Cytokines and adhesion molecules form a unique interacting functional network. This led us to study both systems together. Modulation of this network can disrupt signalling pathway activation and overcome the high resistance to treatment. It may also increase the selectivity of AML treatment, reduce the overall treatment-related toxicity and improve outcomes of AML treatment in all age groups of patients [4,5].

Patients and Methods

Patients

A total of 51 newly diagnosed AML patients, 19 males and 32 females, mean age 52.5 ± 13.4 , median 56.2 years, were studied. According to FAB classification, 2 patients had AML M0, 10 patients AML M1, 25 patients AML M2, 4 patients AML M3, 6 patients AML M4, 3 patients AML M5 and 1 patient

AML M7. The subgroup of secondary AML patients consisted of 15 patients with a previous history of MDS (myelodysplastic syndrome) and 4 patients with previous myeloproliferative disorder. The study was approved by the local Ethics Committee and all patients gave written consent.

Serum collection

Peripheral blood was collected in serum separating tubes, immediately transported to the laboratory and processed within 2 hours of collection by centrifugation at 1500rpm x 5 minutes. All sera were collected before treatment initiation. If specimens were not to be analysed immediately, they were stored frozen in small aliquots at -20°C as recommended by the Cytokine Array manufacturer. Repeat freeze/thaw cycles were avoided.

Methods

All analytes were measured by biochip array technology using chemiluminescent sandwich immunoassays applied to the Evidence Investigator Analyzer (Randox Laboratories Ltd., Crumlin, UK). The Evidence Investigator Biochip Array technology is used to perform simultaneous quantitative detection of multiple analytes from a single patient sample.

We evaluated circulating levels of the following 17 cytokines and 5 soluble adhesion molecules: interleukins (IL-1 alpha, IL-1 beta, IL-2, IL-3, IL-4, IL-6, IL-7, IL-8, IL-10, IL-12p70, IL-13, IL-23), vascular endothelial growth factor (VEGF), tumor necrosis factor-alpha (TNF- α), interferon-gamma (IFN- γ), epidermal growth factor (EGF), monocyte chemoattractant protein-1 (MCP-1), E-selectin, L-selectin, P-selectin, intercellular adhesion molecule-1 (ICAM-1) and vascular cell adhesion molecule-1 (VCAM-1). The results are expressed in nanograms per litre (ng/L) for cytokines and micrograms per litre (μ g/L) for adhesion molecules.

Statistical analysis

Statistical analysis was performed with the "Statistica" software using two tailed T-tests and Mann-Whitney tests in non-parametric analysis. The values were expressed as means \pm standard deviation. Probability values (p) < 0.05 were considered statistically significant.

Results

Age dependent differences

Originally, we analysed 3 subgroups of patients. The first subgroup included patients aged less than 55 years ($n=25$), the second subgroup included patients aged 55-65 years ($n=11$) and the third subgroup included patients aged 65 and older ($n=15$). Because there were no significant differences between younger and 55-65 year old patients, we analysed both subgroups together against patients older than 65 years.

In patients aged 65 or more, we found a significant decrease in IL-12 levels (0.95 ± 1.14 ng/L vs. 4.11 ± 3.76 ng/L, $p=0.025$).

Secondary AML

These patients with secondary AML were much older than those with primary disease (62.9 ± 6.7 vs. 46.6 ± 13.3 years, $p=0.00008$). In secondary AML, we found higher IL-7 (6.13 ± 4.42 ng/L vs. 3.59 ± 1.97 ng/L, $p=0.047$) and EGF levels (26.64 ± 26.58 μ g/L vs. 7.49 ± 8.05 μ g/L; $p=0.004$), see Figure 1. The levels of IL-12 (1.26 ± 1.46 ng/L vs. 4.32 ± 3.87 ng/L; $p=0.021$), IL-13 (2.16 ± 3.02 ng/L vs. 5.09 ± 4.47 ng/L, $p=0.049$) and E-selectin (14.85 ± 10.36 μ g/L vs. 28.84 ± 18.16 μ g/L; $p=0.018$) were decreased in secondary AML (see Figures 2 and 3). The leukocyte counts had a trend to lower counts in the secondary AML group which were significant after exclusion of patients with acute promyelocytic leukemia ($15.93 \pm 15.99 \times 10^9$ /L vs. $53.35 \pm 54.44 \times 10^9$ /L, $p=0.048$). We also found trends towards higher MCP-1 (246.14 ± 128.35 ng/L vs. 167.56 ± 101.96 ng/L, $p=0.055$) and lower IL-10 levels (1.53 ± 1.16 ng/L vs. 4.99 ± 4.86 ng/L, $p=0.075$) in secondary AML.

Discussion

The treatment of secondary AML is complicated. Our results are in agreement with the general finding that patients with secondary AML are usually older than those with primary disease. The finding of lower IL-13 levels in secondary AML is in agreement with previous results, where MDS patients had lower IL-13 levels than AML [6]. Further, the trend to lower IL-10 levels in secondary disease may explain the recently published negative prognostic impact of low IL-10 levels [7]. The decrease in IL-12 levels found in elderly patients is probably attributed to secondary AML. We venture to suggest that the origin of AML is a more important factor for cytokine and adhesion molecule levels than age per se.

Conclusions

The secondary AML has different biology compared to primary disease. The development of innovative treatment approaches in secondary AML should be based on detailed knowledge of these differences. Early detection and choice of appropriate strategy would allow treatment to be more personalized which is the basic aim of modern medicine.

Summary

We evaluated serum levels of 17 cytokines and 5 adhesion molecules in 51 consecutive patients with newly diagnosed acute myeloid leukemia (AML) using biochip array technology. We searched for links between baseline levels, age and secondary origin of AML.

Serum samples were analyzed by biochip based immunoassays on the Evidence Investigator analyzer. For statistical analysis T-test and non-parametric Mann-Whitney test were used.

We found that higher age is associated with lower levels of IL-12. Patients with secondary disease were older, had higher levels of EGF and IL-7 and, lower levels of E-selectin, IL-12 and IL-13.

Some leukemic cell subpopulations have the ability to produce cytokines that modulate the microenvironment by inducing inflammation. Our findings suggest that primary and secondary AML differ in cytokine background and cellular biology. Clinically, the same treatment approach is applied to both diseases, but the outcome is inferior in secondary AML. Reflecting secondary AML biology should stand at the basis of innovative treatment strategies.

Acknowledgements

The work was supported by a long-term organizational development plan 1011 (Faculty of Military Health Sciences, Hradec Kralove) and by a specific research project "Analysis of defined prognostic factors in acute myeloid leukemia" (Faculty of Military Health Sciences, Hradec Kralove).

References

1. Bruserud Ø, Kittang AO.: The chemokine system in experimental and clinical hematology. *Curr Top Microbiol Immunol* 2010; 341, 3-12.
2. Löwenberg B, Touw IP.: Hematopoietic growth factors and their receptors in acute leukemia. *Blood* 1993; 81, 281-292.
3. Coussens LM, Werb Z.: Inflammation and cancer. *Nature* 2002; 420, 860-867.
4. Kupsa T, Horacek JM, Jebavy L.: The role of cytokines in acute myeloid leukemia: a systematic review. *Biomed Pap Med Fac Univ Palacky Olomouc Czech Repub* 2012; 156, 291-301.
5. Kupsa T, Horacek JM, Jebavy L.: The role of adhesion molecules in acute myeloid leukemia and (hemato) oncology: A systematic review. *Biomed Pap Med Fac Univ Palacky Olomouc Czech Repub* 2014; Sep 26. doi: 10.5507/bp.2014.049. [Epub ahead of print]
6. Kornblau SM, McCue D, Singh N et al.: Recurrent expression signatures of cytokines and chemokines are present and are independently prognostic in acute myelogenous leukemia and myelodysplasia. *Blood* 2010; 116, 4251-4261.
7. Sanchez-Correa B, Bergua JM, Campos C et al.: Cytokine profiles in acute myeloid leukemia patients at diagnosis: survival is inversely correlated with IL-6 and directly correlated with IL-10 levels. *Cytokine* 2013; 61, 885-891.

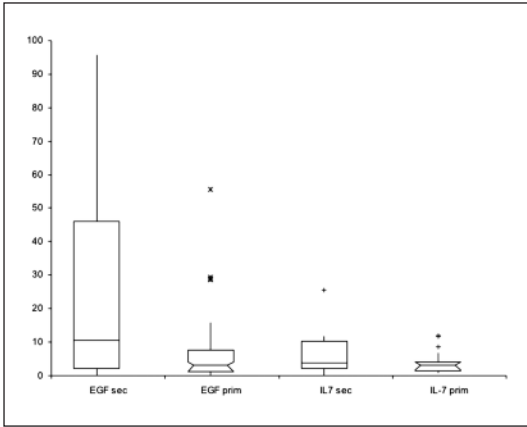


Figure 1. Serum levels of EGF and IL-7 in primary and secondary AML.

Legend: EGF – Epidermal growth factor; IL-7 – Interleukin 7; sec – secondary AML; prim – de novo AML

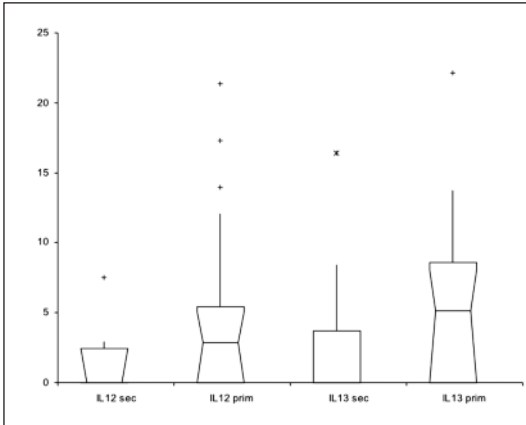


Figure 2. Serum levels of IL-12 and IL-13 in primary and secondary AML.

Legend: IL-12 – Interleukin 12; IL-13 – Interleukin 13; sec – secondary AML; prim – de novo AML

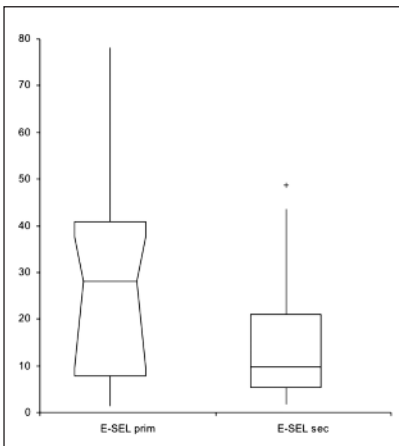


Figure 3. Serum levels of E-selectin primary and secondary AML.

Legend: E-SEL – E-selectin; sec – secondary AML; prim – de novo AML

PACAP CAN AMELIORATE VASCULAR CHANGES IN THE ANIMAL MODEL OF RETINOPATHY OF PREMATURITY

Tímea Kvárík

E-mail: kvarik.timi@gmail.com

Department of Anatomy and Neonatology, Faculty of Medicine, University of Pécs,
in Pécs, Hungary

Co-authors: B. Mammel, D. Werling, B. Bede, A. Váczy, J. Gyarmati, A. Tamás, T. Ertl,
D. Reglődi, T. Atlasz

Tutors: Prof. Dr. Reglődi Dóra, Prof. Dr. Ertl Tibor

Introduction

Thanks to the improving quality of neonatal care more and more premature babies can be saved. As a consequence, neonatologists have to face the increasing number of complications affecting future life quality. One of these conditions is the neurovascular disease of the retina, the retinopathy of prematurity (ROP). Preterm birth results in incomplete retinal vascular development. In ROP, at the junction of vascular and avascular retinal area new, abnormal vessel formation starts and can grow into the vitreous. This process can lead to retinal detachment due to fibrovascular traction. (1) Despite striking effects in therapeutic strategies and understanding the pathophysiology of ROP, it is still one of the major cause of childhood blindness. (2)

The animal models of ROP are widely used in research. The base of these models is the fluctuating oxygen concentration in early life leading to oxygen-induced retinopathy (OIR). Rat model mimics the human disease. On one hand, the retinas of newborn rat pups are similar to that of a 26-week old premature infant, on the other hand the OIR develops on the peripheral area like in humans. (3)

Pituitary adenylate cyclase-activating polypeptide (PACAP) is a member of vasoactive intestinal peptid/secretin/glucagon peptide superfamily, and has a diverse biological action. PACAP has been shown to have antiapoptotic and protective effects in numerous cells and tissues, including the retina. (4) Several studies have revealed the presence of PACAP and its receptors in different layers of the retina. Moreover, the retinoprotective effects of local PACAP treatment were reported after excitotoxic and ischemic retinopathy. (5) (6)

The aim of the study was to examine the effects of local and systemic PACAP treatment in the rat model of ROP.

Materials and Methods

OIR was generated by placing the newborn Sprague-Dawley rat pups with their nursing mother in 24-hour cycles of 10% / 50% oxygen from postnatal day (P) 0 to 14, then returning them to room air. (7) Animals were divided into subgroups according to the treatment strategy. A group of animals were injected with intraperitoneal PACAP (cc. 100µg/ml, dose: 1mg/kg) from P1 – P8. Another group received intravitreal PACAP injection (cc. 100µg/ml, dose: 3µl/treated eye) on P11, P14, P17 with 33G Hamilton syringe. Age- and cage-matched controls were treated with the adequate amount of saline in the same ways; as a control for OIR, animals - divided into the same subgroups - were kept in room air during the whole experiment. On P18-19 – when the neovascularization is maximal – animals were sacrificed and eyes were dissected. Retinas were isolated, stained with fluorescent dye (Alexa Fluor 568) – conjugated isolectin GS-IB4. Sections were washed and coverslipped. The percentages of

avascular to whole retinal areas were defined by using Adobe Photoshop CS6 and ImageJ softwares. Statistical comparisons were made by using ANOVA test followed by Fisher's post hoc analysis.

Results

OIR resulted in obliteration of peripheral vessels and new vessel formation on the edge of vascularized and non-vascularized retinal areas. Intravitreal treatment with PACAP injection markedly reduced the extent of avascular area (13.25 ± 1.47 ; $n=28$) compared to the results of non-treated OIR group (20.45 ± 1.51 ; $n=47$) and to the saline-treated group (20.40 ± 2.58 ; $n=16$). Intraperitoneal PACAP treatment (18.08 ± 1.82 ; $n=42$) did not reveal any differences compared to the control OIR retinas. (fig.1.) Retinal images of controls kept in room air did not show vascular changes.

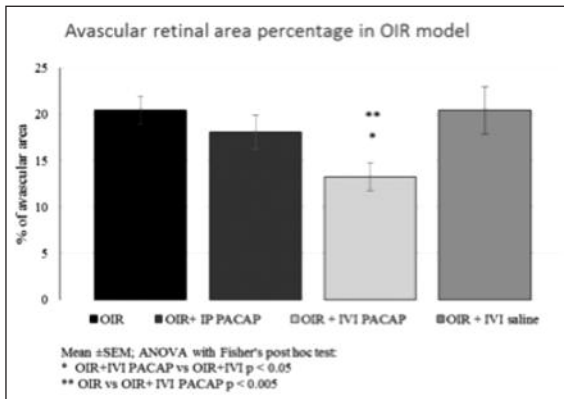


fig. 1. Percentage of avascular to whole retinal area is represented in mean \pm SEM

Discussion

PACAP and its receptors occur throughout the retina. Several papers were published to demonstrate the retinoprotective effects after certain damages. The retina is one of the most sensitive tissues in human body to hypoxia, especially during development. ROP is the disease of prematures with risk factors like oxygen-therapy, infections, transfusions, episodes of hyperglycaemia. (8) The rat model of ROP is based on the alternating oxygen concentration resulting in cessation of vessel growth followed by neovascularization leaving the peripheral retina avascular. We showed that local treatment with PACAP injection into the vitreous body reduced the avascular retinal area by almost 35% compared to non-treated or saline-injected retinas. Further in vitro and in vivo molecular methods are needed to reveal the exact protective mechanism.

Conclusion

The rat retina represents a characterized, readily accessible tissue for angiogenesis research. Large number of studies emphasize that using OIR retina may contribute to our better understanding of the angiogenic pathomechanisms. The exact role of potential retinoprotective PACAP in this process raise further questions.

Summary

This study supports the retinoprotective effect of PACAP, but there is a need to reveal the molecular mechanisms. In the future it may provide the basis for future clinical application of PACAP treatment in retinal degenerations.

References

- 1) Hartnett ME et al. Studies on the pathogenesis of avascular retina and neovascularization into the vitreous in peripheral severe retinopathy of prematurity. *Trans Am Ophthalmol Soc* 2010; 108
- 2) Chen J, Smith LE. Retinopathy of prematurity. *Angiogenesis* 2007; 10:133-140
- 3) Penn JS, Henry MM et al. The range of PaO₂ variation determines the severity of oxygen-induced retinopathy in newborn rats. *Invest Ophthalmol Vis Sci* 1995; 36:2063–2070
- 4) Reglodi D, Szabadfi K, Atlasz T et al. PACAP is an endogenous protective factor – insight from PACAP-deficient mice. *J Mol Neurosci* 2012; 48:482-492
- 5) Atlasz T et al. PACAP-mediated neuroprotection of neurochemically identified cell types in MSG-induced retinal regeneration. *J. Mol. Neurosci.* 2008; 36: 97–104
- 6) Atlasz T et al. Pituitary adenylate cyclase activating polypeptide is protective in bilateral carotid occlusion-induced retinal lesion in rats. *Gen. Comp. Endocrinol.* 2007; 153:108–114.
- 7) Barnett J, Yanni S, Penn J. The development of the rat model of retinopathy of prematurity. *Doc Ophthalmol* 2010; 120:3-12
- 8) Ertl T, Gyarmati J et al. Relationship between hyperglycaemia and retinopathy of prematurity in very low birth weight infants. *Biol Neonate.* 2006; 89(1): 59-6

INVOLVEMENT OF UNFOLDED PROTEIN RESPONSE IN CELLULAR SENEESCENCE ESTABLISHMENT

Liliana Matos

E-mail: lmatos@fena.up.pt

Department of Experimental Biology, Faculty of Medicine (FMUP);
Ageing and Stress Group, IBMC-Instituto de Biologia Molecular e Celular;
and Faculty of Nutrition and Food Sciences (FCNAUP), University of Porto, Portugal

Supervisor: Prof. Henrique Almeida, MD, PhD

Co-supervisor: Prof. Alexandra M. Gouveia, PhD

Introduction

Endoplasmic reticulum (ER) has a “quality control” chaperoning system engaged in protein unfolding, misfolding and aggregation prevention. The efficiency of this system depends on the fine regulation of chaperones and enzymes, such as immunoglobulin binding protein (BiP), calnexin, protein disulfide isomerase (PDI) and ER oxidoreductin-1 (Ero1). However, when proteostasis is disrupted, an adaptive ER stress response or Unfolded Protein Response (UPR) mediated by ER transmembrane sensors, as pancreatic ER kinase (PKR)-like ER kinase (PERK), activating transcription factor 6 (ATF6) and inositol-requiring enzyme 1 (IRE1), is activated [1]. These three pathways aim to limit protein load and alleviate ER stress, but if these pro-survival cellular responses are not able to restore proteostasis, they can lead to cell death.

In aging, this complex quality control system appears to be disturbed on account of the progressive accumulation of damaged biomolecules, such as structurally and functionally abnormal proteins [2]. In this setting, we hypothesized that human cellular models of replicative senescence (RS) and stress-induced premature senescence (SIPS) [3] would present an activation of UPR and an impairment of the ER chaperoning mechanisms. Therefore, our aims were to evaluate the expression of ER chaperones and enzymes, and UPR activation in WI38 models of RS [4], hydrogen peroxide (H₂O₂)-SIPS [5] and copper sulfate (CuSO₄)-SIPS [6]. We also evaluated the impact of UPR inhibition in the establishment of SIPS.

Methods

WI38 fibroblasts were cultivated in BME-10% FBS and, when unable to duplicate for 3 weeks, were considered in RS. For the induction of H₂O₂- and CuSO₄-SIPS, young fibroblasts were exposed to sub-cytotoxic concentrations of H₂O₂ or CuSO₄ for 2 or 24h, respectively. For the inhibition of PERK- or IRE1-mediated ER stress response, 120nM GSK2606414 or 10μM 4μ8c, respectively, were added to the medium 1h prior to SIPS induction and maintained throughout the experiments. Cell proliferation was assessed by performing the sulforhodamine B assay to quantify the increase in cell density along time (0, 1, 2, 3 and 4 days after stress). 48h after each treatment the senescence biomarker SA beta-gal was detected as described [6]. Protein or gene expressions were evaluated 72h after treatments. Protein levels were semi-quantified by western blotting as described [6, 7] using specific primary antibodies at pre-optimized concentrations (anti-BiP, anti-calnexin, anti-Ero1, anti-PDI, anti-IRE1, anti-PERK, anti p-eIF2 from Cell Signaling Technology®; anti-P-JNK and anti-ATF6 from Santa Cruz Biotechnology, Inc.; and anti-Tubulin from Sigma-Aldrich®). Gene expression was evaluated using real-time PCR as described in detail in ref [7].

Results

Upon western blot assessment in the different senescence models (Figure 1), BiP protein was found significantly increased both in RS and CuSO₄-SIPS cells. Both calnexin and PDI protein levels were reduced in the three cellular models of senescence, whereas Ero1 exhibited an augmentation comparatively to controls.

In normal conditions, IRE1, PERK and ATF6 remain inactive while bound to BiP through their luminal domain. However, when unfolded/misfolded proteins accumulate in ER lumen, BiP is recruited to chaperone them and dissociate from these sensors leading to the activation of their transductive pathways. Activated IRE1 acquires kinase and RNase activity and is able to phosphorylate the c-Jun N-terminal kinase (JNK) and to cleave X box-binding protein 1 (XBP1) mRNA generating an mRNA spliced variant (XBP1s), ultimately promoting ER chaperones upregulation. IRE1 and P-JNK proteins, and XBP1s mRNA were significantly increased in RS and CuSO₄-SIPS cells when compared to controls, whereas H₂O₂-SIPS fibroblasts did not present this pathway activated (Figure 2A). BiP dissociation from PERK promotes its activation and leads to eukaryotic translation initiation factor 2 α phosphorylation (p-eIF2 α), which in turn inhibits general protein translation and induces activating transcription factor 4 (ATF4) expression and subsequently CCAAT/enhancer-binding protein homologous protein (CHOP) transcription. PERK and p-eIF2 α protein levels were found increased in the three senescence models (Figure 2B). However, CHOP expression was reduced in CuSO₄-SIPS and RS, while it was increased in H₂O₂-SIPS cells, when compared to controls. As ATF6 is released from BiP, it is transported to the Golgi compartment, where it is activated by proteolytic cleavage. This cleaved form – ATF6(p50) – translocates to the nucleus where it promotes the transcription of ER chaperones and XBP1. ATF6(p50) protein was found increased both in RS and CuSO₄-SIPS (Figure 2C), while H₂O₂-SIPS cells did not show significant variations in ATF6(p50) levels.

The importance of UPR activation during cellular senescence was evaluated by inhibiting IRE1 or PERK activities in WI-38 fibroblasts prior to the induction of CuSO₄-SIPS using 4 μ 8c and PERK and GSK2606414, respectively. IRE1- or PERK-response inhibition prior to CuSO₄-SIPS induction resulted in a decrease of SA beta-gal positive cells (Figure 3A). IRE1 inhibition did not affect the effect of copper on cell proliferation or p21 levels, while CuSO₄-SIPS cells with inhibited PERK presented increased cell proliferation and decreased p21 levels (Figure 3B and 3C).

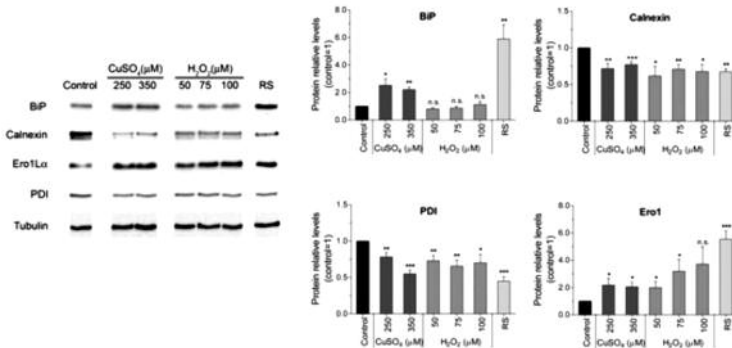


Figure 1: Expression of key ER chaperones and enzymes is altered in both RS and SIPS fibroblasts. BiP, calnexin, Ero1 and PDI proteins were detected by western blot and their relative protein levels were quantified by densitometry relative to tubulin in the cellular extracts from RS, CuSO₄- and H₂O₂-SIPS cellular models. Data are expressed as mean \pm SEM from at least three independent experiments. * $p < 0.05$; ** $p < 0.01$; *** $p < 0.001$; and n.s. non-significant, when compared to control. These results were already published [7].

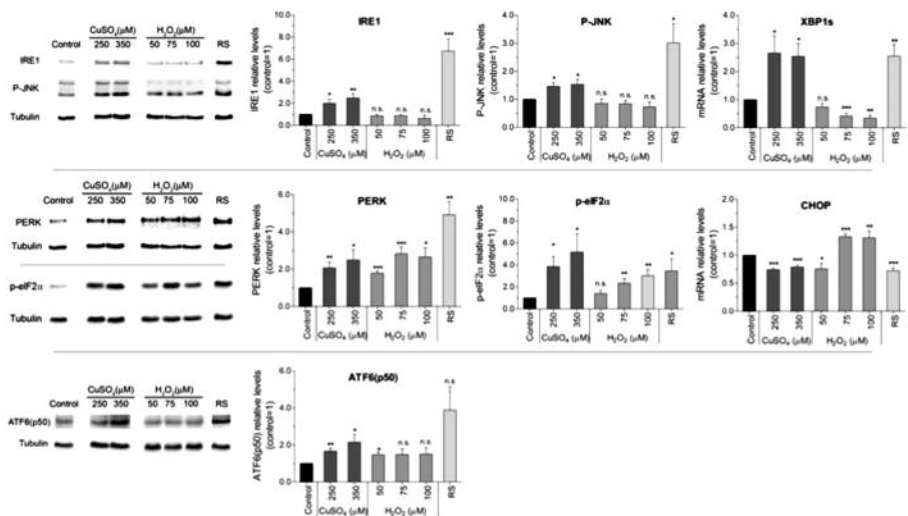


Figure 2: UPR activation in RS and SIPS human cellular models. Western blotting and qPCR techniques were used to evaluate the activation of the three different branches of UPR. (A) IRE1 pathway activation was assessed by the quantification of IRE1 and P-JNK protein, and XBP1s transcript levels. (B) PERK and p-eIF2 protein and CHOP mRNA levels were used as indicators of PERK-mediated UPR. (C) ATF6 activation was demonstrated by the levels of ATF6(p50) cleaved protein. Data are expressed as mean \pm SEM from at least three independent experiments. * $p < 0.05$; ** $p < 0.01$; *** $p < 0.001$; and n.s. non-significant, when compared to control. These results were already published [7].

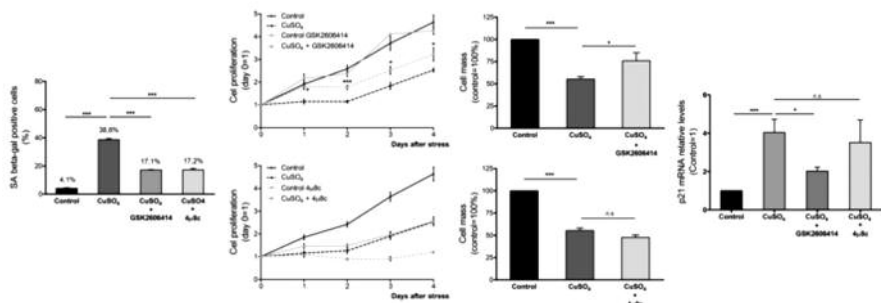


Figure 3: UPR inhibition attenuates the appearance of senescence. (A) The percentage of SA beta-gal positive cells was evaluated in CuSO₄-SIPS in the presence or absence of PERK (GSK260614) or IRE1 (4 μ 8c) inhibitors. (B) Cell proliferation was assessed using sulforhodamine B assay at 0, 1, 2, 3 and 4 days after stress induced in CuSO₄-SIPS cells pre-treated or not with GSK260614 or 4 μ 8c, as indicated in the respective plots. The percentage of cell mass was calculated at the 4th day after stress considering that the respective control cells represented 100% of cell mass. (C) Relative levels of p21 mRNA were quantified by qPCR in CuSO₄-SIPS cells treated or not with GSK260614 or 4 μ 8c, as indicated. Data are expressed as mean \pm SEM from at least three independent experiments. * $p < 0.05$; ** $p < 0.01$; *** $p < 0.001$; and n.s. non-significant, when compared to control. These results were already published [7].

Discussion and Conclusions

In RS and CuSO₄-SIPS cells, BiP, calnexin, PDI and Ero1 levels adjust to restore proteostasis while IRE1-, ATF6- and PERK-mediated UPR are activated. However, H₂O₂-SIPS do not exhibit IRE1 and ATF6 pathways activation but a PERK-mediated upregulation of CHOP. Furthermore, UPR inhibition (PERK- or IRE1-mediated) before CuSO₄-SIPS induction leads to senescence attenuation, but only PERK inhibition resulted in increased cell proliferation and decreased p21 mRNA levels. These results indicate that PERK-mediated UPR is implicated in copper ability to induce cell cycle arrest in CuSO₄-SIPS.

The present study shows that CuSO₄-SIPS model mimics better the ER molecular events of RS than H₂O₂-SIPS, and adds further evidence on the molecular mechanisms regulating senescence induction. Copper has recently been involved in senescence establishment, since its intracellular levels were increased in RS when compared to young cells [8]. Such involvement can be now justified by copper ability to induce UPR activation, which we demonstrate here to be required for senescence induction. Actually, copper homeostasis disruption has been involved in age-related diseases, as Alzheimer's and Parkinson's [9], which turns CuSO₄-SIPS model a valuable tool in their study. In addition, its usefulness may extend to identify new mechanisms and potential targets for pharmaceutical interventions, aiming to ameliorate cellular stress responses during aging and postpone age-related health deterioration.

Summary

The aging process is characterized by progressive accumulation of damaged biomolecules in the ER, as result of increased oxidative stress accompanying cellular senescence and decreased efficiency of the chaperoning capacity. In this setting, we hypothesized that WI-38 human cellular models of RS and SIPS would present ER chaperoning mechanisms impairment and UPR activation. Using RS, H₂O₂- and CuSO₄-SIPS human cellular models, it is shown that BiP, calnexin, PDI and Ero1 levels are adjusted to deal with senescence-associated imbalance in proteostasis. In addition, RS triggers a cellular protective ER stress response mediated by IRE1, ATF6 and PERK. This behavior is mimicked by CuSO₄-SIPS but not by the most frequently used H₂O₂-SIPS model, which does not exhibit the activation of IRE1 and ATF6 axis of ER stress response and, instead, reveals PERK-mediated upregulation of CHOP. The impact of UPR inhibition in the establishment of SIPS was also evaluated. It is shown that UPR activation is required for SIPS induction, since PERK and IRE1 inhibitors decreased SA beta-gal appearance. In CuSO₄-SIPS the decrease in senescence levels is associated with PERK-driven, but IRE1 independent, cell cycle arrest. These results add a step further on the molecular mechanisms that regulate senescence induction; moreover, they validate CuSO₄-SIPS model as a useful tool to study cellular stress responses during aging and in age-related disorders, hoping to improve healthspan.

Acknowledgements

Matos L was supported by POCI 2010, FSE and “Fundação para a Ciência e Tecnologia” (SFRH/BD/61820/2009).

References

1. Schröder M and Kaufman RJ: The mammalian unfolded protein response. *Annu Rev Biochem* 2005; 74, 739-789.
2. Levine RL: Carbonyl modified proteins in cellular regulation, aging, and disease. *Free Radical Biology and Medicine* 2002; 32(9), 790-796.
3. Toussaint O, Remacle J, Dierick JF, et al.: From the Hayflick mosaic to the mosaics of ageing. Role of stress-induced premature senescence in human ageing. *Int J Biochem Cell Biol* 2002; 34(11), 1415-1429.
4. Hayflick L: Limited in Vitro Lifetime of Human Diploid Cell Strains. *Exp Cell Res* 1965; 37(3), 614-636.
5. Chen QM, Bartholomew JC, Campisi J, et al.: Molecular analysis of H₂O₂-induced senescent-like growth arrest in normal human fibroblasts: p53 and Rb control G(1) arrest but not cell replication. *Biochem J* 1998; 332, 43-50.
6. Matos L, Gouveia A, and Almeida H: Copper ability to induce premature senescence in human fibroblasts. *Age (Dordr)* 2012; 34(4), 783-794.
7. Matos L, Gouveia AM, and Almeida H: ER Stress Response in Human Cellular Models of Senescence. *J Gerontol A Biol Sci Med Sci* 2014; in press.
8. Boilan E, Winant V, Dumortier E, et al.: Role of p38MAPK and oxidative stress in copper-induced senescence. *Age (Dordr)* 2013; 35(6), 2255-2271.
9. Scheiber IF, Mercer JF, and Dringen R: Metabolism and functions of copper in brain. *Prog Neurobiol* 2014; 116, 33-57.

USE OF PH-CYCLING CONDITIONS TO MODEL POST-ERUPTIVE MATURATION OF DENTAL ENAMEL *IN VITRO*

Emma Jane Miles

E-mail: e.j.miles@liverpool.ac.uk

Department of Health Services Research, Faculty of Health and Life Sciences,
University of Liverpool, United Kingdom

Supervisors: Prof. S. Higham, Dr. S. Valappil and Prof. R. Lynch

Introduction

Post-eruptive maturation (PEM) refers to the chemical and physical changes that occur in the outer layers of tooth enamel following eruption of the tooth and exposure to the oral environment (Brudevold *et al.* 1982). Newly erupted enamel is more susceptible to the development of dental caries (Brudevold *et al.* 1982) and it has been suggested that this is due to increased porosity and the presence of naturally-occurring chemical impurities that increase enamel solubility (Driessens *et al.* 1985). During PEM chemical and physical changes occur in the outer layers of the enamel (Wöltgens *et al.* 1981), however there is yet to be determined a definitive explanation of how this process occurs. PEM is believed to be caused by the cyclic de- and re-mineralisation that occurs within the oral environment (Nakajima *et al.* 2003), in addition to the actions of ions such as Fluoride (Robinson *et al.* 2000) and Zinc (Brudevold *et al.* 1963). As such, the present study aimed to simulate PEM using an *in vitro* pH-cycling model, the success of which was tested through exposing treated enamel to a subsequent acid challenge. It also aimed to investigate the effects of Zinc and Fluoride upon the model.

Methods

Preparation of Blocks

30 bovine enamel blocks approximately 10x4mm in size were prepared and coated in acid resistant nail varnish (Nailfinity, MaxFactor, Procter and Gamble, UK) leaving an experimental window approximately 9x3mm in size. Blocks were pre-treated in demineralisation solution (pH 5.11, 2.25mM calcium chloride dihydrate, 17.7mM potassium dihydrogen orthophosphate, 32.9mM lactic acid, 4.25µM fluoride (As NaF)) for either 0 or 3h to obtain baseline values. Blocks were mounted using Green Stick Impression Compound (Sybron Dental Specialties, Kerr, Italia, S.p.A) into 50 ml Sterilin disposable containers (Sterilin Ltd. Newport, UK).

pH Cycling with exposure to Zn and NaF

pH-Cycling solutions were designed to emulate ion concentrations and pH values representative of plaque-fluid. The demineralisation solution (outlined previously) was based on ion concentrations and pH values reported previously by Vogel *et al.* (2000) for plaque fluid during an acid challenge. Values selected were the average of values obtained from upper and lower molar sites. The remineralisation solution described by Lynch *et al.* (2007) was used (pH 6.58, 20mM HEPES, 1mM calcium chloride dihydrate, 12.7mM potassium dihydrogen orthophosphate, 130mM potassium chloride), with the addition of 5.7µM Fluoride (From resting levels reported by Vogel *et al.* (2000)). Blocks were exposed to three 30m demineralisations each day for either 0 or 20d and were stored in remineralisation solution in between.

Cycled blocks were assigned to one of five conditions (No Cycling, No Treatment, 231 $\mu\text{mol/l}$ Zn Sulphate treatment, 228ppm NaF treatment and Zn and NaF together) and were exposed to treatment solutions for 2 minutes at each solution change.

Demineralisation of enamel blocks

Following pH-cycling treatment, enamel blocks subjected to a total of 72 hours in a standard demineralising solution with agitation at room temperature. Samples were rinsed in deionised water and allowed to air-dry at room temperature.

Quantitative Light-Induced Fluorescence (QLF-D) and Multispectral Imaging (Nuance) Analysis QLF-D Biluminator™ (Inspektor, Amsterdam, Netherlands) and Nuance™ (CRi, Woburn, USA) images were taken of dry samples at baseline, following pH-cycling treatment and at following 72 hours demineralisation. The change in fluorescence (ΔF) was calculated for both methods using QA2 image analysis software (Inspektor, Amsterdam, Netherlands).

Transverse Microradiography (TMR)

Transverse microradiography was used to determine the change in mineral (ΔZ) at baseline, following pH-Cycling treatment and after 72 hours. TMR was conducted as described previously (Lynch et. al. 2011). Enamel sections were polished to 80 μm and mounted with an aluminium step wedge. Microradiographs were taken using Kodak type 1A high-resolution plates (Kodak, Rochester, USA) exposed to a $\text{CuK}\alpha$ X-ray source operating at 20 mA and 20 kV for 12 minutes. Results were examined microscopically

Results:

QLF-D

A decrease in fluorescence loss (ΔF) was observed for all pH-cycled enamel blocks in comparison to un-cycled controls (with the exception of the 3h Pre-treated Zn/F condition), however none were statistically significant. A decrease in fluorescence loss was observed in all blocks treated with Zn, F or both in comparison to untreated controls.

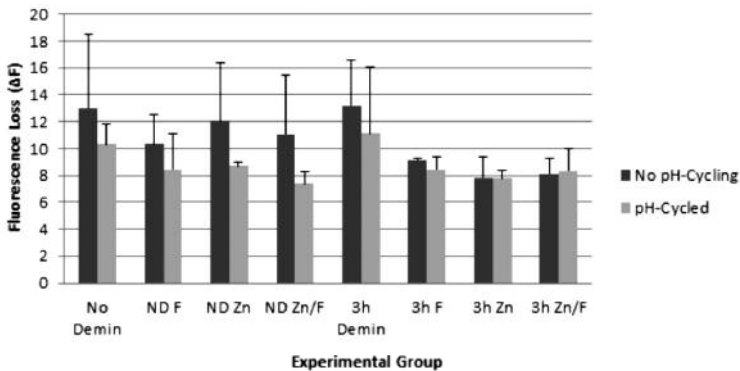


Fig. 1 Graph showing QLF-D values for Fluorescence loss at baseline and following pH- Cycling and subsequent demineralisation.

Nuance

In agreement with QLF-D results, a decrease in fluorescence loss (ΔF) was observed for all pH-cycled enamel blocks in comparison to un-cycled controls, however none were statistically significant. A decrease in fluorescence loss was observed in all blocks treated with Zn, F or both in comparison to untreated controls.

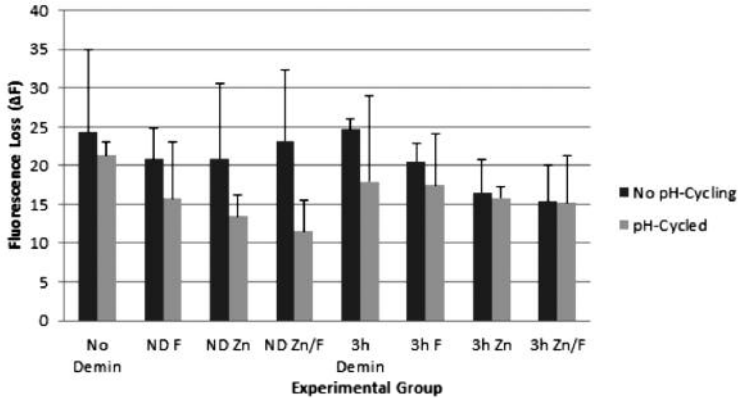


Fig. 2 Graph showing Nuance values for Fluorescence loss at baseline and following pH- Cycling and subsequent demineralisation.

TMR

A decrease in mineral loss (ΔZ) was observed for all pH-cycled enamel blocks in comparison to un-cycled controls, however none were statistically significant. A decrease in mineral loss was observed in all blocks treated with Zn, F or both in comparison to untreated controls (With the exception of 3h pre-treated enamel exposed to both pH-Cycling and F).

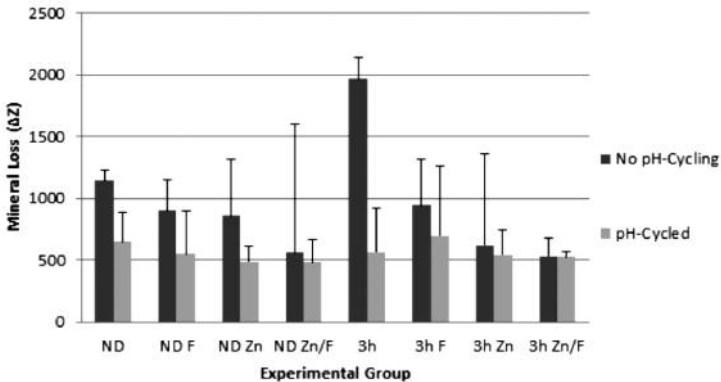


Fig. 3 Graph showing TMR values for Fluorescence loss at baseline and following pH- Cycling and subsequent demineralisation.

Discussion

Results demonstrated a decrease in Fluorescence/mineral loss for enamel subjected to 20 days of pH-Cycling in comparison to non-cycled controls, suggesting that such exposure may confer a degree of protection to subsequent acidic challenges. This provides support for the idea that exposure to the cyclic pH of the mouth may be what drives PEM, however due to the small sample sizes used and the lack of statistical

significance further work is needed to support these findings. These findings also provide support for the use of this approach for attempting to model the PEM process.

Decreased mineral/fluorescence loss was observed in enamel blocks treated with Zinc or Fluoride solutions in comparison to un-treated controls, particularly in the Zn/F condition, supporting their involvement in reducing enamel demineralisation and possible importance for PEM. Once again, however, the observed differences were not statistically significant and, as such, further work with larger sample sizes is needed to confirm this.

Conclusions

The initial results reported here suggest that pH-cycling may be an effective way of modelling the PEM process *in vitro* and that Zinc and Fluoride also appear to be involved. These results need to be further confirmed in a larger sample sizes along with supplementary chemical and physical analysis to further develop this model.

Summary

Post-eruptive maturation refers to the chemical and physical changes that occur in the outer layers of tooth enamel following eruption of the tooth and exposure to the oral environment and is believed to be caused by the cyclic de- and re-mineralisation that occurs within the mouth. The present study aimed to simulate PEM using an *in vitro* pH-cycling model, the success of which was tested through exposing treated enamel to a subsequent acid challenge. It also aimed to investigate the effects of Zinc and Fluoride upon the model through 2m treatments throughout the pH-cycling process. Reduced mineral/fluorescence loss was observed both in 20d pH-cycled enamel in comparison to non-cycled controls and in enamel treated with Zinc and Fluoride compared to non-treated controls. These differences were not, however, statistically significant. Results indicate that pH-cycling may be an effective way of modelling the PEM process *in vitro* and that Zinc and Fluoride may be involved, however this needs to be further confirmed in a larger sample sizes and further chemical and physical analysis conducted.

References:

- Brudevold F, Steadman L T, Spinelli M A *et al.* A study of zinc in human teeth. Arch Oral Biol 1963 8: 135-144.
- Brudevold F, Aasenden R, Bakhos Y: A preliminary study of posteruptive maturation of teeth in situ. Caries Res 1982;16:243-248.
- Driessens FC, Heijligers HJ, Borggreven JM, Wöltgens JH: Posteruptive maturation of tooth enamel studied with the electron microprobe. Caries Res 1985;19:390-395.
- Lynch RJ, Mony U and ten Cate JM: Effect of Lesion Characteristics and Mineralising Solution Type on Enamel Remineralisation in vitro. Caries Res. 2007; 41. 257-262.
- Lynch RJ, Churchley D, Butler A, Kearns S, Thomas GV, Badrock TC, Cooper L, Higham SM: Effects of zinc and fluoride on the remineralisation of artificial carious lesions under simulated plaque fluid conditions. Caries Res. 2011; 45, 3. 313-322.
- Nakajima O, Miake Y, Yanagisawa T: The influence of saliva on post-eruptive maturation in enamel. Shikwa Gakuho 2003;103:289-298.
- Robinson C, Shore RC, Brookes SJ, Strafford S, Wood, SR and Kirkham J: The Chemistry of Enamel Caries. Crit Rev Oral Biol Med. 2000; 11, 4. 481-495.
- Vogel GL, Zhang Z, Chow LC, Carey CM, Schumacher GE and Banting DW: Effect of *in vitro* Acidification on Plaque Fluid Composition With and Without a NaF or a Controlled-release Fluoride Rinse. J Dent Res. 2000; 79, 4. 983-990.
- Wöltgens JH, Bervoets TJ, Witjes F, Driessens FC: Changes in the composition of the enamel of human premolar teeth shortly after eruption. Arch Oral Biol 1981;26:717-719.

PERFORMANCE OF QUANTIFERON-TB GOLD IN-TUBE TEST IN SERIAL TESTING OF LATENT TUBERCULOSIS INFECTION AMONG HEALTHCARE WORKERS IN GEORGIA

Veriko Mirtskhulava

E-mail: verikomir@gmail.com

PhD Program, David Tvildiani Medical University, Tbilisi, Georgia

Tutor: Prof. Nino Tabagari, MD, PhD

Introduction

Health care workers (HCW) are at risk of *M. tuberculosis* (TB) infection, or latent TB infection (LTBI), due to their occupational exposure in healthcare facilities in Georgia. Therefore, the screening of HCW for LTBI is critical as TB infection control program is being implemented.¹

Aims

We conducted retrospective analysis of the LTBI testing results of HCWs from the National Tuberculosis Program (NTP) of Georgia and affiliated primary healthcare centers (PHCs). We evaluated agreement between the tuberculin skin test (TST) and A commercial blood assays for the diagnosis of latent tuberculosis infection (LTBI) - QuantiFERON-TB Gold In Tube (QFT-IT).

Methods

We did subgroup analysis of 163 HCWs screened for LTBI between March 2009 and September 2010 as part of the study already published in 2013.¹ For our analysis HCWs were grouped by their self reported frequency of occupational exposure to infectious TB patient. We assessed agreement between the test using Kappa statistics in different risk groups for LTBI. Concordance between the two diagnostic tests for LTBI (TST and QFT-GIT) was determined using the kappa (κ), where $\kappa > 0.75$ represents excellent agreement, $\kappa = 0.4-0.75$ represents fair to good agreement, and $\kappa < 0.4$ represents poor agreement. The following standards for strength of agreement for the kappa coefficient are usually applied: ≤ 0 =poor, $.01-.20$ =slight, $.21-.40$ =fair, $.41-.60$ =moderate, $.61-.80$ =substantial and $.81-1$ =almost perfect.² Agreement between the tests was assessed at baseline and at the second round of LTBI testing. Occupational TB exposure frequency was categorized as daily (contact ≥ 5 days per week), frequent (contact < 5 days per week and \geq twice per month), rare (contact < 5 days per month and \geq once per 3 months), and very rare (contact < 5 days per 3 months). TST was defined as positive if the induration in HCWs was ≥ 10 mm^{3,4} QFT-IT was defined as positive if the response to the TB antigens minus the negative control was ≥ 0.35 IU/ml as per manufacturer's instructions.⁵⁻⁷ Furthermore based on previous similar studies conducted different cut off points for the QFT-IT such as < 1.0 IU/ml⁵, < 3.0 IU/ml⁷, and < 5.3 IU/ml⁶ were used to evaluate agreement with the TST. Logistic linear regression was used to assess risk factors for discordant results of these LTBI tests.

Results

Data were collected and managed using a REDCap electronic data capture tool. REDCap (Research Electronic Data Capture) is a secure, web-based application designed to support data capture for research studies⁸. Statistical analyses were performed using IBM SPSS Statistics 21. We analyzed LTBI testing results of 163 HCW Seventy eight percent (127/163) of the HCWs worked in TB facilities, and 22% worked in PHCs. The majority of the HCWs were female (n=132, 81%). The mean age was 42 years (standard deviation 10 years). The mean number of years in healthcare was 17 (standard deviation 12 years). Forty five percent of the HCWs reported daily TB exposure at work, 20% reported frequent TB exposure, and 51% reported rare TB exposure at work. Mean delay between sequential LTBI tests was 69 weeks (standard deviation 25 weeks).

Agreement between TST and QFT-IT at baseline and repeated testing is described in table 1. Our study showed highest agreement between TST and QFT-IT at QFT-IT cut off of < 0.35 IU/ml. This agreement was fair with $\kappa = 0.39$ (standard error (SE): 0.065) at baseline and $\kappa = 0.36$ (SE: 0.064) at the second round of testing. We did not find major difference in agreement between TST and QFT-IT at baseline and at the 2nd round of testing at any QFT-IT cut off.

Agreement between TST and QFT-IT at baseline and repeated testing stratified by BCG scar and occupational TB exposure status at QFT-IT Cut off < 0.35 IU/ml is presented in table 2. Concordance between the two LTBI tests was higher among those HCWs with no BCG scar (n=34), $\kappa = 0.58$ (SE: 0.129) at baseline and $\kappa = 0.50$ (SE: 0.129) at the second round of testing compared to the group with a BCG scar (n=129), $\kappa = 0.35$ (SE: 0.074) at baseline and $\kappa = 0.33$ (SE: 0.069) at the second round of LTBI testing. Furthermore agreement between TST and QFT was higher among HCWs with daily occupational TB exposure [$\kappa = 0.41$ (SE: 0.086)] compared to those HCWs who did not see TB patients five days a week [$\kappa = 0.36$ (SE: 0.095)].

In multivariate analysis, we found that the TST+/QFT-IT- group, at the QFT-IT cut-off of < 0.35 IU/ml, less likely to have daily occupational TB exposure (adjusted odds ratio (aOR)=0.4, p<0.02).

Discussion

Retrospective analysis of LTBI testing results of Georgian HCWs from the NTP and PHCs showed higher agreement between TST and QFT among HCWs with daily occupational TB exposure compared to those HCWs who did not see TB patients five days a week. As it was expected agreement between the TST and QFT-IT is higher among HCWs with no BCG scar due to 79.4% concordance between TST and QFT-IT compared to those with BCG scare, highlighting cross-reaction from prior BCG vaccination. TST+/QFT-IT- result was associated with less likelihood of daily occupational TB exposure. This discordance is the most probably due to false positive TST result among BCG vaccinated individuals –Georgia HCWs. Many studies have shown false positive TST results in BCG vaccinated individuals.⁹

Our study had some limitations: first, there is no “gold standard” for detecting LTBI, and second, we did not evaluate a possible booster effect of TST. Also the sample size for this analysis is small.

Conclusions

When LTBI therapy will be introduced for HCWs in Georgia in order to avoid treatment of false positive HCWs for LTBI routine screening with QFT-IT is recommended due to high BCG vaccination coverage in the country and boosting effect of TST when serial testing is done.

Summary

Introduction: Health care workers (HCW) are at risk of M. tuberculosis (TB) infection, or latent TB infection (LTBI), due to their occupational exposure in healthcare facilities in Georgia.

Methods: We conducted retrospective analysis of the LTBI testing results of HCWs from the National

Tuberculosis Program (NTP) of Georgia and affiliated primary healthcare centers (PHCs) to evaluate agreement between TST and QFT-IT among 163 HCWs screened for LTBI in March 2009 - September 2010.

Results: Our study showed highest agreement between TST and QFT-IT at QFT-IT cut off of < 0.35 IU/ml with $\kappa = 0.39$ (standard error (SE): 0.065) at baseline and $\kappa = 0.36$ (SE: 0.064) at the second round of testing. In multivariate analysis, we found that the TST+/QFT-IT- group, at the QFT-IT cut-off of < 0.35 IU/ml, less likely to have daily occupational TB exposure (adjusted odds ratio (aOR) = 0.4, $p < 0.02$).

Conclusion: When LTBI therapy will be introduced for HCWs in Georgia in order to avoid treatment of false positive HCWs for LTBI routine screening with QFT-IT is recommended due to high BCG vaccination coverage in the country and boosting effect of TST when serial testing is done.

Table 1. Agreement between TST and QFT-IT at baseline and repeated testing (N=163)

LTBI Testing	QFT-IT Cut off (IU/ml)	TST-/QFT-IT-No (%)	TST+/QFT-IT+No (%)	TST+/QFT-IT-No (%)	TST-/QFT-IT+No (%)	κ (S.E.)
Baseline	< 0.35	38 (23.3)	76 (46.6)	42 (25.8)	7 (4.3)	0.39 (0.065)
Retesting		24 (14.7)	93 (57.1)	44 (27.0)	2 (7.7)	0.36 (0.064)
Baseline	< 1.0	38 (23.3)	59 (36.2)	59 (36.2)	7 (4.3)	0.25 (0.059)
Retesting		25 (15.3)	74 (45.4)	63 (38.7)	1 (0.6)	0.26 (0.050)
Baseline	< 3.0	40 (24.5)	38 (23.3)	80 (49.1)	5 (3.1)	0.14 (0.045)
Retesting		25 (15.3)	52 (31.9)	85 (52.1)	1 (0.6)	0.15 (0.036)
Baseline	< 5.3	40 (24.5)	26 (16.0)	92 (56.4)	5 (3.1)	0.68 (0.039)
Retesting		25 (15.3)	37 (22.7)	100 (61.3)	1 (0.6)	0.91 (0.027)

Table 2. Agreement between TST and QFT-IT at baseline and repeated testing stratified by BCG scar and occupational TB exposure status (QFT-IT Cut off < 0.35 IU/ml)

LTBI Testing	Occupational TB Exposure Risk	TST-/QFT-IT-No (%)	TST+/QFT-IT+No (%)	TST+/QFT-IT-No (%)	TST-/QFT-IT+No (%)	κ (S.E.)
Baseline	5 days a week (N=106)	22 (20.8)	55 (51.9)	23 (21.7)	6 (5.7)	0.41 (0.086)
Retesting		12 (11.3)	64 (60.4)	28 (26.4)	2 (1.9)	0.31 (0.084)
Baseline	5 days a week (N=57)	16 (28.1)	21 (36.8)	19 (33.3)	1 (1.8)	0.36 (0.095)
Retesting		12 (21.1)	29 (50.9)	16 (28.1)	0 (0.0)	0.43 (0.099)
	BCG Scar					
Baseline	Present (N=129)	29 (22.5)	58 (45.0)	35 (27.1)	7 (5.4)	0.35 (0.074)
Retesting		18 (14.0)	72 (55.8)	38 (29.5)	1 (0.8)	0.33 (0.069)
Baseline	Absent (N=34)	9 (26.5)	18 (52.9)	7 (20.6)	0 (0.0)	0.58 (0.129)
Retesting		6 (17.6)	21 (61.8)	6 (17.6)	1 (2.9)	0.50 (0.154)

References

1. J AW, Mirtskhulava V, Kipiani M, et al. Prevalence and incidence of latent tuberculosis infection in georgian healthcare workers. *PLoS One* 2013;8(3):e58202.
2. Sim J, Wright CC. The kappa statistic in reliability studies: use, interpretation, and sample size requirements. *Phys Ther* 2005;85(3):257-68.
3. Targeted tuberculin testing and treatment of latent tuberculosis infection. This official statement of the American Thoracic Society was adopted by the ATS Board of Directors, July 1999. This is a Joint Statement of the American Thoracic Society (ATS) and the Centers for Disease Control and Prevention (CDC). This statement was endorsed by the Council of the Infectious Diseases Society of America. (IDSA), September 1999, and the sections of this statement. *Am J Respir Crit Care Med* 2000;161(4 Pt 2):S221-47.
4. Blumberg HM, Leonard MK, Jr., Jasmer RM. Update on the treatment of tuberculosis and latent tuberculosis infection. *JAMA* 2005;293(22):2776-84.
5. Fong KS, Tomford JW, Teixeira L, et al. Challenges of interferon-gamma release assay conversions in serial testing of health-care workers in a TB control program. *Chest* 2012;142(1):55-62.
6. Slater ML, Welland G, Pai M, Parsonnet J, Banaei N. Challenges with QuantiFERON-TB Gold assay for large-scale, routine screening of U.S. healthcare workers. *Am J Respir Crit Care Med* 2013;188(8):1005-10.
7. Nienhaus A, Garipey PK, Trouve C, Lhaumet C, Toureau J, Peters C. Tuberculosis screening at the Sainte-Anne Hospital in Paris - results of first and second IGRA. *J Occup Med Toxicol* 2014;9:24.
8. Harris PA, Taylor R, Thielke R, Payne J, Gonzalez N, Conde JG. Research electronic data capture (REDCap)--a metadata-driven methodology and workflow process for providing translational research informatics support. *J Biomed Inform* 2009;42(2):377-81.
9. American Thoracic Society (1990) Diagnostic Standards and classification of tuberculosis. *Am Rev Respir Dis* 142: 725–735.

IDENTIFICATION AND CHARACTERIZATION OF BACTERIA OBTAINED FROM HUMAN SKIN AND SKIN OF MUS MUSCULUS - A PILOT STUDY FOR PREPARING NON-STANDARD MODEL BACTERIA FOR THEIR POTENTIAL USE IN ALTERNATIVE GENE THERAPY

Lenka Pálková

E-mail: lena.palkova@gmail.com

Institute of Molecular BioMedicine, Faculty of Medicine,
Comenius University in Bratislava, Slovakia

Co-authors: L. Tóthová, N. Bratinková, I. Mojžišíková

Tutor: RNDr. Gabriel Minárik, PhD.

Introduction

The number of microorganisms living in association with human body exceeds the number of human cells several times. The sum of genomes of all of these microbes is referred to as a microbiome. Since, microbiome encodes about 100 times more genes than the entire human genome does, it can significantly affect a human phenotype (1). The largest organ of the human body, which is colonized by microorganisms, is a skin (2). Bacteria living on the surface of the body are collectively referred to as skin microflora. As it includes a lot of non-pathogenic bacteria, it provides the potential for the development of new diagnostic and therapeutic approaches in the treatment of dermatological diseases. In our project, we decided to explore the possibility of utilization of non-pathogenic bacteria cultivated after the collection from human skin and skin of *Mus musculus*, that have not been used and genetically modified in the laboratory before. The genome of *Mus musculus* is 99% identical to the human genome (3), moreover, there were found significant similarities between human and mouse skin microflora, that make mouse an excellent model system for investigating of interactions between host and bacteria (4). The primary aim of our study was to optimize the process of cultivation of these bacteria, isolation of genomic DNA and identification of bacterial species present on the skin of both studied organisms. Later, identified and cultivated bacteria will be genetically modified and tested for the possibility of their utilization in an alternative gene therapy.

Methods

DNA isolation and quantification

Bacterial samples were obtained from skin of 4 healthy people forearms, and from skin of 8 mice (*Mus musculus*) by cotton swabs. Subsequently, bacteria were applied to a Petri dish with a solid LB medium and cultivated 24 h. After several rounds of cultivation on Petri dishes single colonies were gained, inoculated into liquid LB medium and cultivated 24 h. In this way, separation of individual bacterial species was achieved. For isolation of genomic DNA, DNeasy® Blood & Tissue Kit 250 (Qiagen, Hilden, Germany) was used. Firstly, we proceeded according to the original protocol. Secondly, we optimized protocol in order to increase the yield of DNA: bacteria were exposed to heat shocks by incubating 5 min / 90 °C and 5 min 20 °C before isolation. Incubation steps were repeated 5 times. The next optimization steps were: incubation 10 min. / 99 °C and 10 min. / 56 °C, after addition of ATL buffer; 10 min / 56 °C and 10 min / 70 °C after addition of Proteinase K and AL solution respectively. DNA concentration was measured on a Nanodrop ND-1000 (Thermo Scientific, Wilmington, USA). The comparison of DNA yield obtained by both protocols was performed using GraphPad Prism 5 (La Jolla, CA, USA). The two-way ANOVA test was used for statistical processing of data. $P < 0.05$ was considered statistically significant.

Bacteria genotyping

16S RNA genes were amplified by the universal primers - forward primer 27F 5'-AGAGTTTGATC-CTGGCTCAG-3' (5) and reverse primer 5'-1492R GGTTACCTTGTTACGACTT-3' (6). For the amplification of target sequences PCR master mix (2x) (Fermentas, Vilnius, Lithuania) was used. Then, PCR products were purified using Exonuclease I and Fast AP Thermosensitive Alkaline Phosphatase (Fermentas, Vilnius, Lithuania). Sequencing of PCR reactions was performed using Big Dye Terminator® v 3.1 Cycle Sequencing Kit (Applied Biosystems, Foster City, USA). The samples were precipitated with NaOAc EtOH + MBG H₂O and 70% EtOH and dried out. To the dried product, Hi-Di formamide (Applied Biosystems, Foster City, USA) was added. ABI 3500 Genetic Analyzer Genetic Analyzer using a 50 cm capillary with POP-7™ polymer (Applied Biosystems, Foster City, USA) was used for electrophoresis. The sequencing data were processed using the Sequencing Analysis Software (Applied Biosystems, Foster City, USA) and compared with a database of 16S RNA genes sequences using the BLAST online tool (<http://blast.ncbi.nlm.nih.gov/Blast.cgi>)

Results

Using 16S RNA bacterial genes we identified six bacterial species obtained from the surface of human body (Table 1), and 5 bacterial species obtained from the skin of model organism *Mus musculus* (Table 2) which we were able to cultivate and to prepare long term stock cultures for further research.

Table 1: Bacteria isolated from the surface of human body

Bacterial species	Gram staining	Phylum
<i>Micrococcus luteus</i>	G+	Actinobacteria
<i>Neisseria subflava</i>	G-	Proteobacteria
<i>Rothia mucilagonosa</i>	G+	Actinobacteria
<i>Staphylococcus epidermidis</i>	G+	Firmicutes
<i>Staphylococcus haemolyticus</i>	G+	Firmicutes
<i>Staphylococcus pasteurii</i>	G+	Firmicutes

Table 2: Bacteria isolated from the surface of *Mus musculus* body

Bacterial species	Gram staining	Phylum
<i>Klebsiella oxytoca</i>	G-	Proteobacteria
<i>Micrococcus luteus</i>	G+	Actinobacteria
<i>Staphylococcus cohnii</i>	G+	Firmicutes
<i>Staphylococcus lentus</i>	G+	Firmicutes
<i>Staphylococcus sciuri</i>	G+	Firmicutes

We have optimized the protocol for isolation of bacterial genomic DNA, which is suitable for use in G+ and G- bacteria. Using the optimized method, 1.9 – 19.7 times higher concentrations of DNA were obtained for all bacterial species compared to standard protocol for DNeasy® Blood & Tissue Kit 250. Significantly higher yields of DNA were obtained in three bacterial species obtained from human skin: *Micrococcus luteus* p<0.001; *Neisseria subflava* p<0.05; *Rothia mucilagonosa* p<0.05; *Staphylococcus epidermidis* p=ns; *Staphylococcus haemolyticus* p=ns; *Staphylococcus pasteurii* p=ns (Figure 1) and three bacterial species obtained from skin of mice: *Klebsiella oxytoca* p<0.001; *Micrococcus lentus* p = ns; *Micrococcus luteus* p <0.001; *Staphylococcus cohnii* p <0.01; *Staphylococcus sciuri* p = ns (Figure 2).

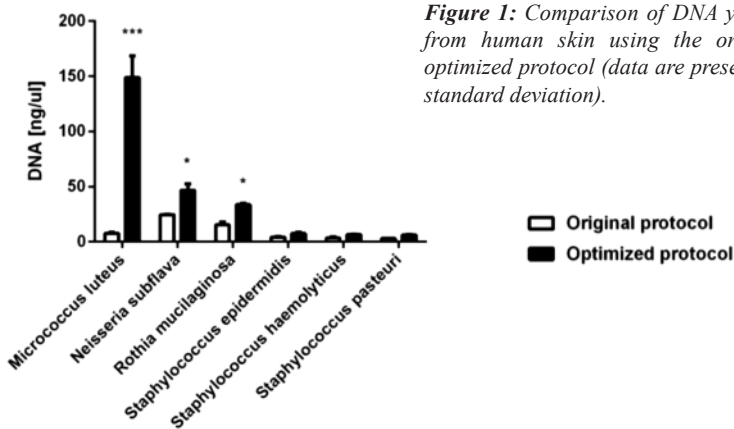


Figure 1: Comparison of DNA yield of bacteria from human skin using the original and the optimized protocol (data are presented as mean + standard deviation).

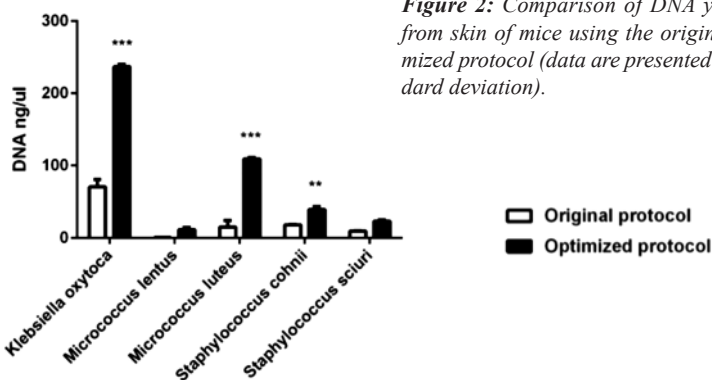


Figure 2: Comparison of DNA yield of bacteria from skin of mice using the original and the optimized protocol (data are presented as mean + standard deviation).

Discussion

The 16S RNA genes represent an ideal tool for identifying bacterial species, as they contain conserved and variable region. Moreover, they offer sufficient length and plenty of interspecific polymorphisms, according to which individual species can be distinguished (7). Based on these sequences, we identified, cultivated and prepared stocks for six bacterial species obtained from the surface of human body and five bacterial species from mice. All of identified bacterial species are non-pathogenic organisms that are present on human skin and skin of mice under natural conditions. In next stages of experiment, we will examine a potential of these bacteria to express heterologous genes. Since these cultivated bacterial species are non-standard bacteria, in which standard protocols may not work properly, several steps such as plasmid isolation or transformation of bacterial cells need to be optimized. Then, we intend to prepare genetically modified bacteria that will be capable of stable reproduction on skin and also will be able to express a heterologous protein that can provide a potential health benefit for the host organism. This method may

potentially be used in treatment of skin diseases, when an active substance could be expressed by the bacteria directly in the affected area, on the skin.

Conclusions

In our study, we identified and successfully cultivated six non-pathogenic bacterial species obtained from the surface of human body and five bacterial species obtained from body surface of *Mus musculus*. We have optimized protocol for genomic DNA isolation from non-standard bacterial species, as standard protocol may not work properly in DNA isolation from these bacteria.

Summary

Most of bacteria living in association with human body are non-pathogenic organisms that are not laboratory used. In our study we optimized protocol for DNA isolation from non-standardly used bacteria obtained from human skin and skin of *Mus musculus*. We also identified and cultivated several bacterial species, which will be tested for the possibility of using in alternative gene therapy.

Acknowledgments

This project was supported by grant UK/334/2014.

References

1. Turnbaugh PJ, Ley RE, Hamady M, Fraser-Liggett C, Knight R, Gordon JI: The human microbiome project: exploring the microbial part of ourselves in a changing world. *Nature* 2007; 449 (7164), 804–810.
2. Grise EA, Segre JA: The skin microbiome. *Nature Reviews Microbiology* 2011; 9, 244-253
3. Waterston RH a spol.: Initial sequencing and comparative analysis of the mouse genome. *Nature* 2012; 420, 520-562.
4. Grise EA a spol.: A diversity profile of the human skin microbiota. *Genome research* 2008; 18, 1043–1050.
5. Lane DJ: 16S/23S rRNA sequencing. *Nucleic acid techniques in bacterial systematics* 1991, 115-175.
6. Turner S, Pryer KM, Miao VPW, Palmer JD: Investigating deep phylogenetic relationships among
7. Clarridge JE: Impact of 16S rRNA Gene Sequence Analysis for Identification of Bacteria on Clinical Microbiology and Infectious Diseases. *Clinical microbiology reviews* 2004; 17 (4), 840–862

MACROPHAGE PTEN REGULATES EXPRESSION AND SECRETION OF ARGINASE I MODULATING INNATE AND ADAPTIVE IMMUNE RESPONSES

Emine Sahin

E-mail: emine.sahin@meduniwien.ac.at

Center for Physiology and Pharmacology, Institute for Physiology
Medical University of Vienna, Austria

Co-authors: S. Haubenwallner, M. Kuttke, I. Kollmann, A. Halfmann, A. M. Dohnal,
L. Chen, P. Cheng, B. Hoesel, E. Einwallner, J. Brunner, J. B. Kral, W. C. Schrottmair,
K. Thell, V. Saferding, S. Blüml, and G. Schabbauer
Tutor: Ass.-Prof. Priv.-Doz. Mag. Dr. Gernot Schabbauer

Introduction

Multiple sclerosis (MS) is the most common autoimmune disease of the central nervous system (CNS) leading to progressive paralysis in adult humans [1]. The most widely used animal model for MS is experimental autoimmune encephalomyelitis (EAE), which recapitulates many features of MS immunopathology [2]. CD4⁺ T cells, especially those polarized towards the Th1/Th17 subsets, play a critical role in the pathogenesis of autoimmune diseases [3]. Therefore, it is important to understand pathways controlling Th17-mediated autoimmunity. However, signal transduction pathways in APCs that govern the development of Th17 cells are incompletely understood. The Phosphatidylinositol-3-kinase (PI3K) pathway is one of the most important signal transduction pathways intricately involved in innate immunity and is strictly regulated by the PI3K antagonist, the lipid phosphatase, PTEN [4]. We found that myeloid PTEN is responsible for the elevated production of cytokines such as IL-6 in response to TLR agonists, and deletion of PTEN results in diminished inflammatory responses [5, 6]. Additionally we observed that PTEN in myeloid cells is required for the development of CIA [6]. We observed that Arginase 1 expression was markedly induced by PTEN deletion in myeloid cells, suggesting an alternative like activation of *pten*^{-/-} macrophages. Therefore, we aimed to elucidate the molecular basis of the PI3K/PTEN signaling axis regulating Arginase 1 expression and the potential role of Arginase 1 in modulating innate immune responses mediated by cell-type-specific PTEN deficiency in cells of monocytic/macrophage origin. Furthermore we aimed to investigate the regulatory mechanisms of intrinsic Arginase 1 or extrinsic pegylated Arginase 1 (recArgI) in experimental autoimmune encephalitis (EAE).

Methods

We induced EAE in animals with a celltype-specific (LysM, CD11c-cre) deletion of PTEN to test the selective role of PTEN-deficient APCs on the induction of autoimmunity without affecting other cell types, especially T cells. In a pharmacological experimental approach we analyzed the possibility that extrinsic recombinant Arginase 1 contributes to the protection of wildtype mice developing experimental autoimmune encephalomyelitis.

Results and Discussion

Here we report that control of PI3K signaling by PTEN specifically in APCs is essential for the development of Th17 mediated autoimmune diseases such as experimental-autoimmune-encephalomyelitis

(EAE). We observed that Arginase I expression and secretion were markedly induced by PTEN deletion, suggesting *pten*^{-/-} antigen presenting cells (APCs) exhibit an alternative -like phenotype. This finding was further corroborated by experiments with recombinant Arginase I present in mixed lymphocyte reactions using LPS-primed ovalbumin laden dendritic cells together with OTII T-cells and in the in vivo autoimmune model EAE. Genetic and pharmacologic experimental approaches in vitro, as well as in vivo models of autoimmunity, provide convincing evidence that PI3K/PTEN -regulated extracellular Arginase I acts as a paracrine regulator of inflammation and immunity.

Conclusion and Summary

Our findings show that the PI3K/PTEN axis in APCs is regulating Th17-dependent autoimmune pathology. PTEN deficient APCs with sustained and enhanced PI3K signaling display an upregulation of markers for alternative activation. This regulatory phenotype leads to a significantly reduced production of inflammatory cytokines IL6 and IL12/23 upon stimulation with TLR agonists.

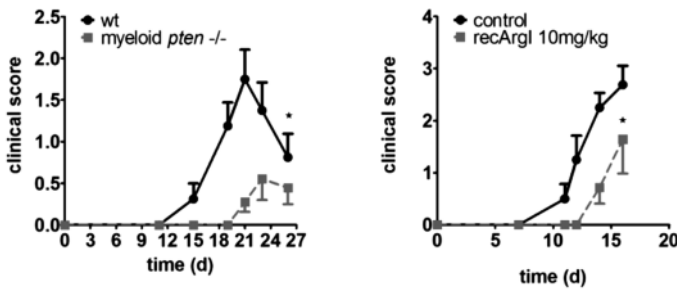


Figure 1: A: Clinical score of wt and myeloid *pten*^{-/-} animals after induction of EAE. B: Disease development as indicated by clinical score in *recArgI*-treated versus control wildtype mice.

References

1. De Jager, P.L., et al., Integration of genetic risk factors into a clinical algorithm for multiple sclerosis susceptibility: a weighted genetic risk score. *Lancet Neurol*, 2009. 8(12): p. 1111-9.
2. Rangachari, M. and V.K. Kuchroo, Using EAE to better understand principles of immune function and autoimmune pathology. *J Autoimmun*, 2013. 45: p. 31-9.
3. Langrish, C.L., et al., IL-23 drives a pathogenic T cell population that induces autoimmune inflammation. *J Exp Med*, 2005. 201(2): p. 233-40.
4. Gunzl, P. and G. Schabbauer, Recent advances in the genetic analysis of PTEN and PI3K innate immune properties. *Immunobiology*, 2008. 213(9-10): p. 759-65.
5. Gunzl, P., et al., Anti-inflammatory properties of the PI3K pathway are mediated by IL-10/DUSP regulation. *Journal of leukocyte biology*, 2010. 88(6): p. 1259-69.
6. Stephan Blüml et al., PTEN in antigen presenting cells controls Th17-mediated autoimmune arthritis. *Arthritis & Rheumatology*, Manuscript in Revision.

EVALUATION OF PARAMETHERS AFFECTING SURVIVAL AND METASTATIC POTENTIAL IN PATIENTS WITH *SDHB* MUTATED PHEOCHROMOCYTOMA/PARAGANGLIOMA

Jan Schovánek^{1,2}

E-mail: schovanej.jan@outlook.com

¹Program in Reproductive and Adult Endocrinology, Eunice Kennedy Shriver National Institute of Child Health & Human Development, NIH, Bethesda, MD, USA

²Department of Internal Medicine III – Nephrology, Rheumatology and Endocrinology, Faculty of Medicine and Dentistry, Palacky University, Olomouc, Czech Republic

Co-Author: Doc. MUDr. Zdeněk Fryšák, CSc. ²

Tutor: Prof. MUDr. Karel Pacák, DrSc. ¹

Introduction

Succinate dehydrogenase subunit B (*SDHB*) mutations are associated with aggressive pheochromocytoma (PHEO)/paraganglioma (PGL) behavior, often resulting in metastatic disease and fatal outcomes. These tumors are often larger, extra-adrenal, and contain lower catecholamine concentrations than other hereditary PHEOs/PGLs. This study evaluated the size and age at diagnosis of primary *SDHB*-related PHEOs/PGLs as independent predictors of their metastatic behavior and outcome (survival).

Methods

One hundred six patients with *SDHB* mutation-related PHEO/PGL were included in this retrospective study. The recorded largest diameters, locations, and patient ages at initial diagnosis of *SDHB*-related primary tumors were analyzed in the context of time to metastasis and patient survival.

Results

First, the development of metastatic disease in patients with primary tumors ≥ 4.5 cm was significantly earlier than in patients with smaller tumors ($P = 0.003$). Second, patients with primary tumors larger than 5.5 cm also had worse overall survival than patients with smaller tumors ($P = 0.008$). Third, age at initial diagnosis was found to be an independent predictor of patient survival (PHEOs: $P = 0.041$; PGLs: $P < 0.001$). Fourth, we did not observe a significant difference in survival based on the specific *SDHB* mutations or patient sex.

Discussion

The importance of the primary tumor size for patient prognosis in general oncology is well established, as manifested by the use of the TNM classification. Thus, previous studies have already agreed that the size of the primary tumor is an important predictor for patient survival and for the metastatic potential of PHEO/PGL, but none of these studies examined whether this finding was true of tumors with specific genetic backgrounds. This study extends this knowledge, due to its unique design, to *SDHB*-related PHEO/PGL. Given the status of the NIH PHEO/PGL program as a national and international referral center, our patient population is typically made up of clinically more severe and complicated cases, usually due to patients with underlying genetic backgrounds, which could possibly lead to some referral bias.

Conclusion

Receiver operating characteristic curves established 4.5 cm as the best value to dichotomize the primary *SDHB*-related PHEO/PGL in order to evaluate the development of metastatic disease and 5.5 cm as the best value for survival prediction. Subsequently, the size of the primary tumor was found as an age-independent predictor of patient survival and metastases development in PGL. In both PHEO and PGL, age at diagnosis was found to be a size-independent predictor of patient survival. No significant difference was found in metastases development or patient survival between males and females or among specific *SDHB* mutations.

Summary

This data further extends and supports previous recommendations that carriers with *SDHB* mutations must undergo early and regular evaluations to detect PHEO/PGL in order to achieve the best clinical outcome.

References

1. Amar L, Baudin E, Burnichon N, Peyrard S, Silvera S, Bertherat J, Bertagna X, Schlumberger M, Jeunemaitre X, Gimenez-Roqueplo AP et al: Succinate dehydrogenase B gene mutations predict survival in patients with malignant pheochromocytomas or paragangliomas. *J Clin Endocrinol Metab* 2007, 92(10):3822-3828.
2. Karasek D, Shah U, Frysak Z, Stratakis C, Pacak K: An update on the genetics of pheochromocytoma. *J Hum Hypertens* 2013, 27(3):141-147.
3. Eisenhofer G, Lenders JW, Siegert G, Bornstein SR, Friberg P, Milosevic D, Mannelli M, Linehan WM, Adams K, Timmers HJ et al: Plasma methoxytyramine: A novel biomarker of metastatic pheochromocytoma and paraganglioma in relation to established risk factors of tumour size, location and *SDHB* mutation status. *Eur J Cancer* 2011.
4. Zelinka T, Musil Z, Duskova J, Burton D, Merino MJ, Milosevic D, Widimsky J, Jr., Pacak K: Metastatic pheochromocytoma: does the size and age matter? *Eur J Clin Invest* 2011, 41(10):1121-1128.
5. Pacak K, Eisenhofer G, Ahlman H, Bornstein SR, Gimenez-Roqueplo AP, Grossman AB, Kimura N, Mannelli M, McNicol AM, Tischler AS: Pheochromocytoma: recommendations for clinical practice from the First International Symposium. October 2005. *Nat Clin Pract Endocrinol Metab* 2007, 3(2):92-102.

NOVEL PROTOCOL FOR DIFFERENTIATION OF INDUCED PLURIPOTENT STEM CELLS (IPS) INTO DOPAMINE AND MELANIN PRODUCING CELLS

Maciej Sulkowski

E-mail: maciej.sulkowski@gmail.com

Department of Transplantation, Faculty of Clinical Immunology and Transplantation,
Collegium Medicum Jagiellonian University, Krakow, Poland.

Co-author: Bogna Badyra

Tutors: prof. dr hab. Marcin Majka, prof. dr hab. Krystyna Ossowska

Introduction

Invented by Yamanaka in 2006, induced Pluripotent Stem cells (iPS) [1] are unlimited source of different adult cells. They can found application not only as in vitro models but also in cell therapy of many disorders, including neurodegenerative diseases.

In Parkinson's disease (PD) degeneration of dopamine-producing neurons takes place. Present therapeutic strategy is symptomatic and its effectiveness decrease in time [2]. There is constant search for new therapies which could cure the cause of the disease. Among most promising approaches, regenerative stem cell therapy appears to be most encouraging.

Aims

The main goal of this study was to develop protocol for in vitro neuronal differentiation of iPS cells into dopaminergic neurons.

Methods

iPS cells cultured on feeder layer were transferred to suspension. Subsequently, progenitor cells were selected and expanded in serum-free medium. In final step cells were terminally differentiated into dopamine-producing cells. On each step cells were characterized for expression of markers on the level of mRNA (by RT-PCR) and protein (by immunocytochemistry). Dopamine production was proved by HPLC, appearing black pigment was identified by EPR. Melanin cellular localization was analyzed by TEM.

Results

Applied neuronal differentiation protocol led to generation of neurons expressing specific markers on the level of mRNA (e.g. dopamine transporter) and protein (tubulin β -III class, tyrosine hydroxylase). Acquired cells were also able to produce and secrete dopamine.

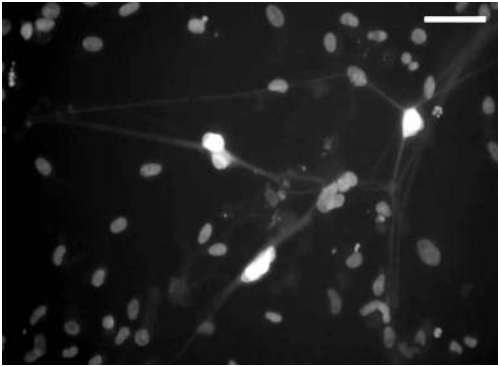


Figure 1. Differentiated cells express tyrosine hydroxylase – marker of dopaminergic neurons. Magnification 400x, white bar - 50 μ m.

Unexpectedly, we also acquired cells producing black pigment. It was identified by EPR as melanin – most probably neuromelanin. Electron microscopy proved that melanin is localized in granules which resemble neuromelanin seeds in substantia nigra.



Figure 2. Differentiated cells sequester melanin. TEM, magnification 51 200x.

Discussion

Applied protocol generated dopaminergic neurons with efficiency corresponding to published data [3]. Acquired cells expressed characteristic markers. They were able to produce dopamine and melanin. To our knowledge this is the first report showing *in vitro* differentiation of iPS cells into neuromelanin-producing cells.

Conclusions

Described protocol efficiently generates dopamine and melanin producing cells. Our results suggest generation of *in vitro* model, which may be used for future research focused on putative role of neuromelanin in the pathogenesis of PD.

Summary

Regenerative therapy of PD involving iPS cells is very promising strategy and in future may become more than *in vitro* model of the disease - a real alternative for present therapies of neurodegenerative diseases.

References

1. K. Takahashi and S. Yamanaka, "Induction of pluripotent stem cells from mouse embryonic and adult fibroblast cultures by defined factors.," *Cell*, vol. 126, no. 4, Aug. 2006.
2. A. E. Lang and A. M. Lozano, "Parkinson's Disease," *N. Engl. J. Med.*, vol. 339, no. 15, 1998.
3. S. H. Lee, N. Lumelsky, L. Studer, J. M. Auerbach, R. D. McKay, and others, "Efficient generation of midbrain and hindbrain neurons from mouse embryonic stem cells," *Nat. Biotechnol.*, vol. 18, no. 6, 2000.

THE VIBRATION PLETHYSMOGRAPHIC METHOD OF ARTERIAL COMPLIANCE ANALYSIS IN DEPENDENCE ON TRANSMURAL PRESSURE

Jana Svačinová

E-mail: svacinova@med.muni.cz

Department of Physiology, Faculty of Medicine, Masaryk University, Brno, Czech Republic

Co-autors: J. Moudr, N. Honzíková

Tutor: prof. MUDr. Nataša Honzíková, CSc.

Introduction

Arterial compliance is a property of the arterial wall enabling a dampening of the amplitude pulse wave. Compliance is defined as a volume difference induced by the pressure difference. Elastance is a reciprocal value of compliance and it decreases with age. A low compliance is frequently a marker of endothelial dysfunction and of changes in the structure of the arterial wall and results in different pathological states and it is one of the predictors of cardiovascular risks like an ischemic heart disease, myocardial infarction, or stroke.

In the last ten years researchers focused on the study of the arterial pressure-volume relationship and the corresponding arterial compliance by photoplethysmographic methods (Tanaka et al. 2011, Talts et al. 2006, Chang et al. 2009). Finger photoplethysmography is a measurement technique enabling detection of arterial blood volume changes in the finger in relationship to pressure changes in the finger arteries.

Previously, we developed a new method for studying the viscoelastic properties of finger arteries and we used for this method a term vibration plethysmography (Penaz et al. 1997). The aim of this study was to develop a new modification of a vibration plethysmographic method of an arterial compliance analysis in dependence on the transmural pressure. Finally, we analysed the compliance of a group of volunteers.

Methods

The pressures acting on the arterial wall are as follows: blood pressure $BP(t)$ is acting on the inner side of the arterial wall, the applied cuff pressure $P_c(t)$ is acting on the outer side of the arterial wall, and the transmural pressure $P_t(t)$ is the resultant pressure originating from the elastance of the arterial wall in dependence on volume. The pressures are time-varying therefore we have to consider additional pressure given by dissipative and inertial forces. Static compliance $C(P_t)$ is defined as a volume difference induced by the pressure difference therefore it can be express as a derivation of volume V in dependence on $P_t(t)$:

$$\frac{d}{dP_t} V(P_t) = C(P_t) = 1/E(P_t), \text{ where } E(P_t) \text{ is an elastance.}$$

Finger cuff (placed on the middle phalanx of the fourth finger) operated on the artery at a pressure $P_c(t) = P_{css} + P_{ca} \cdot \sin(2\pi ft)$, where $P_{ca} \cdot \sin(2\pi ft)$ are the pressure vibrations of a constant amplitude $P_{ca} = 2$ mmHg and frequencies $f_m = (20, 25, 30, 35, 40)$ Hz. Vibrations are sequentially superimposed to each pressure value P_{css} (taking 10 values from 170 to 30 mmHg). Simultaneously, we recorded the arterial volume vibration $V(t)$ as a response to the pressure vibrations $P_c(t)$. The finger cuff for continual

BP(t) measurement and the Pt evaluation (Portapres) was placed on the middle phalanx of the fourth finger. (Figure 1)

Then we computed dynamic compliance as a frequency characteristic of the vibration transmitted by the arterial wall:

$$F(j2\pi f, P_{t0}) = \frac{A(j2\pi f_{m}, P_{t0n}) \cdot e^{j\omega(2\pi t)}}{P_{ca}(P_{t0})} = \frac{1}{E(P_{t0}) - (2\pi f)^2 K_m + j2\pi f K_d(P_{t0})}$$

where $A(j2\pi f_{m}, P_{t0n})$ is the volume difference obtained by a Fourier transform applied on the volume vibrations $\Delta V(t)$ measured by the finger cuff at the frequency f_m and the transmural pressure P_{t0n} .

The compliance $C(P_{t0})$ is a static feature of the arterial wall and it can be considered as a frequency characteristic $|F(j2\pi f_{m}, P_{t0n})|$ at frequencies $f=0$. A reason for this consists in the fact that the amplitudes of transmitted vibrations decrease with increasing vibratory frequency. This is caused by the inertial forces of the moving tissues (implemented as a parameters K_m and K_d). To compute $C(P_{t0})$, we use a real part of the reciprocal form of a frequency characteristic as a regression function with a vector $[f_m]$ as an argument of the predictor. The result is the reciprocal value of $C(P_{t0n})$.

The special original equipment and the especially designed measurement protocol were tested on 6 young healthy normotensive subjects (2 women and 4 men) aged 21 ± 1 years and one healthy man aged 70 years (normotensive).

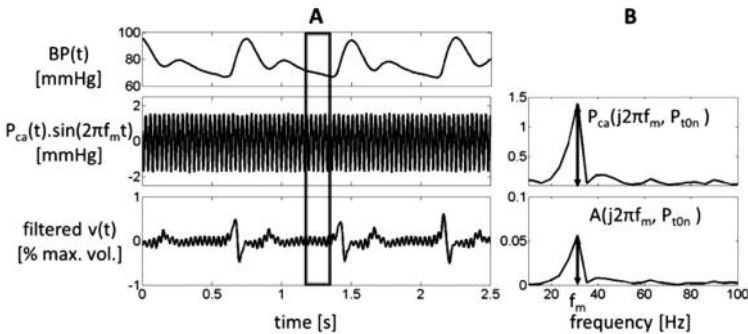


Figure 1: A: an example of 4 second lasting recordings.

$BP(t)$: blood pressure, $P_{ca}(t) \cdot \sin(2\pi f_m t)$: cuff pressure vibration, filtered $V(t)$: volume vibration. The end of the diastolic pulse curve is evaluated.

B above: spectrum of applied pressure vibration; $P_{ca}(j2\pi f_m, P_{t0n})$ is an amplitude of applied pressure vibration at the pressure P_{t0n} and the frequency f_m .

B below: spectrum of volume vibration $V(t)$, where $A(j2\pi f_m, P_{t0n})$ is an amplitude of arterial volume vibration.

Results

The resulting frequency characteristics of arterial wall responses to the applied pressure vibrations differed between the subjects. An example of three-dimensional graphs of the network of the frequency characteristic $|F(j2\pi f_m, P_{t0n})|$ of the arterial wall is shown in Figure 2. This frequency characteristic provides information about the ability of the arterial wall to transmit vibrations of different frequencies from the pressure in the cuff to the arterial volume in dependence on transmural pressure. This graph demonstrated that an increased pressure vibratory frequency caused a decrease of the transmission amplitude. This effect could be influenced by arterial compliance. On the example of frequency characteristics in Figure 2 it appeared that the frequency characteristics of an older individual had lower values compared to the frequency characteristic of a young individual. The compliance $C(P_t)$ of six healthy normotensive young subjects is presented in Figure 3.

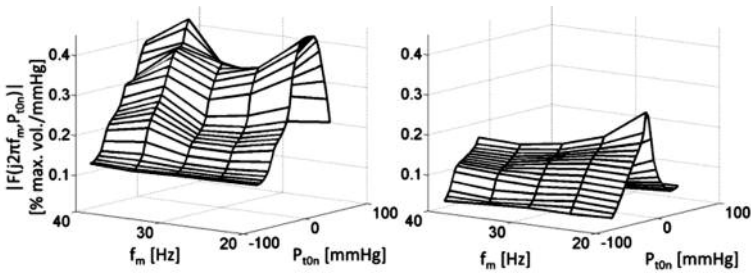


Figure 2: Network of frequency characteristics $|F(j2\pi f_m, P_{t0n})|$ of the pressure vibration transmitted to the volume vibration in dependence on vibration frequency f_m and pressure P_{t0n} .

Left: Frequency characteristic network of the 28 years old woman.

Right: Frequency characteristic network of the 70 years old man.

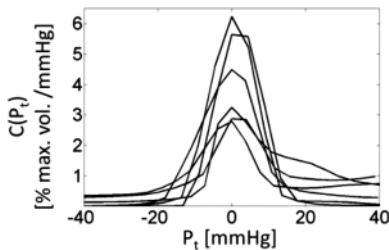


Figure 3: An example of compliance $C(P_t)$ of six healthy normotensive young subjects.

Discussion and conclusion

The main result is a new original method of the determination of dynamic compliance of small arteries, which could serve as a new way to examine small arteries under different physiologic and pathologic states. Some studies estimated arterial compliance based on finger photoplethysmography using pressure-volume changes at changeable transmural pressures (Talts et al. 2006). Our study added additional information on the ability of the arterial wall to transmit vibrations of different frequencies from the applied pressure to arterial volume vibrations by a different gain of the frequency characteristic. We showed that arterial compliance influenced the shape of the frequency characteristic of the arterial wall. Lower compliance seems to be linked with a decrease of the amplitude of transmitted vibrations at higher frequencies.

Supported by MUNI/A/0957/2013.

Summary

The aim of this study was to obtain a detailed analysis of the relationship between the finger arterial compliance C [ml/mmHg] and the arterial transmural pressure P_t [mmHg]. We constructed a dynamic plethysmograph enabling us to set up a constant pressure P_{css} [mmHg] and a superimposed fast pressure vibration in the finger cuff (equipped with a source of infra-red light and a photoelectric sensor for the measurement of arterial volume). P_{css} could be set on the required time interval in steps ranging between 0 and 170 mmHg, and on sinusoidal pressure oscillation with an amplitude P_{ca} (2 mmHg) and a frequency f (20, 25, 30, 35, 40 Hz). At the same time continuous blood pressure BP was measured on the adjacent finger (Portapres). We described the volume dependence of a unitary arterial length on the time-varying transmural pressure acting on the arterial wall (externally $P_{\text{css}} + P_{\text{ca}} \cdot \sin(2\pi f)$, internally BP) by a second-order differential equation for volume. This equation was linearized within a small range of selected BP. In the next step, a Fourier transform was applied to obtain the frequency characteristic in analytic form of a complex linear combination of frequency functions. While series of oscillations [P_{ca}, f] were applied for each P_{css} , the corresponding response of the plethysmogram was measured. Amplitude spectra were obtained to estimate coefficients of the frequency characteristic by regression analysis. We determined the absolute value: elastance E , and its inverse value: compliance ($C=1/E$). Then, $C=C(P_t)$ was acquired by applying sequences of oscillations for different P_{css} (and thus P_t) by the above-described procedure. This methodology will be used for the study of finger arterial compliance in different physiological and pathological conditions.

References

- Chang S, Wang JJ, Su HM, et al.: On calculating the time-varying elastance curve of a radial artery using a miniature vibration method. In: 13th International Conference on Biomedical Engineering 2008 (ICBME) 23: 540-542.
- Penaz J, Honzikova N, Jurak P.: Vibration plethysmography: a method for studying the visco-elastic properties of finger arteries. *Med Biol Eng Comput* 1997; 35, 633-637.
- Talts J, Raamat R, Jagomagi K.: Asymmetric time-dependent model for the dynamic finger arterial pressure-volume relationship. *Med Biol Eng Comput* 2006; 44, 829-834.
- Tanaka G, Yamakoshi K-I, Sawada Y.: A novel photoplethysmography technique to derive normalized arterial stiffness as a blood pressure independent measure in the finger vascular bed. *Physiol Meas* 2011; 32, 1869-1883.

UNIMPAIRED ANABOLIC RESPONSE TO ORAL MEAL FEEDING IN PATIENTS WITH PANCREATIC CANCER CACHEXIA

David P. J. van Dijk

E-mail: d.vandijk@maastrichtuniversity.nl

Department of Surgery, Maastricht University Medical Centre and NUTRIM
School of Nutrition, Toxicology and Metabolism, Maastricht University, The Netherlands

Co-authors: M.C.G. van de Poll, A.G.W. Moses, T. Preston, S.W.M. Olde Damink,
S.S. Rensen, N.E.P. Deutz, P.B. Soeters, J.A. Ross, K.C.H. Fearon, C.H.C. Dejong
Tutor: Prof. Peter B. Soeters, MD, PhD

Background

Pancreatic cancer is often accompanied by cachexia, a syndrome of severe weight loss, muscle wasting, and inflammation. A suboptimal response to nutritional support may further aggravate cachexia. The influence of nutrition on protein kinetics in these patients is poorly understood. This study investigates the effect of feeding on whole-body protein kinetics in cachectic pancreatic cancer patients using labelled amino acids.

Methods

Eight cachectic pancreatic cancer patients and seven control patients received a primed continuous intravenous infusion of L-[ring- $^2\text{H}_5$]phenylalanine and L-[3,3- $^2\text{H}_2$]tyrosine for eight hours. In addition, an enteral L-[1- ^{13}C]phenylalanine tracer was administered orally. After four hours, oral sip feeding was started (0.083 g protein/kg/h, one sip every 30 minutes). Whole body protein breakdown was measured as total rate of appearance (Ra) of phenylalanine corrected for exogenously administered phenylalanine. Protein synthesis was calculated as total phenylalanine Ra minus rate of phenylalanine hydroxylation. Net protein synthesis was calculated by subtracting protein breakdown from protein synthesis. Measurements were corrected for lean body mass. C-reactive protein (CRP) was measured as marker for systemic inflammation.

Results

Baseline protein breakdown and protein synthesis were higher in cachectic patients compared with controls (breakdown: 63.0 ± 6.5 versus 43.9 ± 1.7 , $p=0.049$; and synthesis: 59.1 ± 6.2 versus 39.3 ± 2.2 , $p=0.021$). During feeding, protein breakdown decreased significantly to 40.0 ± 5.1 ($p=0.012$) in the cachexia group and to 29.3 ± 4.4 ($p=0.018$) in the control group. This decrease did not differ between groups ($p=0.132$). Protein synthesis was not affected by feeding in cachectic patients: 58.6 ± 6.6 ($p=1.000$) but was stimulated in controls: 49.1 ± 3.1 ($p=0.018$). Both groups achieved a positive and comparable net protein synthesis during feeding: 18.6 ± 3.3 (cachexia) and 19.8 ± 3.3 (control), $p=0.908$. Basal protein breakdown was positively correlated with CRP levels ($rs=0.658$, $p=0.008$).

Conclusions

Cachectic pancreatic cancer patients have a higher basal protein turnover than controls which is correlated with systemic inflammation. Both cachectic patients and controls show a comparable protein anabolism during feeding, albeit through a different pattern of protein kinetics. In cachectic patients this is primarily related to reduced protein breakdown, whereas in controls both protein breakdown and protein synthesis alterations are involved. Interventions targeted at stimulating protein synthesis may further boost the anabolic response and increase the efficacy of nutritional support in cancer cachexia.

INDEX

Avaliani Tamar	12
Babinská Zuzana	15
Bibby Becky	19
Biedermann Julia	23
Botz Balint	27
Brocklesby Kayleigh	33
Castro José Pedro	38
Danihel Vojtěch	41
Fabrik Ivo	43
Filipová Alžběta	46
Howard Anthony	49
Chrenko Robert	54
Ivák Peter	59
Janovská Zuzana	63
Kazimierová Ivana	66
Koelfat Kiran	70
Krajčová Adéla	71
Kramná Lenka	75
Krychtiuk Konstantin	76
Kupsa Tomáš	81
Kvarik Timea	85
Matos Liliana	88
Miles Emma Jane	93
Mirtskhulava Veriko	98

INDEX

Pálková Lenka	102
Sahin Emine	106
Schovánek Jan	108
Sułkowski Maciej	110
Svačinová Jana	113
van Dijk David	117

Vydala: Univerzita Karlova v Praze, Lékařská fakulta v Hradci Králové
prof. MUDr. RNDr. Miroslav Červinka, CSc.
Sazba: TAH reklamní agentura, s.r.o. Hradec Králové

2014